



**Science Research
Publishers**



**Journal of Chemistry and
Environment**
Vol. 1 No. 1 (2022)

Journal of Chemistry and Environment **(ISSN: 2959-0132)**

Vol.1, No.1

December 2022

Editor in Chief	Dr Asad Ali
Edited by	Science Research Publisher (SRP)
Published By	Science Research Publisher (SRP)
Email	jceeditorial@gmail.com JCE@jspae.com
Website	https://www.jspae.com
Journal Link	https://www.jspae.com/index.php/jce



Table of Contents

S.N	Title	Authors	Pages No.
1	Determination of Antioxidant Activity of Acacia Nilotica Linn from different Regions of Baluchistan (Pakistan)	Muhammad Haroon, Zainab Ali Ahmad, Naeem Ullah, Fazal Haq, Muhammad Junaid, Amir Zeb, Mehwish Kiran, Sahid Mehmood, Farzana Kamalan, Aisha Hamid	1-4
2	Synthesis, characterization and antibacterial activity of ethylene di-amine and 2-hydroxybenzadehyde Schiff base and its metal complexes	Muhammad Junaid, Jianhua Yan, Zhongquan Qi, Muhammad Haroon	5-16
3	Comprehensive Review on Synthesis of Abox Material and its Catalytic Applications	Syeda Mehak Batool, Khushbo e Kainat, Suqqyana Fazal, Fawad Ahmad	17-55
4	Fractionation and Characterization of the Bioactive Compounds of the Extracts of Buds of Syzygium aromaticum	Agu Chukwuemeka Leonard, Omeje Nelson Osita	56-73
5	Evaluation of Heavy Metals in Drinking Water of Tribal Districts Ex-FATA Pakistan	Rahim Ullah, Muhammad Suleman, Hina Fazal, Zafar Ali Shah, Muhammad Nauman Ahmad, Yaseen Ahmed, Naik Nawaz, Aiman Niaz, Kashif Ahmed	74-79
6	Advancement and Future Perspectives of Prostate Cancer Treatment by Using Plant Bio-actives: A Review	Hira Zulfiqar, Hunain Zulfiqar, Muhammad Furqan Farooq, Iqbal Ahmed, Iqra Rani, Farman Ullah	80-106

Edited By

Dr. Asad Ali (Editor) JCE@jspae.com

Proof Editor. Dr. Izhar Ali (Managing Editor)

Contact journal email: jceeditorial@gmail.com

Contact Publishers: thesrp.journals@gmail.com

Doi: <https://doi.org/10.56946/jce.v1i01>

Scan QR to view full volume





ARTICLE

Determination of Antioxidant Activity of *Acacia Nilotica* Linn from different Regions of Baluchistan (Pakistan)

Muhammad Haroon^{1*}, Zainab Ali Ahmed¹, Naeem Ullah¹, Fazal Haq², Muhammad Junaid³, Amir Zeb⁴, Mehwish Kiran⁵, Sahid Mehmood⁶, Farzana Kamalan¹, Aisha Hamid¹

¹Department of Chemistry, University of Turbat, Balochistan, Pakistan

²Institute of Chemical Science, Gomal University, DI Khan

³Medical College, Guangxi University, Nanning 530004, Guangxi, China.

⁴Department of Natural and Basic Science, University of Turbat, Balochistan, Pakistan

⁵Department of Horticulture, Faculty of Agriculture, Gomal University, Dera Ismail Khan 29050, Pakistan

⁶College of Chemical and Biochemical Engineering, Zhejiang University, China
Correspondence: burmy_chem@yahoo.com

Abstract

Free radicals are naturally occurring species with unpaired electrons that are formed during normal metabolic processes. Their formation in a high amount may cause oxidation of essential structural molecules of cell, the condition is known as oxidative stress which results in several health issues such as cancer, diabetes, heart diseases, inflammatory diseases, arthritis and a lot more. To overcome these effects, antioxidants, both synthetic and natural ones are consumed by people. Due to recent evidences about the long term harmful effects of synthetic antioxidants the interest towards the natural sources has increased. The aim of the current research is to comparatively analyze the antioxidant activity of *acacia Nilotica* Linn samples collected from different regions of Makran by using 2, 2-diphenyl-1-picrylhydrazyl (DPPH) assay on which no work has been done so far. The DPPH assay of the samples gave the following results with antioxidant activity values as 18.51851%, 4.47761%, and 8.25958% for the samples of *acacia Nilotica* Linn from Shahrak, *acacia* from Turbat, *acacia* from Pedrak. The results revealed that *acacia Nilotica* Linn from Shahrak exhibits maximum free radical scavenging activity. More work on chemical composition of the tested samples has to be done.

Keywords: *Acacia Nilotica* Linn, free radical, antioxidants, DPPH assay

1. INTRODUCTION

Antioxidants play a significant role for the protection of health. According to scientific confirmation antioxidants decrease the risk for many chronic diseases which include heart and cancer diseases [1]. Naturally occurring major sources of antioxidants are vegetables, fruits, leaves etc [2]. The antioxidant compounds are phenol and polyphenols, flavonoids, carotenoids, steroids and thiol these are natural supplements [3]. The benefits of these antioxidants is that they provide antioxidant defense against oxidative stress and show low chances of causing diseases. The antioxidants of the body are insufficient to protect the body thus supply

of external antioxidants is also necessary [4]. Potential approaches for natural antioxidants have been examined in different plant materials. A number of diseases affected by (ROS) which are formed during metabolic processes of cell [5]. In normal conditions for immunity of the biological system since it protects the body from being infected by bacterial and viruses. But their excessive production can harm the tissues [6]. These free radicals cause lipid peroxidation in membrane which is considered to be the starting step towards the cell-injury [7]. These free radicals are stabilized by antioxidants by reacting with them before they oxidized any cellular component and in this way they protect the cell from

oxidative injury [8].

Pakistan, which is an agricultural country, rich in aromatic and medicinal plants which are used as traditional medicine for health care [9]. *Acacia nilotica* is a plant which has known for its useful sources of bioactive properties. *Acacia nilotica* which gives number of bioactive components that shows anti-hypertensive, anti-platelet, aggregatory, anti-inflammatory, spasmogenic, antispasmodic and vasoconstrictor properties [10]. An inexpensive and a fast simple method for the measurement of antioxidant activity involves the use of (DPPH) which is being used to test the ability of compounds which act as hydrogen donor or free radical scavengers to determine antioxidant activity [11]. The technique of (DPPH) test is based on the (DPPH) reduction which is a stable free radical. The unpaired electrons of free radical (DPPH) shows extreme absorption at 517 nm with (purple color) [12]. As the antioxidant and DPPH react with each other which was the stable radical it becomes paired off because due to the existence of a H-donor and it will become DPPH-H and as concerns the absorptions reduced from the DPPH [13]. The DPPH-H is form, which results in decolorization (yellow color) with respect to total taken electrons [14]. This plant has been testified to own antioxidant properties. So this work has been carry out to assess *Acacia nilotica* plant for their possible potential to antioxidant action by DPPH Scavenging method [15].

2. EXPERIMENTAL WORK

2.1 Materials and Methods

2.2 Sample collection

Leaves of *acacia Nilotica* commonly known as desi-kiker were collected from three regions of Makran division of Baluchistan (Pakistan). Each sample were given a number as sample 1, sample 2, sample 3. Sample 1, collected from Shahrak in 25th October 2020, sample 2, collected from Turbat in 30th October 2020, sample 3, collected from Pedrak in 3rd November 2020.

2.3 Chemicals and reagents

All the chemicals and reagents used were of analytical evaluation. Ethanol from sigma Aldrich (www.sigma-aldrich.com), distilled water, and DPPH (2, 2-reagent 95%) from Alfa Aesar, united states.

2.4 Extraction

Air-dried leaves of this plant were ground into powered. 1 gram of each sample was dissolved individually in of 100ml 70% ethanol (absolute). After stirring each sample solution for 5 minutes they were stirred and kept for 5 days at room temperature [11]. After the given period of interval each solution was stirred by magnetic stirrer for 30 minutes and then these were filtered by wattman filter paper to remove the solid residues.

2.5 DPPH radical scavenging assay

Free radical scavenging activities of different leaves extract were measured by (DPPH). In brief, 0.5ml sample solution, 3ml ethanol absolute and 0.3ml of freshly prepared solution of 2, 2-diphenyl-1-picrylhydrazyl (DPPH) solution were mixed to get four tests of each sample. Four blanks for each sample were prepare by mixing 3.3 ethanol absolute and 0.5ml sample solution. A control was prepared by adding 0.3ml (DPPH) solution in 3.5ml ethanol and all these were kept in dark for 2hours at room temperature. After that absorbance of control, blacks and tests were measured at 517nm (UV-visible Spectrophotometer (UV 752 (D), China). Ascorbic acid which is a synthetic antioxidant was used as a standard. A 25ppm ethanolic solution of ascorbic acid as standard. The blank and test of ascorbic acid solution were prepared by following the same protocol as was used for the sample and absorbance was measured [12, 13].

2.6 Statistical analysis

Reduction in absorbance is a degree of better potential of substance is scavenging activity. The antioxidant activity is determined and calculated by using the equation 1.

DPPH Scavenging effect (%) or percent inhibition = A° -

$$A^1 / A^0 * 100 \quad (\text{equation. 1})$$

Where A^0 was the absorbance of control reaction and A^1 was the absorbance in presence of test or standard sample.

3. RESULTS AND DISCUSSION

The acacia nilotica leaves showed greater antioxidant potential when these are compare with the standard ascorbic acid by DPPH method [14]. The absorbance is measured at 517nm the analysis involves UV-visible spectrophotometer which shows maximum absorbance of sample 1 (18.51851%) and 8.25958%, 4.47761% shown by the sample of Turbat and Pedrak. For standard ascorbic acid value were obtained as 22.28571%.

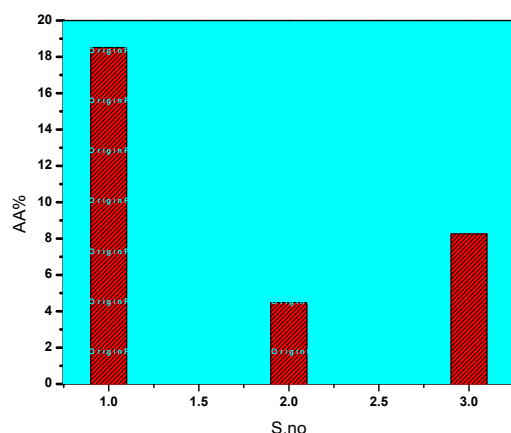


FIGURE 1. Absorbance of different extract of acacia nilotica at 517nm by uv-visible spectrophotometer by DPPH Scavenging assay method.

It means that plant species gives better antioxidant activity by free radical scavenging method as they are compared with standard. So, we can say that acacia nilotica has potential antioxidant activity and it can get a way towards the pharmaceutical uses. The values of control and blank are given in Table 1. Determination of AA% in real samples of acacia Nilotica Linn is given Table 2. AA% of standard (Ascorbic acid) is given Table 3. Absorbance of different extract of acacia nilotica at 517nm by uv-visible spectrophotometer by DPPH Scavenging assay method is given Figure 1.

TABLE 1. Values of control and blanks.

Solution	Absorbance	Mean± SD	Co variance
Blank 1	0.200 0.201 0.202	0.201	0.00082
Blank 2	0.152 0.153 0.154	0.153	0.00082
Blank 3	0.148 0.149 0.151	0.1493	0.00129
Control	0.270 0.271 0.272	0.271	0.00082

TABLE 2. Determination of AA% in real samples of acacia Nilotica Linn.

S. No	Sample type	Absorbance	Mean± SD	Co variance	AA%
1	Acacia from Shahrak	0.420 0.421 0.422	0.421	0.00082	18.51851%
2	Acacia from Turbat	0.344 0.345 0.346	0.345	0.00082	4.47761%
3	Acacia from Pedrak	0.459 0.460 0.461	0.46	0.00082	8.25958%

TABLE 3. AA% of standard (Ascorbic acid).

Absorbance	Meann± SD	Co variance	AA%
0.220 0.221 0.222	0.221	0.00082	22.28571%

4. CONCLUSION

Antioxidants are one of the major requirements of our body in today's world where there are higher risks of disease due to increasing environmental pollution. Since the pollution and several other factors contribute as exogenous source of free radical formation resulting in oxidative stress that results in a number of chronic health issues. For a long period of time the attention of health care institutions and product manufacturers are seeking for the best natural source of antioxidants that are of high value due to their safety assurance. The long term harmful effects of synthetic antioxidants have grabbed the attention of researchers to seek for the safe natural and low cost antioxidant sources. Plants and the derivatives of plants have been proven as the best source of antioxidants. This work

reveals new essential natural sources of antioxidants that are regional acacia samples from three different regions of Makran. The results indicate that all these natural products are significant antioxidants that need to be further analyzed for their chemical composition.

Authors Contribution

M.H supervised research work and has the main idea. ZAA did practical work and wrote the manuscript. FH, AZ, MH, SM, NU and MJ revised the manuscript and provided suggestions. FK is coworker in research. AH coworker in research.

Acknowledgment

We are thankful to Government of Balochistan and University of Turbat for financial assistance through UOTRF project.

Conflict of Interest

The authors declare no conflict of interest. All the authors approved the submission of the manuscript.

Data Availability statement

The data presented in this study are available on request from the corresponding author.

REFERENCES

1. Koleva, I.I., et al., Screening of plant extracts for antioxidant activity: a comparative study on three testing methods. *Phytochemical Analysis: An International Journal of Plant Chemical and Biochemical Techniques*, 2002. 13(1): p. 8-17.
2. Hegazy, G.A., A.M. Alnoury, and H.G. Gad, The role of Acacia Arabica extract as an antidiabetic, antihyperlipidemic, and antioxidant in streptozotocin-induced diabetic rats. *Saudi Med J*, 2013. 34(7): p. 727-733.
3. Patel Rajesh, M. and J. Patel Natvar, In vitro antioxidant activity of coumarin compounds by DPPH, Super oxide and nitric oxide free radical scavenging methods. *Journal of advanced pharmacy education & research*, 2011. 1: p. 52-68.
4. Lü, J.M., et al., Chemical and molecular mechanisms of antioxidants: experimental approaches and model systems. *Journal of cellular and molecular medicine*, 2010. 14(4): p. 840-860.
5. Sivanandham, V., Free radicals in health and diseases-a mini review. *Pharmacologyonline*, 2011. 1(1): p. 1062.
6. Bouayed, J. and T. Bohn, Exogenous antioxidants—double-edged swords in cellular redox state: health beneficial effects at physiologic doses versus deleterious effects at high doses. *Oxidative medicine and cellular longevity*, 2010. 3(4): p. 228-237.
7. Kähkönen, M.P., et al., Antioxidant activity of plant extracts containing phenolic compounds. *Journal of agricultural and food chemistry*, 1999. 47(10): p. 3954-3962.
8. Gowri, S.S., S. Pavitha, and K. Vasantha, Free radical scavenging capacity and antioxidant activity of young leaves and barks of *Acacia nilotica* (L.) Del. Del. *Int. J. Pharm. Pharm. Sci*, 2011. 3: p. 160-164.
9. Atif, A., et al., *Acacia nilotica*: A plant of multipurpose medicinal uses. *Journal of medicinal plants research*, 2012. 6(9): p. 1492-1496.
10. Yadav, A., et al., In vitro antioxidant activities and GC-MS analysis of different solvent extracts of *Acacia nilotica* leaves. *Indian Journal of Pharmaceutical Sciences*, 2018. 80(5): p. 892-902.
11. Villaño, D., et al., Radical scavenging ability of polyphenolic compounds towards DPPH free radical. *Talanta*, 2007. 71(1): p. 230-235.
12. Marinova, G. and V. Batchvarov, Evaluation of the methods for determination of the free radical scavenging activity by DPPH. *Bulgarian Journal of Agricultural Science*, 2011. 17(1): p. 11-24.
13. Okawa, M., et al., DPPH (1, 1-diphenyl-2-picrylhydrazyl) radical scavenging activity of flavonoids obtained from some medicinal plants. *Biological and Pharmaceutical Bulletin*, 2001. 24(10): p. 1202-1205.
14. Leaves, L. and L. Leaves, Antioxidant activity by DPPH radical scavenging method of *ageratum conyzoides*. *American Journal of Ethnomedicine*, 2014. 1(4): p. 244-249.
15. Ahmad, M., F. Saeed, and M. Noor Jahan, Evaluation of insecticidal and antioxidant activity of selected medicinal plants. *Journal of Pharmacognosy and Photochemistry*, 2013. 2: p. 153-158.

How to cite this article: Harron M, Ahmed ZA, Ullah N, Haq F, Junaid M, Zeb A, Kiran M, Mehmood S, Kamalan F, Hamind A. (2022). Determination of Antioxidant Activity of *Acacia Nilotica* Linn from different Regions of Baluchistan (Pakistan). *Journal of Chemistry and Environment*. 1(1).p.1-4.
<https://doi.org/10.56946/jce.v1i01.40>



ARTICLE

Synthesis, characterization and antibacterial activity of ethylene di-amine and 2-hydroxybenzadehyde Schiff base and its metal complexes

Muhammad Junaid^{*1}, Jianhua Yan¹, Zhongquan Qi¹, Muhammad Haroon²¹ Medical College, Guangxi University, Nanning 530004, Guangxi, PR China²Department of Chemistry, University of Turbat, Balochistan, Pakistan

Correspondence:

JunaidSunny42@gmail.com**Abstract**

A number of modern techniques have been developed for the synthesis of Schiff bases. We reported the synthesis of ethylene di-amine and 2-hydroxybenzadehyde Schiff base (SB) via the condensation method. To remove phenolic hydrogen to form Schiff base it was reacted with sodium hydroxide and then treated with M(II) chloride (M=Fe, Cu, Zn, Ni and Sn) to fabricate their respective metal complexes. The synthesis of SB metal complexes and detailed functional group characterization were validated via Fourier transform infrared (FT-IR) spectroscopy. In the final SB, FT-IR results revealed a vibrational peak at 1614 cm⁻¹, which was credited to the –C=N part. The absence of a vibration band for –OH vibration on 1613 cm⁻¹ and the presence of a novel band in the 659 to 586 cm⁻¹ range were due to the metal-oxygen bond, confirming the synthesis of metal complexes. The Schiff base showed high antibacterial activity against *E. coli*, *Pseudomonas aeruginosa*, *Salmonella typhi*, *S.aureus* and *Bacillus* whereas *Streptococcus* was found resistant. Cu, Fe and Sn coordination improved Schiff base activity while Ni coordination did not affect the activity. Similarly, Fe and Sn complex had no effect on *E. coli*. In comparison with standard Ciprofloxacin, the activities of respective metal complexes were low.

Keywords: Ethylene di-amine and 2-hydroxybenzadehyde Schiff base; metal complex of Schiff base; FT-IR; antibacterial activity; standard ciprofloxacin.

1. Introduction

In 1864, a German chemist named Hugo Schiff developed Schiff base (SB) by condensing primary amines and aldehyde [1]. The following compound, R₁R₂C=NR₃, is known as an SB since R₁ is an aryl group, R₂ is a hydrogen atom, and R₃ is an aryl or alkyl group, which is also known as a Schiff base. SBs with aryl substituents are the most stable and easy to synthesize, whereas those with alkyl substituent's are more unstable [2]. SBs and their metal complexes have been used since the mid-nineteenth century. Jorgensen and Warner, the two

physicists, addressed the role of SBs and their metal complexes in coordination chemistry [3]. From salicyl aldehyde SBs and their substituted analogues, Pfeiffer and his colleagues built a chain of complexes [4]. The development of SBs complexes, their chelation properties, and stereochemistry are all studied [5]. These are generally bidentate, tridentate, tetradentate or polydentate ligands and form stable complexes with transition metals by forming five or six member ring at the condensation site[6].

1.1 SB metal complexes and their properties

SB based complexes have earned a vital position in coordination chemistry. In this connection, S and N have

been the key elements in the coordination chemistry related biomolecules [7]. SB metal complexes have some intriguing properties of chelation [8, 9] oxygen affinity [10] and hence can be used as a catalyst and in the processing of dyes [11].

1.2 SBs and their metal complexes' biological significance

Malaria is a parasitic disease caused by the Plasmodium genus that kills one million people per year [12]. More than 500 million people are affected according to WHO data, with 90 percent of those affected being children from Sub-Saharan Africa. For controlling malaria, SB based molecules have been effectively applied, especially their Ruthenium complexes from aryl and ferrocyl groups [13]. The development of drug resistance against available antibiotic drugs has been a growing concern for the researcher. This has also led to a significant rise in the mortality rate [14]. SBs made from 2-hydroxy-1-naphthaldehyde and alpha amino-acids possessed exceptional antibacterial action. Apart from these, SBs resulting from salicylaldehyde show strong antibacterial activity against *Mycobacterium tuberculosis* [15].

Some SBs and their complexes like N-salicylidene-2-hydroxyaniline and 3-Fluoro salicylaldehydeOxo vanadium (IV) have also been reported with promising antifungal activity. Similarly, SB derived from chitosanareis effective against *Botrytis cinerea* and *Colletotrichum lagenarium* [16]. SBs produced from isatin and bisisatin. Abacavir (Ziagen), a pro-drug, has been shown to have potent antiviral and anti-HIV properties [17]. Furthermore, SBs of 2-phenylquinazoline-4(3H)-one have been shown to have potent antiviral properties against corona virus, influenza, and HSV types 1 and 2 [18]. In addition to these activities, SBs have been shown to possess anticancer (Cumarin and pyrazole) [19]. 2, 6-dichloroanilino and 4 amino, 5-di methyl and similarly, some SBs possess activities against insects like bollworm (o-vanillin and its metal complexes). SBs derivative from o-vanillin and their metal complexes

have anti-bollworm properties [20].

Hydrazine carboxoamide and metal complexes of di-oxo Manganese have the anti-fertility ability to alter reproductive physiology [21]. Some of the SBs possess anti-allergic, analgesic, radical scavenging and anti-oxidative activities [22]. Attributed to these reports of SBs against various biotic cultures, herein we report the synthesis of ethylene di-amine and 2-hydroxybenzaldehyde Schiff base and its metal complexes and their activities analysis against biological cultures. Fourier transform infrared (FT-IR) spectroscopy was used to classify the prepared SBs, which aided in the interpretation of the experimental findings.

2. Materials and Methods

2.1 Reagents

Sodium Hydroxide (NaOH), 2 hydroxy-Benzaldehyde, Ethylene-diamine, Iron (II) chloride (FeCl_2), Copper (II) chloride (CuCl_2), Tin (II) chloride (SnCl_2), Zinc Chloride (ZnCl_2), Nickel (II) chloride (NiCl_2), Ethanol, Methanol, and Chloroform, Except for metal chloride salt, which was purchased from Sigma Aldrich, these chemicals were extremely pure and purchased from Fluka.

2.2 Methods

The condensation method was used to synthesize SB and its metal complexes while the antibacterial properties of these compounds were investigated using the agar well diffusion process.

2.3 Instruments

By using an electrochemical melting point apparatus, the difference in melting points of precursors and final products was calculated. FT-IR was used to analyze the chemistry and nature of bands and functional groups noted in a range of 4000 to 400cm^{-1} by using KBr-disc methods.

2.3 Synthesis of SB and respective metal complexes

The synthesis of SB and its metal complexes are schematically shown in Figure 1.

2.4 Synthesis of 2,2' (1E, 1E')-(ethane-1,2-diylbis (azan-1-yl-1-ylidene) bis(methan-1-yl-1ylidene)-diphenol

First, ethylene diamine was reacted in 1:2 ratios with 2

hydroxy Benzaldehyde in a two-necked flask linked to a reflex condenser and Deane-Stark apparatus.

The extra solvent was evaporated while the methanol was refluxed for 3-4 hours, and the yields were washed away by ethanol and re-crystallized with chloroform. Figure 2 depicts the chemical reaction for SB synthesis.

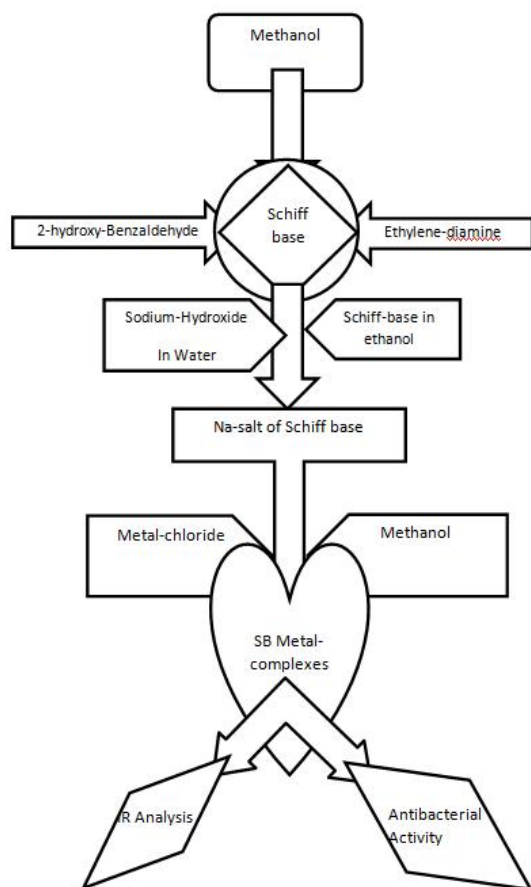


Figure 1: Overall pattern adopted throughout this study

2.5 Synthesis of the Sodium salt of SB

The solutions were combined with intense stirring and continuous heating for 1 hour after sodium hydroxide and SB were dissolved in water and ethanol in 1:2 ratios. The solvents were evaporated at 120°C, leaving a white substance that was cleaned, collected then preserved for coming experimentations. Figure 3 illustrates the chemical reaction of SB sodium salt.

2.6 SB synthesis of copper complex

Copper (II) chloride was added in a 1:2 ratio to a hot methanolic solution of SB-Na salt, then the mixture was

refluxed for 6-7 hours and then chilled overnight while the additional solvent was vaporized under reduced pressure. With the aid of chloroform, the finished product was re-crystallized.

2.7 Synthesis of the iron complex with SB

For the Creation of the SB-iron complex, a similar procedure was followed as that for the copper complex, and the reaction scheme is summarized in figure 5.

2.8 Nickel complex synthesis with SB

The nickel complex of SB was prepared by applying an equimolar solution of Nickel (II) chloride to a hot methanolic solution of SB-Na salt and refluxing it for 6-7 hours. With the aid of chloroform, the finished product was re-crystallized. Figure 6 shows the chemical reaction.

2.9 Synthesis of Tin and Zn complexes with SB

Similar procedures for the preparation of Sn and Zn complexes with SB were followed while their respective reaction schemes are shown in Figures 7 and 8.

2.10 Anti-bacterial activities evaluation

The anti-bacterial activity of SB and respective complexes were used against Gram-positive bacteria such as *Bacillus cereus*, *Staphylococcus aureus*, *Streptococcus*, and Gram-negative bacteria such as *Bacillus subtilis*, *Escherichia coli*, *Pseudomonas aeruginosa* and *Salmonella typh*). Bacterial cultures were inoculated on media, and SB and their metal complexes solutions were poured into these cultures under aerobic condition and incubated for 24 hours at 37°C. The plates were analyzed for inhibition zones after 24 hours (IZ).

3. Results and discussion

The SB was synthesized by condensing ethylene-di-amine with 2-hydroxy-benzaldehyde (salicyl-aldehyde) in 1:2 ratios, and then react it with various metal salts to make its metal complexes. The empirical and structural formula of SB and its metal are summarized in Table 1.

3.1 SB and its metal complexes physical parameters

The Schiff base has a melting point of 113 to 115°C, while its metal complexes have a melting point of 262-293°C. Table no 2 lists the physical characteristics of SBs

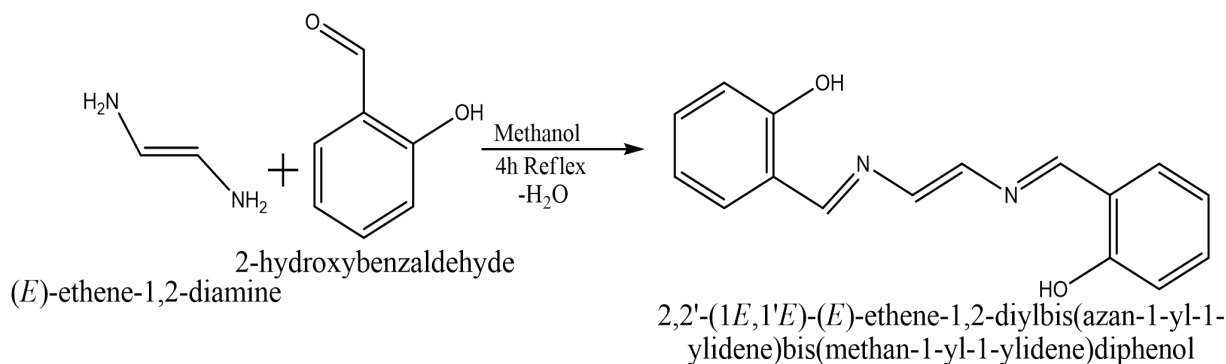


Figure 2: Chemical reaction for the synthesis of 2,2'-(1E, 1E')-(ethane-1,2-diylbis (azan-1-yl-1-yidene)bis(methan-1-yl-1-ylidene)-diphenolpreparation

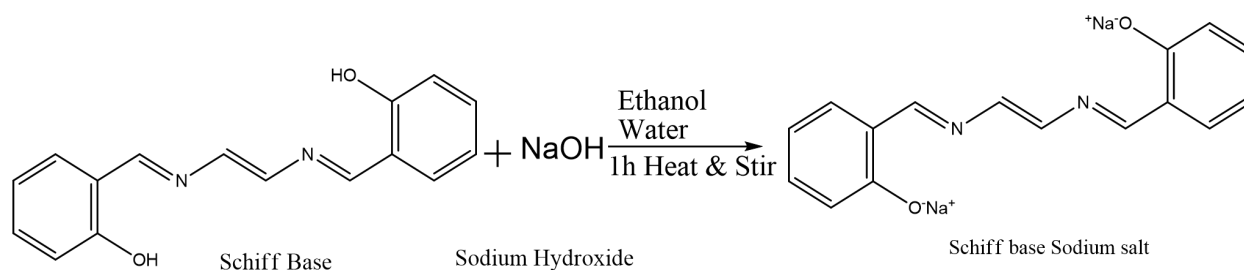


Figure 3: Schiff base reaction with sodium salt

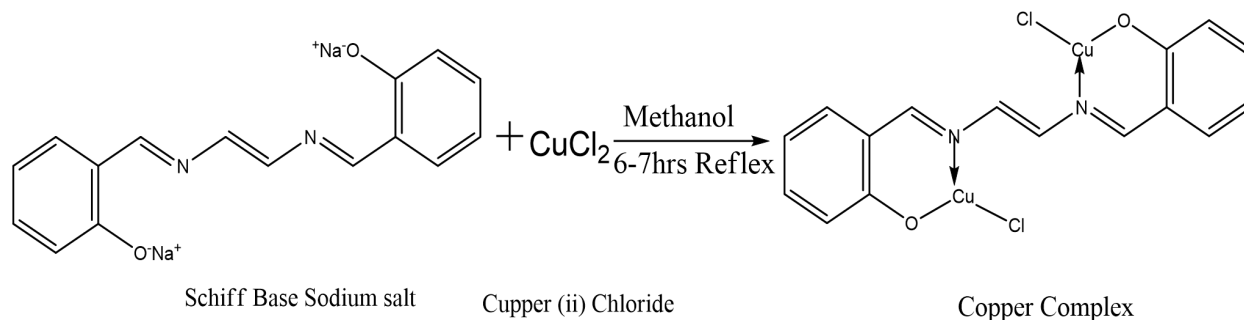


Figure 4: Schiff base Na-salt with copper chloride reaction

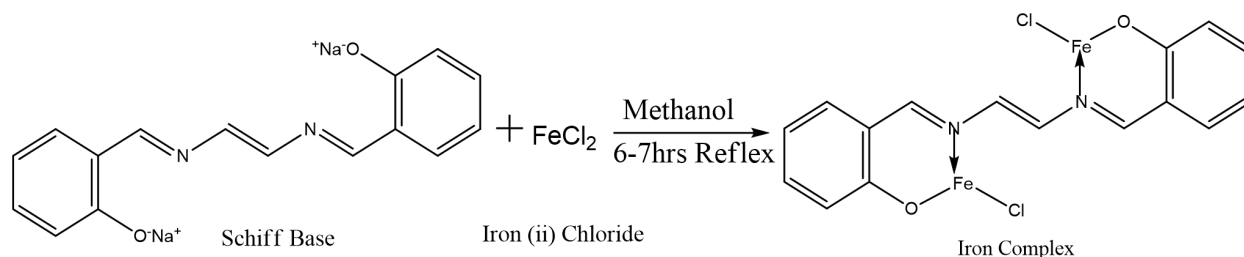
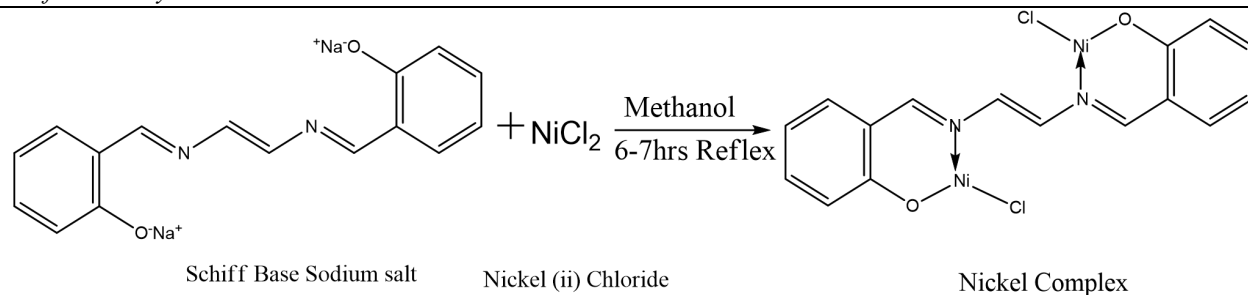
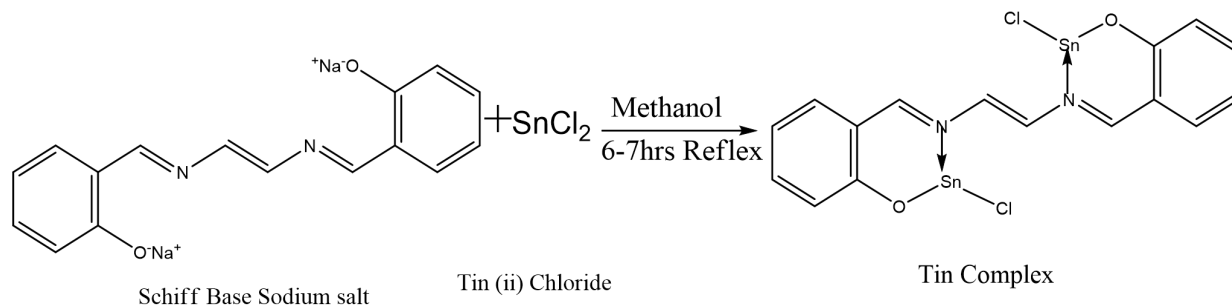
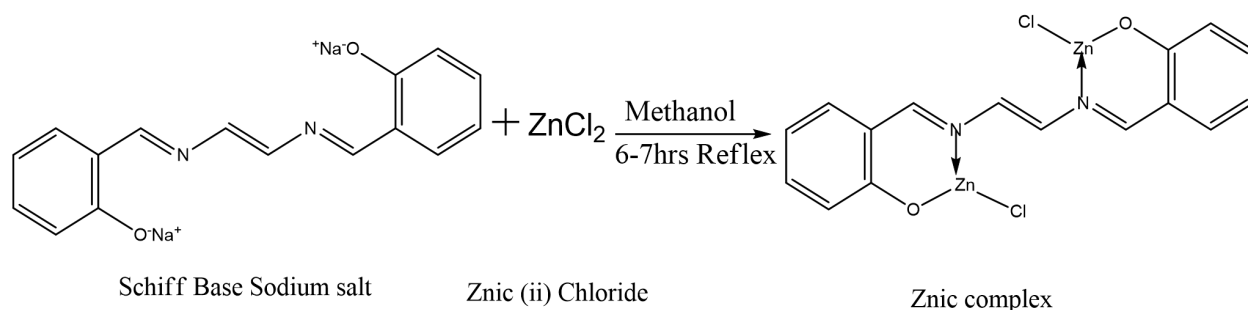


Figure 5: Schiff base with Iron chloride reaction

**Figure 6:** Schiff base Na-salt with Nickel chloride reaction**Figure 7:** Schiff base Na-salt with Tin chloride reaction**Figure 8:** Schiff base Na-salt with Zn chloride reaction

and their complexes, such as color, melting point, molecular weight, and physical state. FT-IR in the range of 4000-400 cm^{-1} was used to perform spectroscopic analysis of SB and metal complexes, yielding valuable information about the chemistry and functional groups of different SBs and their corresponding complexes. Table 3 shows some of the most significant FT-IR bands of the synthesized SBs and metal complexes.

3.2 FT-IR characterization of SBs and their respective metal complexes

FT-IR research revealed a new vibration peak at 1614 cm^{-1} assigned to $-\text{C}=\text{N}-$, created by the reaction of ethylene diamine's amine ($-\text{NH}_2$) and carbonyl-group ($-\text{C}=\text{O}$) of 2-hydroxyl-benzaldehyde. The hydroxyl group was attributed to a strong band in the FT-IR spectra of SB in the range of 3578-

3450 cm^{-1} ($-\text{OH}$). The absorption bands at 3086, 1588 and 1436 cm^{-1} were attributed to the carbon-hydrogen and aromatic carbon-carbon ($\text{C}=\text{C}$) double bonds correspondingly, while the absorption band at 1249 cm^{-1} was attributed to a carbonyl group. The existence, absence, and shifting of certain bands in FT-IR analysis determined the active preparation of SBs and their metal complexes. The absence of a vibration band for $-\text{OH}$ vibration at 1614 cm^{-1} and the occurrence of a new band in the series of 659-586 cm^{-1} were due to the formation of metal complexes, confirming their synthesis [23]. Further groups at 536-516 cm^{-1} and 439-406 cm^{-1} are attributable to metal-chloride band, and imine- nitrogen similar by metal ion ($\text{N} \rightarrow \text{M}$) as well confirmed the successful synthesis of metal complexes [24]. The shifting of the band for the imine group ($-\text{C}=\text{N}-$) to a lower wave number due to the shifting of electron density from

Nitrogen to metals ions in the FT-IR spectra of metal complexes is a clear confirmation of metal nonmetal coherence and production of metal complexes.

3.3 Anti-bacterial action

The synthesized compounds were dissolved in DMSO with a 1:10 ratio to test the biological activity of SB and its metal complexes. After 24 hours of incubation at 37°C, the diameter of IZ is visually determined. The PC was Ciprofloxacin, and the NC was DMSO.

3.4 Antibacterial activity of synthesized compounds against *Escherichia coli*, *streptococcus* and *Bacillus cereus*

By using the good diffusion process, the SB and its metal complexes were added to the cultures above. The synthesized complexes were effective against *E. coli* and *Bacillus cereus*, but had no effect on *Streptococcus* growth, which was unaffected by any metal complexes except SB, which has negligible activity. The IZ measures are tabulated in table 4.

Table 1: Titles, empirical and structural formulation of SBs and respective metal complexes

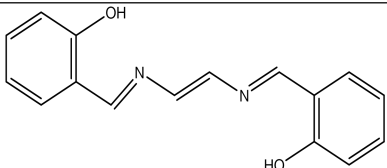
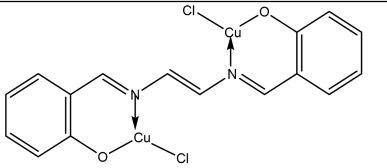
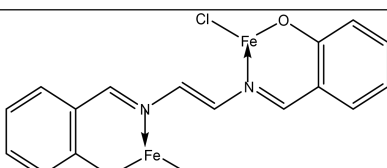
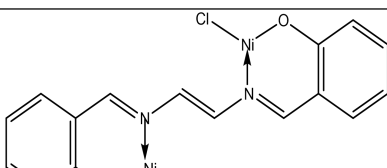
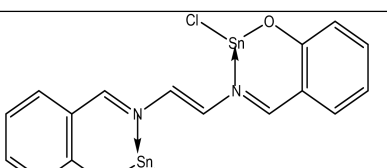
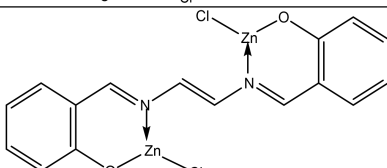
Serial	Titles	Empirical formulation	Structural formulation
1	2, 2'- (1E,1E)- (ethane- 1,2-diylbis(azan-1yl-1-ylidene)bis-(methan-1yl-1ylidene)-diphenol	$C_{16}H_{14}N_2O_2$	
2	(2- (E-(2- (E- 2-hydroxy benzalieneamine)ethylimino)methyl) phenoxy)di-copper (II) di-chloride	$C_{16}H_{12}C_{12}Cu_2N_2O_2$	
3	(2-(E-(2-(E-2-hydroxybenzalieneamine)-ethylimino)methyl)phenoxy)di-iron (II) di-chloride	$C_{16}H_{12}C_{12}Fe_2N_2O_2$	
4	(2-(E-(2-(E-2-hydroxybenzalieneamine)-ethylimino)methyl) phenoxy)di-nickel (II) dichloride	$C_{16}H_{12}C_{12}Ni_2N_2O_2$	
5	(2-(E-(2- (E-2-hydroxybenzalieneamine)-ethylimino)methyl)phenoxy)di-tin (II) dichloride	$C_{16}H_{12}C_{12}Sn_2N_2O_2$	
6	(2-(E- (2-(E-2-hydroxybenzalieneamine)-ethylimino)methyl)phenox) di-zinc (II) dichloride	$C_{16}H_{12}C_{12}Zn_2N_2O_2$	

Table 2: SBs and their metal complexes physical parameters

Serial	Molecular-Formulas	Physical-state	Color	Molecular weight(g/mol)	Melting point(°C)	Yield%
1	C ₁₆ H ₁₄ N ₂ O ₂	Solid	Yellowish	227.28	114-116	88
2	C ₁₆ H ₁₂ C ₁₂ Cu ₂ N ₂ O ₂	Solid	Light blue	462.26	234-236	77
3	C ₁₆ H ₁₂ C ₁₂ Fe ₂ N ₂ O ₂	Solid	Brownish	446.83	292-294	72
4	C ₁₆ H ₁₂ C ₁₂ Ni ₂ N ₂ O ₂	Solid	Green	452.58	268-270	76
5	C ₁₆ H ₁₂ C ₁₂ Sn ₂ N ₂ O ₂	Solid	White	573.56	207-209	68
6	C ₁₆ H ₁₂ C ₁₂ Zn ₂ N ₂ O ₂	Solid	White	466.02	228-230	77

Table 3: FT-IR statistics of SBs and their metal complexes

S.No	Complexes	-O- H	=C -H Aro	-C= N	-C =C Aro	=C -O	M -O	M- N	N→ M
1	SB	3579- 3451	3086	1614	1589 1437	1249			
2	Cu(II)	-	3095	1598	1539 1406	1227	586	516	406
3	Fe(II)	-	3109	1586	1545 1391	1231	616	551	439
4	Ni(II)	-	3131	1571	1569 1376	1211	659	511	426
5	Sn(II)	-	3111	1585	1581 1372	1222	650	536	411
6	Zn(II)		3127	1579	1576 1381	1216	631	523	416

Table 4: IZ of synthesized complexes against *E. coli*, *streptococcus* and *bacillus cereus*

Esherichia Coli				
Serial	Complexes	Dilution 1:10	Ciprofloxacin(Positive control)	DMSO(Negative control)
1	SB	6mm	19.6mm	0 mm
2	Cu- complex	4.4mm		
3	Fe-Complex	Resistant		
4	Ni-complex	3.7mm		
5	Sn-complex	Resistant		
6	Zn-complex	4.2mm		
Streptococcus				
1	SB	0.5mm	14mm	0mm
2	Cu-complex	Resistant		
3	Fe-complex	Resistant		
4	Ni-complex	Resistant		
5	Sn-complex	Resistant		
6	Zn-complex	Resistant		
Bacillus Cereus				
1	SB	5.1mm	15.4mm	0mm
2	Cu-complex	2.7mm		
3	Fe-complex	6.7mm		
4	Ni-complex	4.1mm		
5	Sn-complex	3.7mm		
6	Zn-complex	5.2mm		

Table 5: IZ of SBs and its metal complexes against *Staphylococcus Aureus*, *pseudomonas aeuroginosa* and *salmonella typhi*

Staphylo-coccus aureus				
Serial	Complexes	Dilution 1:10	Ciprofloxacin (Positive control)	DMSO (Negative control)
1	SB	3.1mm	15.6mm	0mm
2	Cu-complex	6.3mm		
3	Fe-complex	3mm		
4	Ni-complex	2.3mm		
5	Sn-complex	2.6mm		
6	Zn-complex	4.3mm		
Pseudomonas aeuroginosa				
1	SB	3.2mm	16.3mm	0mm
2	Cu-complex	3.1mm		
3	Fe-complex	7.3mm		
4	Ni-complex	2.3mm		
5	Sn-complex	4mm		
6	Zn-complex	3mm		
Salmonella typhi				
1	SB	3.7mm	12.4mm	0mm
2	Cu-complex	4.5mm		
3	Fe-complex	7.1mm		
4	Ni-complex	3.2mm		
5	Sn-complex	3.4mm		
6	Zn-complex	2.7mm		

The copper complex has high activity against *staphylococcus aureus*, followed by zinc complex, and Ni complex has low activity, while the iron complex has high activity against *Pseudomonas aeruginosa* and *salmonella typhi*, as shown in Table 5.

The Agar well diffusion method was used to design an in-vitro antibacterial study of SBs and their metal complexes for some specific bacteria [25].

The impact of the synthesized SBs and their metal complexes against the growth of *streptococcus* was negligible; however marginal activity shown by some SBs was greatly dependent on the central metal atoms upon coordination with SB against *Bacillus Anthracis*. After reacting iron with SB, the activity of the iron complex increased, while the zinc complex has the same activity as pristine SB. The cell wall surrounded by a lipid membrane favored the route of lipid-soluble constituents which is a vital aspect of controlling anti-microbial action. The IZ showed that the copper complex has the highest activity against *Staphylococcus aureus*, followed by the Zinc complex, and Ni complex has the lowest activity among the synthesized compounds. The iron complex possesses high activity as related to other synthesized compounds upon exposure to *Pseudomonas aeruginosa*. The activity of SB was enhanced by coordinating Fe and Sn metals while it remained unaffected by the addition of other metal ions.

SBs and their metal complexes inhibited the growth of *Salmonella typhi* as iron complex has high activity with IZ of 7mm followed by copper complex with IZ 4.3 mm while zinc complex with 2.6 mm IZ has the least activity. The coordination of SB with transition metal complexes is the main reason for the increased activity [26]. The different variations in the activity of complexes may be due to the impermeability of microbe's cells or can be the difference in ribosomes in microbial cells [27].

4. CONCLUSION

This study focused on the synthesis of SBs and their metal complexes which were in turn applied for the treatment of various pathogenic bacteria as tested by standard biotic cultures and their results were compared with standard

antibiotics (Ciprofloxacin). With the exception of *streptococcus*, which showed resistance, the SBs and their metal complexes exhibited strong anti-bacterial activity against selected bacteria. Metal complexes synthesized with SBs may be a feasible alternative to currently available antibiotics.

Authors Contribution

M.J and M.H supervised the research work and has the main idea and wrote the manuscript. ZY and ZQ revised the manuscript and provided suggestions.

Conflicts of Interest

The authors declare no conflict of interest. All the authors approved the submission of the manuscript.

Acknowledgment

I owe a great debt of gratitude to Professor Zhong-quan Qi, Dean of Guangxi University's Medical College. Definitely working with him is both a privilege and a pleasure for me.

Data Availability statement

The data presented in this study are available on request from the corresponding author.

REFERENCES

1. Schiff, H. (1864). Mittheilungen aus dem Universitätslaboratorium in Pisa: eine neue Reihe organischer Basen. *Justus Liebigs Annalen der Chemie*, 131(1), 118-119.
2. Hine, J. and Yeh, C.Y., 1967. Equilibrium in formation and conformational isomerization of imines derived from isobutyraldehyde and saturated aliphatic primary amines. *Journal of the American Chemical Society*, 89(11), pp.2669-2676.
3. Pfeiffer, P., Hesse, T., Pfitzner, H., Scholl, W. and Thielert, H., 1937. Innere Komplexsalze der Aldimin- und Azoreihe. *Journal für Praktische Chemie*, 149(8-10), pp.217-296.
4. Calligaris, M., Nardin, G.T. and Randaccio, L., 1972. Structural aspects of metal complexes with some tetradentate Schiff bases. *Coordination Chemistry Reviews*, 7(4), pp.385-403. M. Hariharan, M. and Urbach,

- F.L., 1969. Stereochemistry of tetradentate Schiff base complexes of cobalt (II). *Inorganic Chemistry*, 8(3), pp.556-559.
5. Hariharan, M. and Urbach, F.L., 1969. Stereochemistry of tetradentate Schiff base complexes of cobalt (II). *Inorganic Chemistry*, 8(3), pp.556-559.
6. Cimerman, Z., Miljanić, S. and Galić, N., 2000. Schiff bases derived from aminopyridines as spectrofluorimetric analytical reagents. *Croatica Chemica Acta*, 73(1), pp.81-95.
7. Singh, K., Barwa, M.S. and Tyagi, P., 2007. Synthesis and characterization of cobalt (II), nickel (II), copper (II) and zinc (II) complexes with Schiff base derived from 4-amino-3-mercapto-6-methyl-5-oxo-1, 2, 4-triazine. *European journal of medicinal chemistry*, 42(3), pp.394-402. P.G. Cozzi,
8. Costamagna, J.U.A.N., Vargas, J.U.A.N., Latorre, R., Alvarado, A. and Mena, G., 1992. Coordination compounds of copper, nickel and iron with Schiff bases derived from hydroxynaphthaldehydes and salicylaldehydes. *Coordination Chemistry Reviews*, 119, pp.67-88.
9. Calderon, J., Navarro, M.E., Jimenez-Capdeville, M.E., Santos-Diaz, M.A., Golden, A., Rodriguez-Leyva, I., Borja-Aburto, V. and Diaz-Barriga, F., 2001. Exposure to arsenic and lead and neuropsychological development in Mexican children. *Environmental Research*, 85(2), pp.69-76
10. Park, J.S., Chew, B.P. and Wong, T.S., 1998. Dietary lutein from marigold extract inhibits mammary tumor development in BALB/c mice. *The Journal of nutrition*, 128(10), pp.1650-1656.
11. Kaul, T.N., Middleton, E. and Ogra, P.L., 1985. Antiviral effect of flavonoids on human viruses. *Journal of medical virology*, 15(1), pp.71-79.
12. World Health Organization. (2018). World malaria report 2018. World Health Organization
13. Adams, M., Li, Y., Khot, H., De Kock, C., Smith, P.J., Land, K., Chibale, K. and Smith, G.S., 2013. The synthesis and antiparasitic activity of aryl- and ferrocenyl-derived thiosemicarbazone ruthenium (II)-arene complexes. *Dalton Transactions*, 42(13), pp.4677-4685.
14. Theuretzbacher, U., 2012. Accelerating resistance, inadequate antibacterial drug pipelines and international responses. *International journal of antimicrobial agents*, 39(4), pp.295-299.
15. Sakiyan I, ozdemir R. ogutcu, H.: *Synth. React. Inorg. Met. Org. Chem.* 44, 417 (2014).
16. Rice, L.B., 2006. Unmet medical needs in antibacterial therapy. *Biochemical pharmacology*, 71(7), pp.991-995.
17. Ali, I., Haque, A., Saleem, K. and Hsieh, M.F., 2013. Curcumin-I Knoevenagel's condensates and their Schiff's bases as anticancer agents: Synthesis, pharmacological and simulation studies. *Bioorganic & medicinal chemistry*, 21(13), pp.3808-3820.
18. Kumar, D. and Rawat, D.S., 2013. Synthesis and antioxidant activity of thymol and carvacrol based Schiff bases. *Bioorganic & medicinal chemistry letters*, 23(3), pp.641-645.
19. Sathiyaraj, S., Sampath, K., Butcher, R.J., Pallepogu, R. and Jayabalakrishnan, C., 2013. Designing, structural elucidation, comparison of DNA binding, cleavage, radical scavenging activity and anticancer activity of copper (I) complex with 5-dimethyl-2-phenyl-4-[(pyridin-2-ylmethylene)-amino]-1, 2-dihydro-pyrazol-3-one Schiff base ligand. *European journal of medicinal chemistry*, 64, pp.81-89.
20. Zhu, L., Chen, N., Li, H., Song, F. and Zhu, X., 2002. Synthesis, characterization and biological activities of Schiff bases of 2-amino-5-mercapto-1, 3, 4-thiadiazole and their Mo (VI) complexes. *Journal of Central China Normal University. Natural sciences edition*, 37(4), pp.499-502.
21. Ferreira, G.C., Neame, P.J. and Dailey, H.A., 1993. Heme biosynthesis in mammalian systems: evidence of a Schiff base linkage between the pyridoxal 5'-phosphate cofactor and a lysine residue in 5-aminolevulinic synthase. *Protein Science*, 2(11), pp.1959-1965.

22. Luo, X.Y., Zhao, J.Z., Lin, Y.J. and Liu, Z.Q., 2002. Antioxidative effect of schiff bases with off-hydroxybenzylidenegroup on free radical induced hemolysis of human red blood cell. *Chemical Research in Chinese Universities*, 18(3), pp.287-289
23. Sigee D, Dean A, Levado E, Tobin SMJ. Fourier-transform infrared spectroscopy of *Pediastrum duplex*: Characterisation of a micro-population isolated from a eutrophic lake. *Eur J Phycol.* 2002;37:19–26
24. Saleh, A. A., Tawfik, A. M., Abu-El-wafa, S. M., & Osman, H. F. (2004). Formation of iron (III) cluster complexes with a new (N2O2) Schiff base. *Journal of Coordination Chemistry*, 57(14), 1191-1204.
25. Qil F., Khan M.S.A., Ahmed I. (2005) Effect of certain bioactive plant extracts on clinical isolates of beta-lactamase producing methicillin resistant *Staphylococcus aureus*. *J. Basic Microbiol.* ;45:106–114.
26. Gulcan M., *et al.* “Synthesis, characterization and antimicrobial activity of a new pyrimidine Schiff base and its Cu(II), Ni(II), Co(II), Pt(II) and Pd(II) complexes”. *Turkey Journal of Chemistry* 36 (2012): 189-200.
27. Nika, K., Anupama, B., Pragathi, J. and Gyanakumari, C. (2010) Synthesis Characterization and Biological Activity of a Schiff Base Derived from 3-Ethoxy Salicylaldehyde and 2-Amino Benzoic acid and its Transition Metal Complexes. *Journal of Scientometric Research*, 2, 513-524.

How to cite this article:

Junaid M, Yan J, Qi Z, Haroon M. (2022). Synthesis, characterization and antibacterial activity of ethylene di-amine and 2-hydroxybenzadehyde Schiff base and its metal complexes. 1(1).p.5-16



REVIEW

Comprehensive Review on Synthesis of Abox Material and its Catalytic Applications

Syeda Mehak Batool¹, Khushbo e Kainat¹, Suqqyana Fazal¹, Fawad Ahmad^{1*}

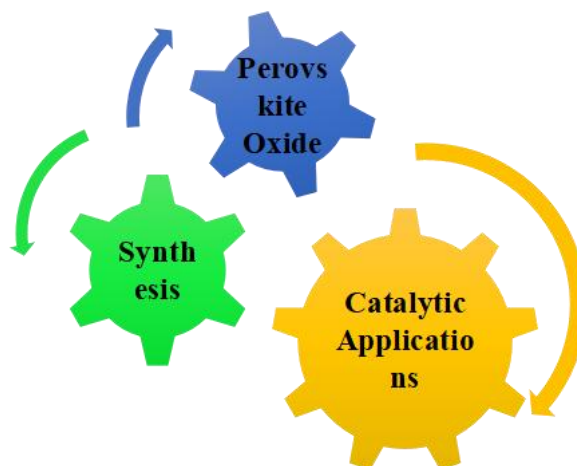
¹Department of Chemistry, University of Wah, Quaid Avenue, Wah Cantt., (47010), Punjab, Pakistan

Corresponding author:
fawad.ahmad@uow.edu.pk

Abstract

Perovskites are materials with crystal structures comparable to perovskite (mineral). The backbone of perovskite is calcium titanium oxide (CaTiO_3). Perovskite oxides with the general formula ABO_x are highly important. In the general formula of perovskite ABX_3 , A & B are cations, where X is an anion that binds with two cations. Perovskites have proven their versatility in catalysis, photovoltaics, solar cells, electrode conducting material, etc. Due to their unique structural properties and applications, they are compatible with elements having metallic approximately 90% of the periodic table. This review discusses the synthesis and catalytic application of perovskite oxides. There are five sections to this review: (a) a brief description of perovskite oxides, (b) the synthesis of perovskite oxides with various properties, (c) general characterization, (d) catalytic applications, and (e) conclusions and future perspectives.

Keywords: perovskite oxides, synthesis, catalysis.



Graphical Abstract

1. Introduction

The term perovskite is used to explain oxides produced from Ca-Ti-O_3 with the structural formula ABO_3 or A_2BO_4 . Oxides of A_2BO_4 , are often known as perovskite-like oxides. They are synthesized by alternating ABO_3 and AO layers. The cations A and B were replaced by a new cation with a

different oxidation state and radius, and the material noted for its structural stability. The oxidation state of the B-site cation and the number of oxygen vacancies may be regulated when a desired external cation is used, providing a practical and workable technique for connecting physicochemical characteristics with the catalytic ability of the material [1].

According to several experts, perovskite oxides have been used to generate a range of oxygenated molecules [2]. Due to their significant thermal stability, the exceptional activity of oxidation and low cost, perovskites have been examined for a range of automobile exhaust purification, fuel cells, N_2O decompositions and Water Gas Shift (WGS) reactions. Perovskite oxide having lanthanide at the A site and transitional metals at the B site is more frequently utilized within heterogeneous catalysis, possibly to use transition metals' catalytic capabilities. Noble metals are recommended as a catalyst owing to their excellent stability in these circumstances. Whereas transition metals have good catalytic activity because of their electronic structure, transitional metals could oxidize in higher temperatures within oxygen presence [3]. Larger ionic radius cations have oxygen atoms and there is 12-fold coordination accommodating sites A and a cation having lower ionic radius with 6-folded coordination accommodating sites B. Perovskite oxides have a structure of the cubical crystal. B is located in the cubic closet packing's octahedral gaps formed by A and O [3].

As stated in "Witness to grace" Professor John began his research to explore perovskite materials 60 years ago and explored perovskite materials for their applications for storage and energy conversion [4]. Most catalysts used are made of mixed metal oxides. Out of mixed metal oxides, a perovskite-type oxide was highlighted. Despite ionic radius requirements, another requirement is electro-neutrality, which means the sum of charges on cations is equal to the charge on anion, which can be achieved only by proper distribution of charge on A, B, and O, respectively. According to Pena and Flerro et al., [5] perovskite oxide materials, such as ABO_3 , have exceptional properties of physical like (BaTiO_3) Ferroelectricity, (SrRuO_3) ferromagnetism, (LaFeO_3) weak ferromagnetism, $(\text{YBa}_2\text{Cu}_3\text{O}_7)$ superconductivity and thermally conductive. They also examined the adsorption features of many perovskite materials by studying their shape to find their active sites, which they then investigated for catalytic activity. Perovskite oxides with different morphologies are shown in Fig (1).

Catalysis is a reaction in which the outcome is influenced by a chemical known as the catalyst, which is not consumed during the reaction. Catalysis can be either homogeneous or heterogeneous. The mixture reaction and the catalyst are in the uni-phase in homogeneous catalysis, whereas the mixture reaction and the catalyst are in separate phases in heterogeneous catalysis. Both types of catalysis have high activity, but heterogeneous catalysis has low selectivity than homogeneous catalysis.

Heterogeneous catalysis requires high reaction temperature than homogeneous catalysis. However, our main aim in this study is to focus on the preparation method of perovskite oxide and explore its catalytic application, which provides the basis for all.

1.1 Perovskite Materials' (Properties of Electronic, Magnetic, and Optical)

The study of oxides of perovskite magnetic properties has attracted a lot of curiosity, among other things. There have already been findings of magneto-optical materials, sensors, catalysts, fuel cells, and other applications. Transition metal perovskite oxides have recently gotten attention because of their significant magnetic properties. Because of the great interaction of electron-electron to the manifold 3D, and their physical strength, these perovskite oxides have remarkable magnetic properties.

Perovskites are used within solar cells, and light detectors and light-emitting diodes are examples of this, for example, optoelectronic applications (LEDs). Because of their outstanding optical features, which are required for both light absorbers and light-generating materials, they are prominent. Higher coefficients of absorption and configurable bandgaps of direct, for example. As a result, in the dye of solid-state comparison sensitized solar cells, the thickness of TiO_2 within perovskite solar cells is relatively lower. It could enhance to some extent, that perovskite solar cells are commercialized and developed.

2. Perovskite Oxides Synthesis with different morphologies

2.1 Perovskite Oxides synthesis in Bulk

Mixed oxides of perovskites are generated by simply annealing a metal oxide mixture at a high temperature, which is a straightforward process. This synthesis is environmentally beneficial because it occurs without the release of any hazardous gases as a result of the reaction. Although it is necessary to homogenize the metal oxide precursors for them to react completely and generate pure perovskite oxides, this is not required. In this case, the mixture could be processed in ethanol with a ball mill or stabilized ZrO_2 balls. When good mechanical attributes are required, this approach generates a sample with a lesser surface area and a greater particle size, which is often used in ceramics [1].

Because catalysis is a surface reaction, it necessitates strong contact between the catalyst and the substrate. And, to put catalysis into practice, perovskite oxides must have a larger surface area and a smaller particle size. As a result, high-surface-area perovskite oxides must be synthesized. Because the precursor and synthesis processes have complex organic that is employed to correlate, burn, and finally, metal oxide particles disperse, replacing metal oxides with soluble metal nitrates is one of the most successful approaches. Citric acid combustion, for example, uses metal nitrates as a precursor and citric acid as a complex organic to metal coordinate ions. Because of its simple operating technique and high catalytic performance, this technique is frequently used to make oxides of perovskite catalysts within catalysis [1].

Undesirable gases like NO_2 and CO_2 are emitted in the process due to nitrates and organic compounds. As a result, synthesis should be done in a fume cupboard or somewhere with good ventilation. It should also be highlighted that because the organic complex contains a carbon source, the creation of carbonates is unavoidable. Carbonates may influence the material's catalytic effectiveness in some reactions; hence their amount should be kept as low as feasible [1].

2.2 Nano-Sized Perovskite Oxides

Following is the procedure for making perovskite oxides from polyvinyl pyrrolidone (PVP):

A solution of water containing metal stoichiometric nitrates and Poly-Vinyl-Pyrrolidone was heated to 100 degrees Celsius. Perovskite-type oxide precursor produced after 1 hour of drying at 150°C . The polymerized precursors were burned in the presence of air for 6 hours at 300–600 degrees Celsius, yielding perovskite-type oxides [6].

Also in the PVP technique, a reaction of solid-state and a procedure of citrate was used to make $\text{La}_{0.6}\text{Sr}_{0.4}\text{Mn}_{0.6}\text{Fe}_{0.4}\text{O}_3$. La_2O_3 , MnO_2 , SrCO_3 , and Fe_2O_3 were used as starting particles for the solid-state reaction. The powders were mixed well in an agate mortar, and the mixture was sintered in the air for 10 hours at $400\text{--}1300^\circ\text{C}$. Nitrates of metal and citric-acid-monohydrate ($\text{C}_6\text{H}_8\text{O}_7\cdot\text{H}_2\text{O}$; 2 times total cation moles; double the times of total moles of cations) dissolve in water and agitate at about 100°C till gel formation. A precursor was created after gel drying for 1 hour at about 150°C . The precursor was calcined within the atmosphere for 10 hours about 4–8 hundred degrees Celsius. Temperature raised with a continuous rate of about $20^\circ\text{C min}^{-1}$ for calcination [6].

According to SEM analysis, the oxide manufactured with PVP was 20nm to 30nm in size, whereas those made with the process of citrate and the reaction of solid state were 50 nm and 10 nm in size. $\text{La}_{0.6}\text{Sr}_{0.4}\text{Mn}_{0.6}\text{Fe}_{0.4}\text{O}_3$ obtained from PVP had the lowest sized particle and the biggest surface-area specific of the several synthetic techniques, probably due to calcination could be done for low temperatures of about 600°C [6]. The typical preparation technique for perovskite-type oxides using polyol mediates synthesis is presented in scheme 1 [7].

2.3 Porous Perovskite Oxides

2.3.1. Synthesis in solid state

To manufacture perovskite oxides, a reaction of solid state is typically utilized, characterized by a simpler process, higher calcination temperature, mass-production capabilities, and lesser manufacturing cost, among other things [8]. In a typical synthesis, the solid raw components are thoroughly mixed before being calcined at a higher temperature for a long enough period to generate a suitable phase of perovskite oxide.

A calcination temperature of over 900°C is required to produce phase-pure perovskite oxides due to the significance of

overcoming the diffusion barrier for perovskite phase formation during the synthesis [8-10]. Particularly for perovskite oxides, including several components and alkaline earth elements, higher calcination temperatures and a lengthy calcination duration of several hours are necessary to produce a high-purity perovskite phase [11-13]. On the other hand, such high synthesis temperatures usually lead to poor sintering and nearly pore-free products. A lower phase formation temperature is required efficiently synthesize porous oxides of perovskite utilizing the reaction of solid-state methodology, and achieving good perovskite phase purity at a lower annealing temperature is a severe difficulty [14].

Solid-state synthesis with the help of high-energy ball milling (HEBM) [13,15-20] and Solid-state reaction injected into the molten salt [21-24] are two recently founded solid-state reaction processes that have been updated. In the solid-state synthesis of HEBM-assisted, known as mechano-chemical manufacture, mechanical energy is frequently used to aid the reaction of solid-state. In process of preparation, mechanical force is used to break down the reactants and products into small particles and appropriately mix them. As a result, the phase formation diffusion barrier can be reduced effectively, the preparation temperature may be properly reduced, and the product surface specific area can successfully be increased. Various perovskite oxides have been successfully generated using this process to utilize as electrodes in metal atmosphere batteries and Solid Oxide Fuel Cell SOFCs [25-28]. The ball-milling period, ball mass ratio to powder solid and other operational factors influence the product surface specific area, pores structure, and size of crystalline [26-29]. High Energy Ball Milling HEBM-assisted solid-state synthesis still has poor porosity which is a severe disadvantage [14]. When a sample is placed under stress calcination, the pores structure is prone to collapse. Kaliaguine's team changed the HEBM-assisted solid-state synthesis technique by adding various alkali additives to the $4-105\text{ m}^2\text{ g}^{-1}$ ball-milling process to make porous perovskites, which maximized porosity [30,31]. As a result, they all have outstanding catalytic characteristics in a variety of procedures. To our knowledge, no study on

applying this fascinating technique to the fabrication of perovskite electro-catalysts in ORR or OER processes has been published, emphasizing that much more research is needed in this domain. If this novel method was used to create porous perovskites as ORR/OER electro-catalysts, the impurity from the alkali additive could potentially be introduced into the perovskite phase and the potential change in activity could be attributed to such impurity doping because most elements can be doped into the perovskite lattice [14]. Inadequate porosity is produced by the reformative HEBM-assisted synthesis method described above because insufficient amounts of alkali are supplied. The molten salt synthesis method, which uses a large amount of alkali metal salts to generate crystallized, chemically purified single-phase powder has gotten more attention in recent history due to its simple, versatile, cost-effective approach [21-24, 32-34]. The molten salt additions serve as a soft template as well as a heat source [33-35]. In synthesis low melting point salts are combined to reactants in non-solvent freshly ground form crystals and the combined precursors are then heated to temperature over the salts melting point. Because reactants have a defined solubility in liquid salts, the molten salt methodology is used [18,19,31]. As catalysts for the formation of higher alcohols, porous $\text{LaCo}_{1-x}\text{Cu}_x\text{O}_{3-\delta}$ (LCCu) perovskite oxides were produced in 2007. In this synthesis process, Elements of Group I was utilized as additive alkalis, successfully controlling the growth grain of phases of perovskite while acting as a soft template. The LCCu perovskite displayed a large specific surface area and many holes when the alkali (0.08wt% of alkali ions) was washed away in water, indicating increased catalysis activity for high alcohol preparation by syngas. Furthermore, the surface-specific areas of the resultant compound changed with a radius of cationic metals of alkali utilized and the increase is in order of $\text{Li} < \text{Na} (\approx \text{Cs}) < \text{K} < \text{Rb}$ respectively. During the ball milling procedure porous $\text{La Fe}_{0.8}\text{Cu}_{0.2}\text{O}_3$ and $\text{LaCo}_{1-x}\text{Fe}_x\text{O}_3$ were also used as perovskite oxides and was well synthesized in the presence of numerous additives and displayed a higher surface specific area for synthesis which uses convection, diffusion processes, permits for speedy transfer of mass transit in the

phase of liquid and allows reactant to mixed on an atom scale [21,36-37]. The salt of a resulting sample could be eliminated by washing it with water that is de-ionized after pyrolysis resulting in porous products.

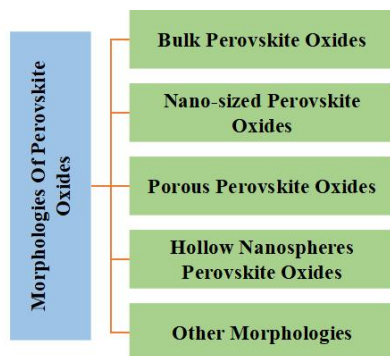


Figure. 1 Perovskite Oxide different structures

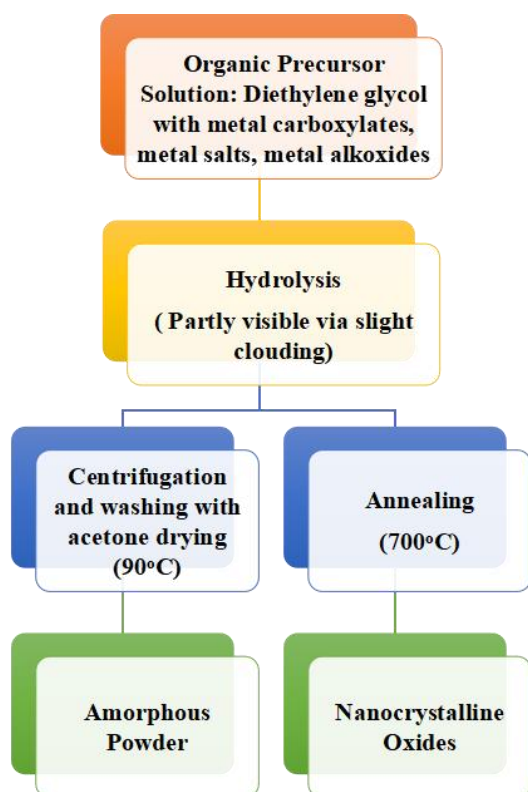
The ratios weight of metal salts of alkali (e.g., ZnCl_2 , NaCl , KOH , and NaNO_3) to solid precursors have ranged from 1:1-15:1 in prior investigations [32-40]. According to some experts, a high ratio can aid in mesopores formation [35-40]. As a result, particle size, morphology, porosity, and other parameters may be effectively modified with molten salt. For decades, molten salt synthesis has been effectively utilized to generate perovskite oxides, particularly ferroelectric oxides such as BaTiO_3 and SrTiO_3 [32]. Furthermore, molten salt synthesis was used to create single-crystalline BaZrO_3 particles, allowing for rational control of the structure of perovskite oxides [41]. Aside from these, other perovskite oxides can be made using this process [21, 32-34, 37-39].

Li and his colleagues reported a molten salt solid-state precursor methodology for the fabrication of LaCoO_3 perovskite. To conduct the precursor reaction, they mixed solid-state $\text{Co(NO}_3)_3 \cdot 6\text{H}_2\text{O}$ and $\text{La(NO}_3)_3 \cdot n\text{H}_2\text{O}$ with a preset amount of KOH after several hours of calcination nanoparticles in porous form having diameters of 15nm to 40 nm were formed [39]. By significantly altering the calcination period various porous nanostructured LaMnO_3 including spheres and cubes were well created employing a co-assisted molten salt method involving NaNO_3 and KNO_3 [24]. LaMnO_3 took on a porous spherical shape after calcination at 550°C for 4 hours with the pore's mean size of 34.7 nm. SEM

and TEM images are shown in Fig 2-(b,c,d,e). After increasing the time of reaction up to 6 hours, reveal single-crystal porous cubic LaMnO_3 particles. The production mechanisms of several LaMnO_3 nanostructures are prepared as shown in Fig (2-f). XRD pattern of LaMnO_3 is shown in Fig (2-g). It was discovered that shape significantly impacted activity in the catalytic elimination of toluene.

Song et al. recently synthesized $\text{La}_{0.6}\text{Sr}_{0.4}\text{Co}_{0.2}\text{Fe}_{0.8}\text{O}_{2.9}$ porous using a standard molten salt process in which the mixed oxide precursors were combined with a 2:1 weight ratio eutectic salt mixture of NaCl and KCl [21]. Fig (2-h) shows scanning electron microscopy (SEM) pictures of porous nanoparticles interconnected with a macroporous cores diameter of 200 nm. The porous arrangement made a huge interfacial surface, exposing more active sites and even perhaps strengthening OER catalytic activity. When compared to the benchmark IrO_2 precious metal-based catalyst, the $\text{La}_{0.6}\text{Sr}_{0.4}\text{Co}_{0.2}\text{Fe}_{0.8}\text{O}_{2.9}$ porous catalyst had a lower over-potential of 345mV and a density of current of 10mA cm^{-2} (360mV). Molten salt techniques are also used to make Sr, Mg doping in perovskite form LaAlO_3 porous for electrolyte SOFC and $\text{La}_{0.8}\text{Sr}_{0.2}\text{MnO}_3$ perovskite powders for the SOFC cathode [22].

However, according to what has been observed, excellent molten salt synthesis perovskite oxides still make up just a tiny proportion of the whole perovskite oxide group. This could be owing to some variables, including the relatively high temperatures at which phases occur (usually $> 1000^\circ\text{C}$) or the likelihood of molten salt reacting and reactants. Even though most modified solid-state approaches do not involve pore size management, they have been shown to improve the surface area and reduce particle size. Several modified solid-state synthesis methodologies have been utilized to target pure phase formation, controllable particle sizes, and associated specific areas. However, due to the unforeseen and random pore-forming processes, controlling the porosity and/or pore size is difficult. More research is needed to better understand phase formation and pore growth in molten salt synthesis, which would greatly improve the design of porous perovskites for applications such as electro-catalysis [14].



Scheme 1. Synthetic technique for perovskite-type oxides using polyol mediates the synthesis.

2.3.2. Wet Chemical Process

Wet chemical techniques for developing porous metal oxides have been widely used and have made significant progress in recent decades [42-55], while multi-metal oxides still need to be studied further. Porous materials have been developed using surfactants and templates. After the template, the surfactant was removed under mild conditions, and with additional calcination procedures, porous solid material can be well generated [14].

Wet chemical synthetic methods such as the process of sol-gel, methodology of complexation, combustion solution technique, route of hydrothermal, synthesis of electro-spinning, and a few others have been developed. Controlled morphology and porous structures, as well as perovskite oxide nanoparticles, are of particular interest [14,21,54-60].

2.4. Hollow Nano-spheres Perovskite Oxides

Nanospheres with hollow interiors are a newer type of nanosphere. Perovskite has a bigger surface area and energy

than mixed perovskite because of its hollow structure, allowing for the doubled face (inner and exterior) interaction with the reactant. Good perovskite oxide performance of catalysis may be achievable as a result. Hollow perovskite is made using a variety of techniques, including One approach for simulating the material using a spherical template, like spheres of carbon [61] or directly synthesizing hollow materials using organic guiding agents and a hydrothermal technique [62,63]. Scheme 2 depicts the synthesis of LCMO nanospheres using template-assisted growth.

The carbon spheres might be made by either exfoliating organic precursors (such as glucose) or replicating hollow perovskite oxides utilizing a silica template, which would be utilized as a template (secondary) to duplicate the hollow oxides of perovskite in the first stage. This image shows the usage of a carbon spheres template with silica as a template secondary for the synthesis of hollow oxides of perovskite [64]. Firstly, sucrose was added to the template of silica, which was subsequently carbonized, to create a carbon-silica composite. The composite of carbon silica etched in the 48% of aqueous HF solution, revealing carbon copy, removal of template of the silica. The pores on the carbon copy were then filled with a pre-prepared solution with the required metal cations. Finally, the mixture was dried and calcined at particular temperatures to achieve the desired result. Zhang et al. [63] suggest a quick procedure. The hydrothermal approach is described in the next paragraphs. The nitrates of metals, citric acid, P123, and urea were initially mixed in ethylene glycol, water, and ethanol. The solution was placed in an autoclave and boiled at about 100°C for 48 hours after which it was completely dissolved. The product solid was centrifuged and dried before being calcined for 8 hours at 600°C in the flow of air to get perovskite oxides. On the other hand, the carbon spheres template technique necessitates manufacturing carbon spheres before the creation of hollow perovskite oxide, making the process more complicated overall. Because of the homogeneous particle size of the silica template, spheres of carbon, eventually, oxides of perovskite having particle that is uniform in size could be

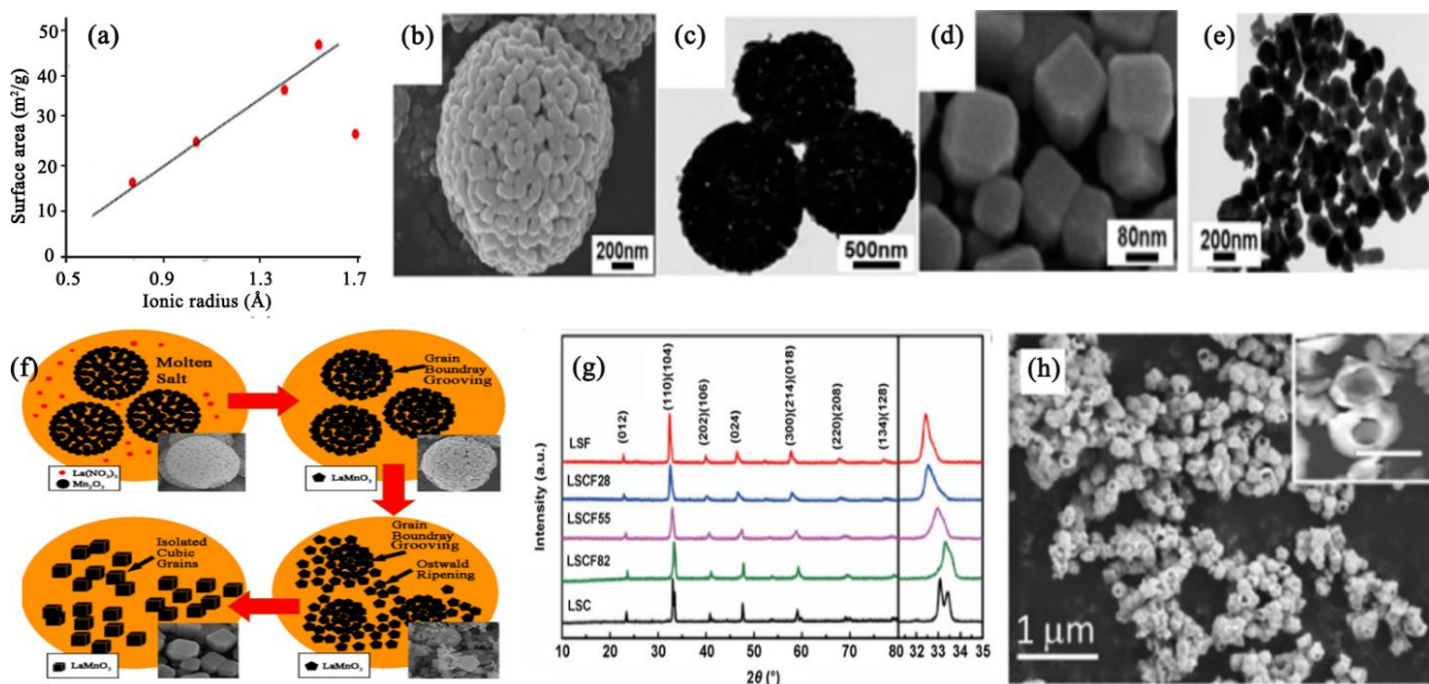
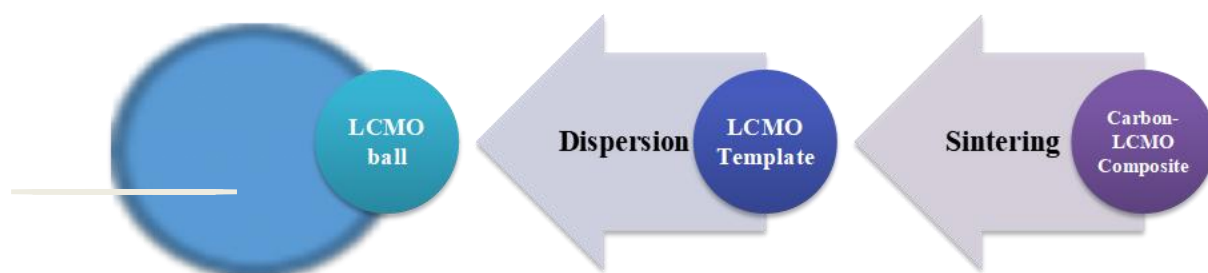


Fig. 2-a) Relation among radius of cationic metal of alkali with a surface area of oxides of perovskite generated. Having the consent of ref. [18] this image has been reproduced. Copyright 2007 Journal of Catalysis b) SEM c) Images showing transmission electron microscopy (TEM) of a porous spherical LaMnO_3 sample. d) Scanning Electron Microscopy Analysis and e) Having TEM, porous cubic images of LaMnO_3 materials were captured. f) suggested the production process of different LaMnO_3 Nanostructures in molten salt media, where the structure of LaMnO_3 was modified from porous-cubic nanoparticles. This image has been reproduced with the permission of ref. [24]. Copyright 2014 ACS applied materials and interfaces g) XRD patterns h) SEM images of the synthesized porous nanostructured perovskite $\text{LaO}_{0.6}\text{SrO}_{0.4}\text{CoO}_{0.2}\text{FeO}_{0.8}\text{O}_{2.9}$. Inset (h) the equivalent enlarged image. Reproduced from ref. [21]. Copyright 2018 Nano Res.



Scheme 2 The creation of LCMO nanospheres using a template-assisted approach is depicted in a series of schematic illustrations [64].

duplicated. Moreover, the particle of perovskite oxides could change from silica to having the required particle size [1].

2.5 Other Morphologies

With the evolution of materials research and the growing need for innovative applications, oxides of perovskite have different techniques, such as nanoporous perovskite oxide, a nanoplate,

nanofibers, nanotubes, flower-like, and cubic, have been created. These various morphologies would allow perovskite oxides to have a wider range of surface characteristics and uses. We went over nanoporous perovskite oxides in great depth.

2.5.1. Nanoporous Perovskite oxides

Hard template, soft template, hydrothermal, colloidal crystal template, and electrospinning procedures are some of the most common ways to make nanoporous perovskite oxides. We only go into detail on the synthesis of soft and hard templates and colloidal crystal templates.

(a) Soft-Template Method

Soft templates have been highlighted [65] in the creation of materials of nano-porous like silica of mesoporous like MCM-41 [66], and SBA-15 [67]. One of the most efficient ways to make mesoporous oxides is to use evaporation-induced self-assembly (EISA). Direct co-condensation methods are typically combined with soft templates. The EISA approach has four steps: (a) Synthesis of a homogenous initial sol including the soft templates and inorganic precursors in the proper stoichiometry; (b) During the dip-coating methodology, solvent evaporation caused inorganic precursors to self-assemble into micelles with a poorly compacted network and a steadily increasing strength over Critical Micelle Concentration CMC. (c) Additional inorganic condensation and film equilibration with its surroundings are responsible for the final mesostructured adjustment. (d) Temperature treatment is produced before consolidation, template removal, and chain crystallization. Even though “EISA” technology was utilized to generate mesoporous oxides of single-metal several times, it was only utilized to make mesoporous perovskite oxides a few times. The cations from the first gel mixed homogeneously on a molecular scale throughout the entire procedure to generate mesoporous oxides of perovskite having pure phases. In as-prepared samples, however, variations within the solubility of components that are non-volatile in the evaporation of solvent procedure frequently result in the separation of phase or secondary phases. Furthermore, because the EISA method

uses a lower temperature for the breakdown of organic surfactants than for the crystallization of perovskite oxides, mesostructures destroy due to a lack of support at calcination of high temperatures, allowing amorphous phases or impurities to emerge. Despite these difficulties, a few papers have been published on the EISA technique for the preparation of mesoporous oxides of perovskite [68]. In 2004 Grosso and company utilized a semi-commercial template of organic for making mesoporous oxide of perovskite films [68] Brezesinski and company [69] effectively generated many Nano porous oxides of perovskite films with honeycomb 3D structures using the “EISA” technique of associated dip coating onto a polar substrate with several amphiphilic block copolymers with high thermal stability. Although the methodology of EISA, when paired with dip coating can make nanoporous perovskite oxides, it is often challenging and limited to small-scale production. A modified EISA method for manufacturing nanoporous perovskite oxides without the need for precipitants or chelating agents was recently devised by certain researchers which eliminates the necessity for dip-coating. These chelating chemicals would result from the further solution that is homogenous and greater dispersion of cation in the process of evaporation, yet they would have an impact on surfactant self-assembly and interactions with ions of metal. As a result, hierarchically nanoporous perovskite oxides such as BaTiO_3 , and SrTiO_3 may be generated using these improved EISA techniques [70,71].

Because of the great ability of hydrolysis of titanium precursors, there is still much research utilizing the self-assembly of soft template technique for generating higher structured mesoporous oxides of perovskite. BaTiO_3 oxide of perovskite having mesostructure inside crystallites was produced directly from solution using the cationic surfactant cetyltrimethylammonium chloride using a simple sol precipitation technique (C16TMAC) [72]. Yan and company developed a higher ordered mesoporous ZnTiO_3 with a greater pore volume, a large surface area, and narrow pore dispersion size utilizing the method of sol-gel in combination with EISA with ethanol and F127 Pluronic being structure guiding reagents [73].

(b) Method of Using a Hard Template

Nanocasting, also known as repeated templating, is a process for manufacturing nanostructured materials with unique features. A method employed in this procedure is to fill metal precursors into porous templates made of mesoporous carbon or mesoporous silica, which are subsequently calcined and etched away using acid or alkaline etching [74].

The template of the hard approach utilized to make nanoporous oxides of perovskite for the past decade includes mesoporous LaNiO_3 utilizing template SBA-15 and $\text{LaFe}_x\text{Co}_{1-x}\text{O}_3$ utilizing KIT-6. There are several distinctions between hard-template procedures for perovskite and single metal oxides due to the usage of multiple precursors metal for oxides of perovskite. Mesoporous silicas (such as SBA-15, MCM-48, and KIT-6) and mesoporous carbons (such as CMK-3, CMK-1) are frequently used as "hard templates," as seen in [75]. After calcination, agents of Chelating were added to the metal salt precursor solution to obtain a stoichiometrically correct homogenous metal salt precursor solution. When silica is removed with NaOH or HF aqueous solution, mesoporous oxides of perovskite with an organized structure of mesoporous and a high specific surface area are formed. An image of TEM of mesoporous oxide of perovskite is shown in

Because of the complicated interactions between silica and ion of metal precursors filtrated, it can be difficult to fill the mesoporous silica at once, necessitating the observation of a comprehensive impregnation of metal precursors over long periods. Larger oxides of perovskite particles are frequently found outside the pores of mesoporous silica. As a result, various innovative approaches have been devised to increase metal precursor impregnation while reducing external pore loading, such as functionalizing mesoporous silica templates to a group of organic compounds [76]. Similarly, the mesoporous perovskite oxides reported using mesoporous silica as a hard template are confined to little varieties, namely those having composition $\text{LaB}_{1-x}\text{B}'_x\text{O}_3$ (B, B' = Mn, Co, Fe, Ni). Chelating chemicals such as citric acid must be added to metal nitrate precursor solutions to form pure-phased

perovskite oxides in lesser calcination temperatures. Another drawback of the hard template method is that correctly draining the silica utilizing a solution of NaOH/HF is difficult, silica residue impacts the hard-characteristic template progress [77]. These issues can be solved by utilizing mesoporous carbon as a template-hard since high-temperature calcination can completely obliterate the carbon template. Based on a silica Aerosil, the process of nano casting in a micro-mesoporous carbon resulted in $\text{LaFe}_{1-x}\text{Co}_x\text{O}_3$ perovskite oxides with a high specific surface area Fig 4(A) [78]. The inorganic precursors are converted into perovskite oxide nanoparticles in the process of calcination at 800°C in air, while the carbon is removed by oxidation. However, there are several drawbacks to employing mesoporous carbon as a template, including inadequate aqueous precursor solution wetting of the pore walls and a low decomposition temperature. Normal impregnation fails to properly fill the pores resulting in perovskite particles developing outside the pores, which is the underlying problem with the hard-template approach. As a result, it will be necessary to build more user-friendly solutions. Due to high interfacial tension in mesoporous structures, the double-solvent method which combines a significant amount of hydrophobic solvent with an aqueous metal precursor solution with a pore volume, may provide an effective method for enhanced metal precursor penetration [79].

The mesoporous structure of LaFeO_3 material is shown in Fig (4B). Silica modification of the surface with different groups that are functional on the interior or exterior surfaces will promote metal precursors to be impregnated due to interactions between metal precursors and functional groups [73,80].

(c) Method for Creating Colloidal Crystal Templates

Another typical production method for the crystalline technique uses nano-porous materials of perovskite having 3D organized macro-pores. Inorganic porous materials with sizes of pores ranging from nanometers-micrometers have been successfully produced using organic polymer spheres. Depending on the synthesis approach, three methods for manufacturing periodic structures of macro-porous using a colloidal crystal template are presented in Fig (5) [81]. The vacant gaps between

monodisperse spheres packed close together e.g., Polystyrene (PS) or Polymethyl methacrylate (PMMA) and in-situ precursor solidification are filled or covered with liquid metal precursors in these colloidal-crystal-template techniques. The three-dimensionally organized macroporous (3DOM) structures may be made by removing the templates and calcinating them at a high temperature. Inverse opals have a three-dimensional interconnected structure that allows big molecules to move swiftly and gas to diffuse quickly.

Two benefits of employing the template of colloidal crystal technique for generating nanoporous oxides of perovskite are the capacity to manufacture ordered nanoporous perovskite oxides and employing calcination at a high temperature. The 3DOM $\text{La}_{0.7}\text{Ca}_{0.3}\text{MnO}_3$, $\text{La}_{0.7}\text{Ca}_{0.32-x}\text{Sr}_x\text{MnO}_3$ was created by Hur et al. [82] by dissolving stoichiometric metal acetates and 2-methoxy ethanol in HNO_3 then gently dumping the thick solution until the millimeter PMMA template was completely immersed. The SEM and TEM images of $\text{La}_{0.7}\text{Ca}_{0.3}\text{MnO}_3$ are shown in Fig (3A, B). Sintering at 800°C in an oxygen environment was used to remove PMMA colloids. On the other hand, making a metal alkoxide solution is labor-intensive and expensive. Using a colloidal-crystal-template technique, researchers created 3DOM oxides of perovskite precursors including solutions of ethylene glycol methanol of different metal nitrates.

Zhao and co-created 3DOM $\text{LaCo}_x\text{Fe}_{1-x}\text{O}_3$ perovskite oxide using this method [83]. Various Surfactants of Organic, chelating compounds are utilized to equally distribute nitrates of metal throughout the crystal colloidal template process in the formation of oxides of 3DOM perovskite. Dai and co, for example, employed a surfactant-assisted PMMA templating procedure to make 3DOM $\text{La}_{0.6}\text{Sr}_{0.4}\text{FeO}_3$ with a mesoporous or nano void-like framework, and the findings demonstrated that the nature of the solvent and surfactant affects the surface area and pore structure of the end product [84].

According to researchers processing the $\text{La}_{0.6}\text{Sr}_{0.4}\text{FeO}_3$ a precursor in the development of $\text{La}_{0.6}\text{Sr}_{0.4}\text{FeO}_3$ 3DOM would be favored at 500°C by N_2 for amorphous carbon and so in the air about 7500°C . Dai's group synthesized many types of

3DOM perovskite oxides using citric acid, PEG (Polyethylene Glycol), and triblock copolymer (pluronic P123) including EuFeO_3 , $\text{Eu}_{0.6}\text{Sr}_{0.4}\text{FeO}_3$, LaMnO_3 , $\text{La}_{0.6}\text{Sr}_{0.4}\text{MnO}_3$ and La_2CuO_4 [85].

The noble metal nanoparticle-assisted crystal colloidal template approach was used to create 3DOM oxides of perovskite in a single step. 3DOM, for example, supports silver nanoparticles. PMMA was employed as a template in a dimethoxytetraethylene glycol (DMOTEG) solution to generate $\text{La}_{0.6}\text{Sr}_{0.4}\text{MnO}_3$ with larger areas of surface ($38.2\text{--}42.7\text{ m}^2/\text{g}$), and the DMOTEG-mediated procedure resulted in size-controlled silver nanoparticles that were also stabilized against agglomeration without the need of extra styrene [86].

In a methanol solution by combining stoichiometric quantities of $\text{La}(\text{NO}_3)_3$, $\text{Pd}(\text{NO}_3)_2$, and $\text{Mn}(\text{NO}_3)_2$ with PEG and lysine in an aqueous HNO_3 solution, Wang and co-created a 3DOM Pd- LaMnO_3 composite [87]. The 3D porous structure may still collapse or be lost during or after the template removal due to the delicate material nature, which has considerably lower wall thickness than the pore size. As a result, the stability of the pore structure of 3DOM perovskite oxide should be checked frequently throughout manufacture and usage.

Another disadvantage of the crystal colloidal template strategy is the cost and time required to create templates of polymer, which confine the practical applicability of metal 3DOM oxide of perovskite. To generate pure phase 3DOM perovskite oxides, organic matter or detergent must be added to the possibility for molecules that are organically interacting with CCT must be addressed when using a precursor solution of metal ion to evenly divide the ions of metal [73]. Different Synthetic protocols with their corresponding positive and negative aspects are shown in Scheme 3.

3. Methods for Making 1D Perovskite-Type Oxide Nanostructures

In the last ten years, many uni-dimensional oxide nanostructures of perovskite have been produced. The most commonly used techniques are "top-down", and "bottom-up". There are two types of preparation procedures for 1D perovskite nanostructures.

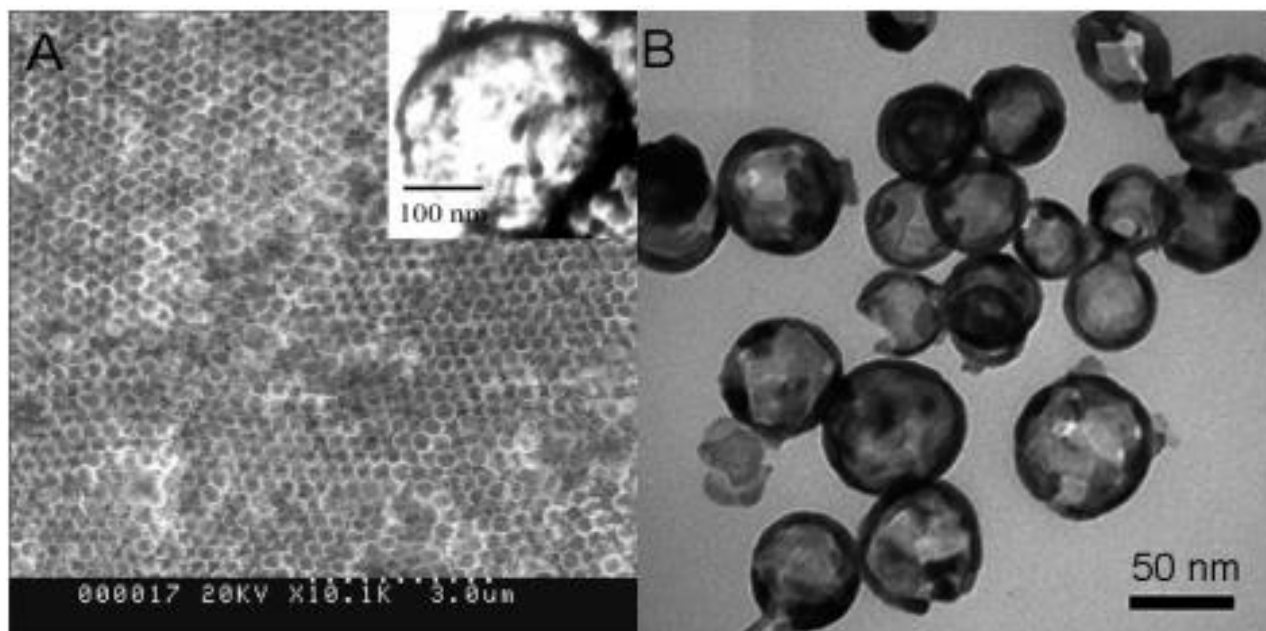


Figure. 3 (A) $\text{La}_{0.7}\text{Ca}_{0.3}\text{MnO}_3$ spherical array duplicated from the carbon template, as seen in SEM. A TEM picture of a $\text{La}_{0.7}\text{Ca}_{0.3}\text{MnO}_3$ sphere with a hollow sphere feature is shown in the inset. (B) TEM picture of hydrothermally produced LaCaMnO_3 . Reproduced with permission from ref. [1]. Copyright 2014 ACS catalysis

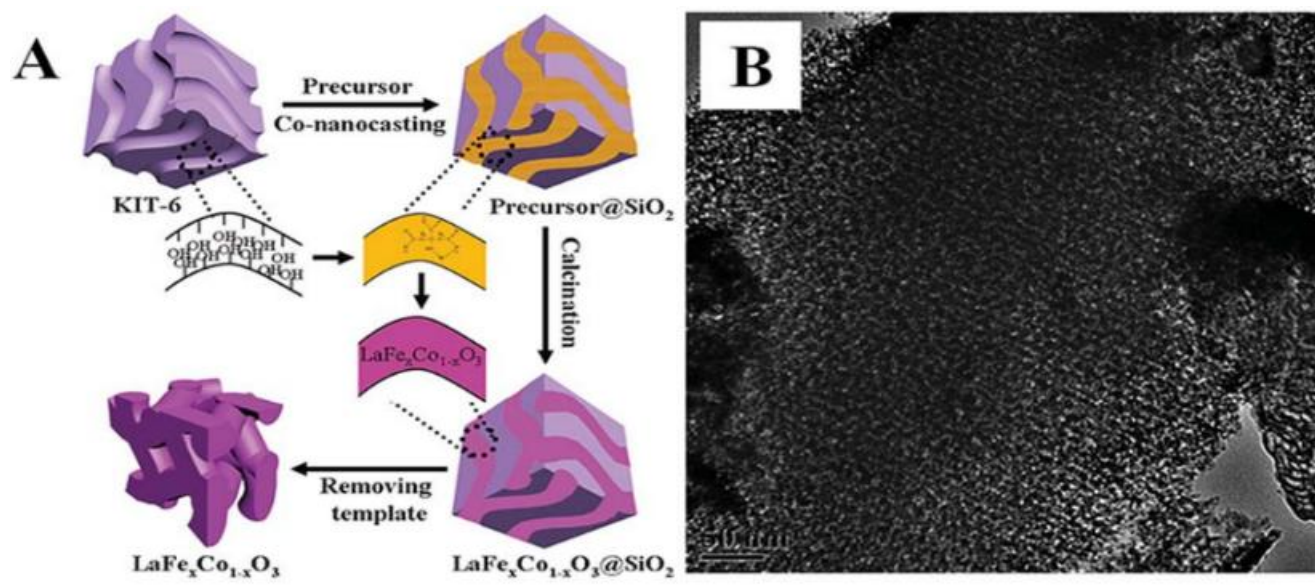


Figure. 4(A) The mesoporous $\text{LaFe}_x\text{Co}_{1-x}\text{O}_3$ perovskite oxides were made using a co-nano casting process using a rigid template of mesoporous KIT-6, (B) LaFeO_3 that has been developed as a mesoporous material. Reproduced with permission from ref. [73]. Copyright 2018 Chemical Science

The first method does not use a template, but the second does.

The following section examines recent advances in manufacturing unidimensional oxide nano-structures of perovskite.

3.1 Template Free Synthesis

Hydrothermal or solvothermal preparation, the salt of molten approach, and the process of electro-spinning having used to build uni-dimensional oxide nano-structures of perovskite without the need for a template.

For example, Joshi and co [88] created perovskite of single crystalline BT (BaTiO_3), ST nano-wires using a solution-based approach of free templates. Piezoelectric (PZT) single crystalline nanowires were also made using the template-free hydrothermal method [89]. The templates need not be removed after the perovskite oxide nanowires are generated because this approach does not require organic templates. BT, ST, and PT single crystalline nano-wires are made using the methodology of molten salt. Precursors' surface and interface energies, as well as the molten salts used, are crucial in the synthesis of molten salt nanowires. To make monocrystalline BT nanowires, the metal of alkali titanates is employed as precursors of synthetic in a modified hydrothermal method. Tetragonal Pt uni crystalline nano-wires with a necklace-like shape have also been made via electrospinning. Their lengths range from tens to various tens of micrometers, while their diameter range from 100-200nm. Sol-gel electrophoresis was also used to make tetragonal PZT nanofibers for mechanical energy harvesting nanogenerators [90-92]. Despite its time-consuming and low-throughput nature, the advantage of this technology is that the nanostructures generated can be morphologically controlled. Perovskite nano-tubes' oxides are also made using free template methods like hydro-thermal manufacturing (PONTs). For example, the hydrothermal method was utilized to make BT and BST nanotube arrays on titanium substrates. Constant BT crystalline and ST PONTs were also made employing a low-temperature hydrothermal method using TiO_2 nanotubes as a bonafide precursor material [93-95].

3.2 Synthesis using Templates

The template-assisted approach is an excellent way to mass-produce regular nanostructured arrays in large numbers. The most frequent templates so far have been colloidal monolayers, anodic aluminum oxide, block-copolymers, and nanoimprint molds. Unidimensional oxide of perovskite nano-structures have been created using template-assisted procedures, which have the following benefits: (1) regular nanostructured arrays with a high density; (2) a high surface-to-volume ratio; and (3) finished product dimensions with excellent control over the template channels. With success in the procedure, the oxide of perovskite $\text{La}_{0.825}\text{Sr}_{0.175}\text{MnO}_3$ nanowires having a polycrystalline perovskite structure was also generated [96,97]. Perovskite oxide nanotubes are created utilizing a sol-gel template-based approach in addition to perovskite oxide nanowires. Hernandez et al. [98] published ground-breaking research using (Anode Aluminium Oxide) AAO templates and the so-gel process to synthesize perovskite PbTiO_3 (PT) and BaTiO_3 (BT) nanotubes. PZT and multiferroic BiFeO_3 BFO nanotubes were made using the same approach. Even though the nano-tubes sizes and shapes can be feasibly controlled through templates, template-based approaches produce polycrystalline nanotubes in general, attributed to nucleation of heterogeneous on walls pore; this process produces tiny uni-crystalline oxide of perovskite nano-tubes. Anti-ferroelectric PZ PONTs were formed utilizing pulsed laser deposition in templates of AAO made up of nanoparticles with diameters ranging from 3 to 7nm and a wall thickness of roughly 10nm. Sol-gel electrodeposition would be utilized to produce PZT nanotube arrays, in which the channels of the templates of AAO are filled with PZT-prepared sol driven from electrophoretic DC voltages. As a result, the filling effect was substantially improved. Manganite nanotube arrays of perovskite were categorized by utilizing microwave irradiation and AAO template-assisted synthesis [99]. This approach allows for the production of arrays of nano-tube at lesser temperatures.

Perovskite $\text{La}_{0.59}\text{Ca}_{0.41}\text{CoO}_3$ nanotubes are also made using sol-gel templates. A template-inorganic precursor and low-

temperature calcination were also used to make perovskite LaNiO_3 nanotubes [100]. LaNiO_3 nanotubes have a polycrystalline structure with very tiny crystals ranging in size from 3–5 nm [95].

4. 2 D Perovskite-Type Oxide Nanostructure Preparation

Methods

Thin-film, arrays of nano-dot, lamellae patterns, nanosheets, nanoplates, and nanowalls are only a few examples of perovskite oxide 2D nanostructures essential in today's microelectronics. As a result, numerous methods for generating perovskite oxide 2D nanostructures have been discovered in the last few years. This section discusses the two-dimensional perovskite ferroelectric nano-structures oxide based upon planar-structures and oxide of perovskite nanosheets, as well as oxide of perovskite thin films and multilayers.

4.1 Multilayer Perovskite Oxide Thin Films

The process that transforms the gaseous state of atoms, molecules, or ions into substrate films or multilayers is known as the oxide of perovskite thin film or multilayer growth. For growing oxide of perovskite thin-films/multilayers, PVD physical vapor deposition methods like PLD, magnetron-sputtering RF, and chemically methodologies like CSD, CVD, and MOCVD, as well as MBE, are all commonly used methods (MBE). This section briefly discusses PLD, CSD, CVD, MOCVD, as well as MBE.

4.2 Laser Deposition using Pulses (PLD)

Smith and co initially used the PLD approach to create dielectric thin films in 1965 [99] and it has since become a prominent thin film growth method. The capacity of the PLD technique to yield film compositions that are almost equal to those of the target, despite the target's complicated stoichiometry, is its most crucial property. Several thin films of oxide of perovskite or multi-layers are generated by altering the PLD process parameters. The literature has an excellent review of the epitaxial development of thin films oxide of perovskite and super lattices.

4.2.1. Chemical Solution Deposition

Because of its low cost, ease of setup, and ability to coat large

areas, Chemical Solution Deposition (CSD) is a promising approach for generating thin films. It was first developed for the oxide of thin films of perovskite in the mid-1980s. To date, the CSD method has been used to make a large number of oxide of perovskite thin films. Four processes are involved in the production of oxide of perovskite thin films: Preparation of the precursor solution, spin coating/dip-coating of solution on the substrate, deposited solution of pyrolysis in lesser temperatures, and high-temperature crystallization of the films [101-103].

4.2.2. Chemical Vapour Deposition (CVD) & Metal Organic Vapour Deposition (MOCVD)

CVD is a widely used method for producing high-quality and performance thin films of perovskite oxides across a vast area (CVD). The synthesized materials must have a high vapor pressure when used as a precursor in the CSD process. The substrate compulsorily increases temperature to a specific temperature to improve the reaction's deposition and adatom mobility. To successfully install complicated multi-component thin films oxide of perovskite with homogenous compositions across a vast region, the utilized precursors must have matching thermal properties and acceptable vapor pressures. Improved film quality control has been accomplished using modified CVD methods based on liquid or aerosol generation injection. Liquid injection CVD was used to deposit PZT perovskite, lanthanum-barium-manganite ($\text{La}_{1-x}\text{Ba}_x\text{MnO}_3$) thin films, whilst aerosol and plasma-assisted CVD was used to create $\text{La}_{1-x}\text{Sr}_x\text{MnO}_3$ perovskite thin films [104].

Perovskite oxide thin films and super lattices are made using metal-organic chemical vapor deposition (MOCVD). Improved film stoichiometry control, greater crystallization quality, and the ability to cover complicated structures and wide areas are just a few of the benefits of this procedure over standard physical deposition methods. Some of the MOCVD variants that have been developed to satisfy a range of applications include MOCVD at low pressures, MOCVD at atmospheric pressures, MOCVD with direct liquid injection, and MOCVD with plasma enhancement. In the MOCVD injection process, the creation of micro-droplets of solution of the precursor is

controlled with a high-speed electro valve pumped in the system of the evaporator. The injection frequency and timing are used to change the optimal growth rates of different deposited materials. Injection MOCVD is now being utilized to produce ferroelectric oxide of perovskite thin films including Barium strontium Titanate (BST), PT, PZT, and BFO, as well as oxide of perovskite super lattices like (BT/ST)_n & (LSMO/STO)_n [105].

4.2.3. Molecular-Beam Epitaxy (MBE)

In the same way that atomic spray painting employs alternatively shuttered elemental sources to maintain cation stoichiometry carefully, the MBE process for producing perovskite oxide thin films uses alternatively shuttered elemental sources to produce high-quality perovskite oxide thin films. Major problems in MBE multicomponent oxide synthesis in only a few applications include regulating oxide substrates terminated at well-defined ionic planes and monitoring the deposition of individual molecular/atomic layers. Reflection high energy electron diffraction) RHEED is frequently utilized for in situ monitoring of the developing surface in MBE. MBE has previously been utilized to fabricate high-quality thin-films oxide of perovskite and epitaxial heterostructures [95].

5. Planar Perovskite Oxide Nanostructures in 2 Dimensions

5.1 Top-Down Methods

A diversity of "top-down" 2D perovskite oxide nanostructured materials based on planar topologies have been constructed thus far using methodologies such as transmission electron microscopy, electron beam lithography (EBL), and nanoimprint lithography (NIL). Alexe and his colleagues were the first to construct a slightly elevated ferroelectric memory based on multiple perovskite ferromagnetism oxide nanostructure formations. Regular arrays of SrBi₂ Ta₂O₉ & PZT nanoisland capacitors with lateral dimensions less than 100 nm were safely manufactured using the EBL procedure.

After the BT nanodots were cut from the BT single crystal using Focused Ion Beam FIB technology, the zone structures inside the BT dots were evaluated [95,106].

5.2 Bottom-up Methods

Bottom-up techniques, including syntax synthesis, have been employed to create two-dimensional oxide of perovskite nanostructures based on lateral arrays of nanodots in addition to top-down solutions. Using template-assisted "bottom-up" synthetic technologies, nanosphere lithography was applied to produce BT, PZT, and SrBi₂Ta₂O₉ ferroelectric oxide nanodots with narrow size and distribution. Lee et al. [107] utilized ultrathin AAO membranes as a stencil mask and PLD method to build PZT arrays on Pt/ MgO substrates. Ultra-high density ferroelectric memory might be allowed by Pt/PZT/Pt nano-capacitors with a density of 176 Gb/inch² [95].

6. Methods for making 3D Oxide Nano-structures of Perovskite-Type

Both "bottom-up", and "top-down" methodologies can be employed to create 3D nanostructures. "Top-down" nanostructure production options include using FIB technology to cut away bulk ferroelectric material and construct logically and continuously ordered nanosized structures. Exact placement and effective control over the shapes and sizes of the nanostructures formed are two major advantages of using "top-down" methodologies for FIB milling to make 3D perovskite oxide nanostructures. On the other hand, the FIB milling machine has a range of negative effects, including slower milling and patterning frequencies, thus causing difficulties for volume patterning nanostructures, specifically bigger ones [108].

Furthermore, difficulties have occurred at the nanoscale as a result of impact ions causing damage to the sample surfaces. Because the features of 3D oxide of perovskite nanostructures are highly influenced by their morphologies and ordered alignments, large-scale nanostructure arrays with the required shape and structure are important. A glass substrate, electron

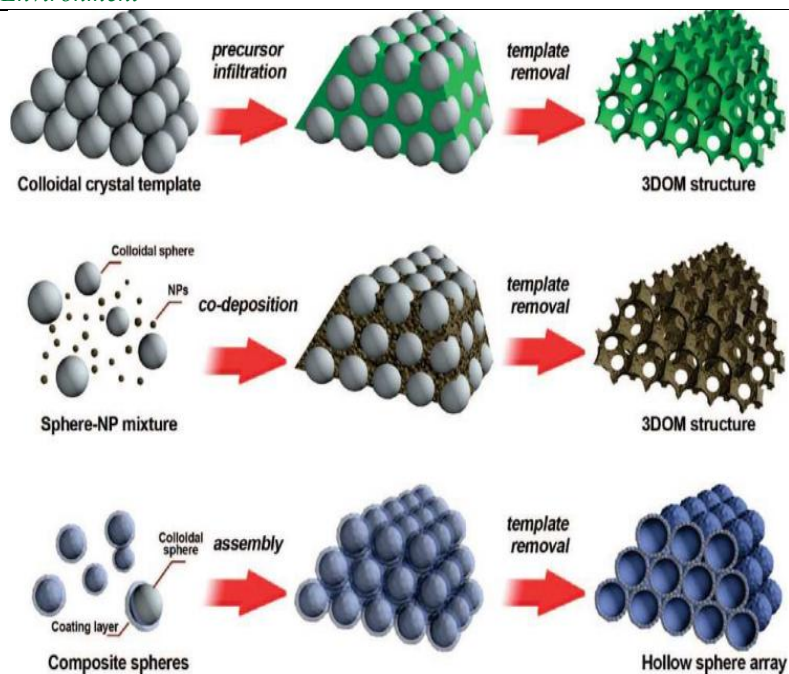
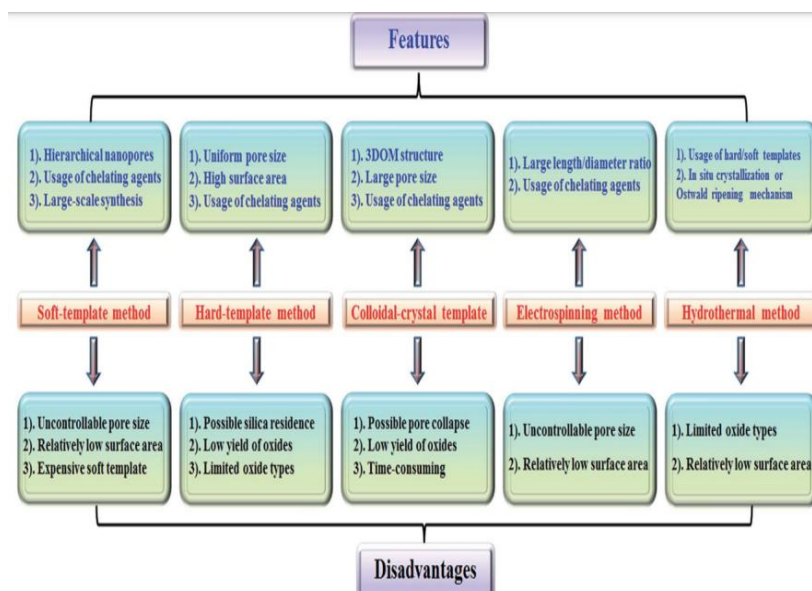


Figure. 5 Three colloidal-crystal-template methods for producing periodic macroporous structures. Top: Precursor material is infiltrated into a preformed colloidal crystal, which is then treated to generate the 3DOM structure once the template is removed. Middle: To make a 3DOM structure homogenous, once the template is removed the nanoparticles (NPs) and templating spheres are co-deposited. Bottom: Hollow shells are produced by regularly arranging core-shell components. This diagram has been reproduced with the permission of ref. [73]. Copyright 2018 Chemical Science



Scheme 3 Synthetic approaches for nanoporous perovskite metal oxides are summarized from ref. [73].

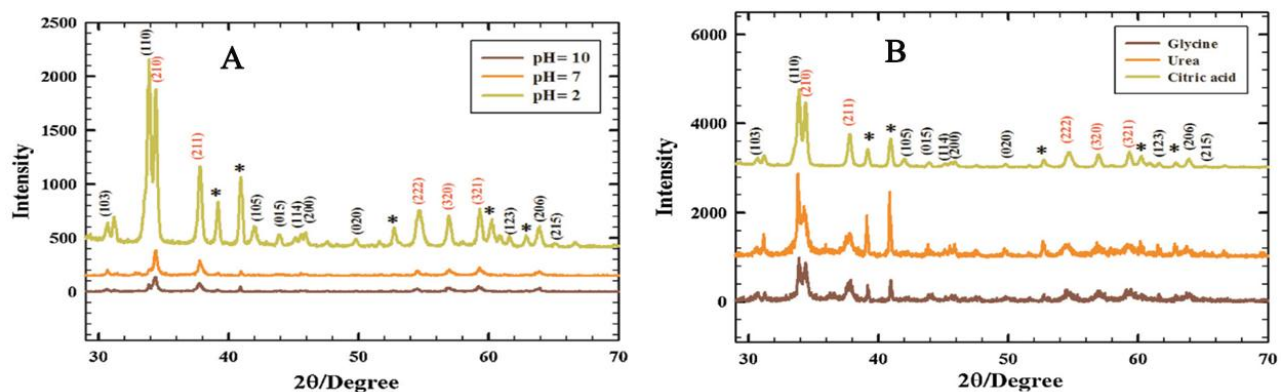


Figure. 6 Patterns of XRD of SrPdO₃ created from a combustion process at varied pH levels (A) for various fuels (B) SrPdO₃, SrPd₃O₄, and SrCl₂. Miller indices (h, l, k) are given in black for SrPdO₃, red for SrPd₃O₄, and the sign (*) for SrCl₂... Reproduced with permission Ref. [110]. Copyright 2014 Electrochimica Acta

Table 1. Lattice parameters of SrPdO₃ synthesized by different methods

	Lattice Structure	Particle Size (nm)	Lattice Parameters (Å)	Lattice Volume (Å ³)	Theoretical Density (g/cm ³)
Standard SrPdO ₃ (ICCD card, 00-025-0908)	Orthorhombic		a=3.977 b=3.350 c=12.82	179.98	4.47
Citrate-nitrate method	Orthorhombic	34.0	a=3.983 b=3.541 c=12.80	180.59	4.45
Urea-nitrate method	Orthorhombic	45.4	a=3.954 b=3.563 c=12.82	180.63	4.45
Glycine-nitrate method	Orthorhombic	25.7	a=3.972 b=3.527 c=12.83	179.69	4.47

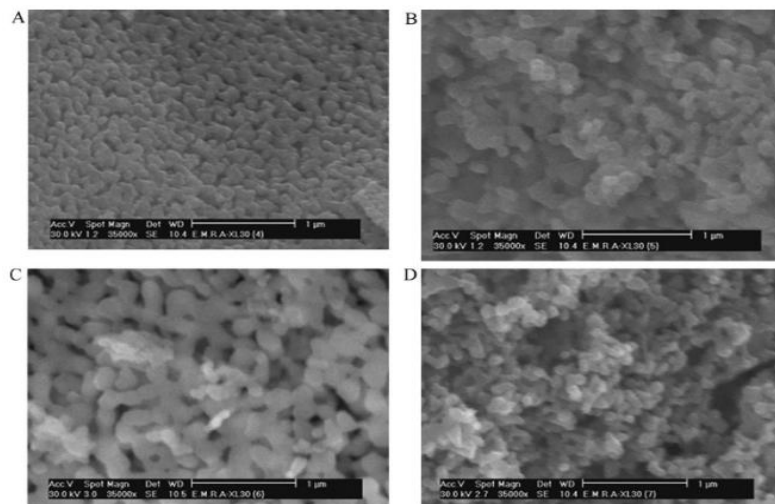


Fig. 7 Images showing SEM analysis of (A) 'LaNiO₃', (B) 'LaCoO₃', (C) 'LaFeO₃' and (D) LaMnO₃ was produced using a microwave-assisted citrate technique at 720W for 30 minutes, magnified 35,000 times. From ref. [112]. Copyright 2014 Electrochimica Acta

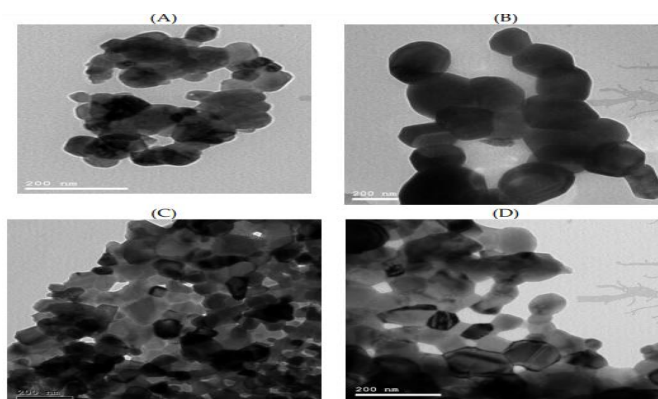


Figure 8. Images showing HRTEM analysis of (A) 'LaNiO₃', (B) 'LaCoO₃', (C) 'LaFeO₃', and (D) For 30 minutes, microwave-assisted citrate was employed to generate LaMnO₃ @ 720W. according to the source ref. [111]. Copyright 2008 Journal of magnetism and magnetic materials

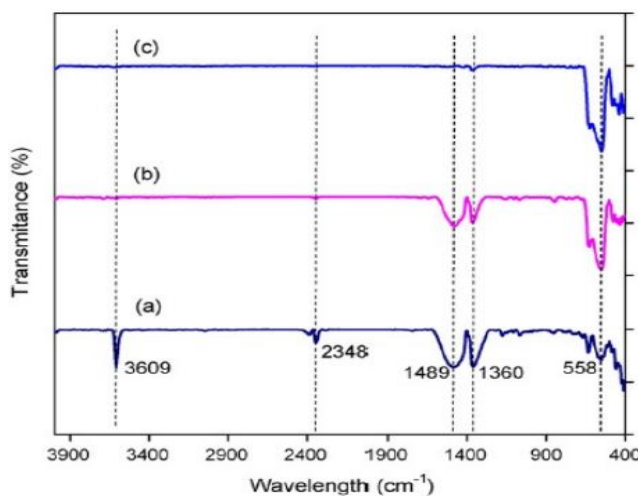


Figure. 9 FTIR spectra of LaFeO₃ produced with permission From ref. [113]. Copyright 2008 Bulletin of materials sciences

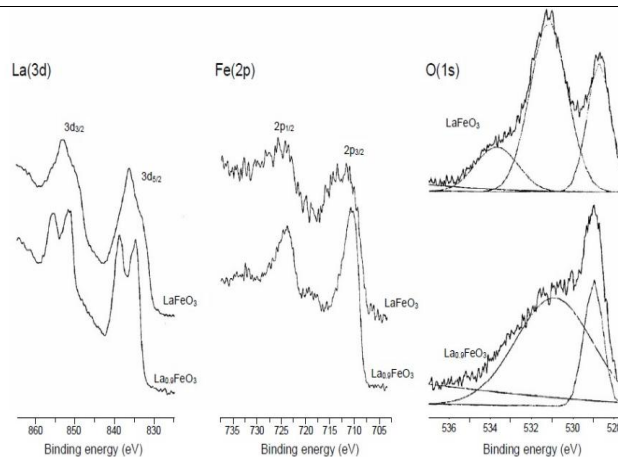


Figure 10: La (3d), Fe(2p), and O(1s) XPS spectra in $\text{La}_{0.9}\text{FeO}_3$ and LaFeO_3 samples. From ref. [114]. Copyright 2009 Bulletin of the Korean chemical society

beam lithography, and scanning probe lithography are used to achieve results [95].

7. Perovskite Characterization

The distinct phases of the perovskites generated may be distinguished by X-ray powder diffraction (XRD). Another approach for determining the structure of perovskites is single-crystal XRD. Thermal analytic techniques such as TGA, DTA, and DSC can be used to study the thermal stability of the produced perovskites. SEM & TEM, on the other hand, may disclose a variety of structural and surface properties of the perovskites created [109]. We chose a variety of perovskites from earlier research as examples for characterization investigations in this study.

7.1. SrPdO_3 perovskite

a. XRD

Galal et al. [109] Fig. (6A) show the XRD patterns of SrPdO_3 synthesized at pH values of 2, 7, and 10 for 3 hours at a calcination temperature of 750 °C. The Intensified Charge Couple Device (ICCD) results for SrPdO_3 were compared to those of the XRD. The real and theoretical pH 2 values are very close. This helps form the primary orthorhombic phase of perovskite of SrPdO_3 (major diffraction peak 110) and the secondary phase of SrPd_3O_4 emerged (210). In prepared samples of pH 7 & 10, only the SrPd_3O_4 phase was visible, while the (110) peak vanished. XRD patterns of SrPdO_3 , SrPd_3O_4 , and SrCl_2 are shown in Fig (6B).

Consequently, the optimal pH for generating SrPdO_3 is pH 2.

XRD may also be used to optimize the kind of (citric-acid, urea, and glycine) SrPdO_3 made with this material. In all cases, SrPdO_3 was the dominant phase, albeit with differing percentages of SrPdO_3 (110) compared to SrPd_3O_4 (210). The proportion was greater in the case of urea, but low in the case of citric acid. Table 1 lists the structural parameters that were calculated as well as well-matched theoretical data [109].

b. SEM and TEM

Perovskite nanoparticles' morphology and physical features may be explored using SEM and TEM. The SEM of the formed perovskites was strongly influenced by the preparation environment, synthesis methodology, types of A- & B-site ions of metal, and doped A- and/or B-sites. Galal and co. [109] employed 720W as the working power for 30 minutes of microwave irradiation to synthesize LaNiO_3 , LaCoO_3 , and LaFeO_3 are all oxides of nickel, cobalt, iron., and LaMnO_3 using the microwave-assisted citrate technique.

The SEM images of several perovskites i-e LaNiO_3 , LaCoO_3 , LaFeO_3 , LaMnO_3 are displayed in Fig (7). LaNiO_3 had a surface as compact with a greater degree of order, whereas LaCoO_3 and LaMnO_3 had spherical grain agglomerations with smaller grain sizes in LaMnO_3 and greater grain sizes in LaCoO_3 and LaMnO_3 , respectively. LaFeO_3 has a unique shape, with a porous surface filled with bonelike particles. LaFeO_3 has greater electro-catalytic activity than other perovskites in the hydrogen evolution process [109].

In addition, HRTEM may demonstrate the various

morphologies and particle properties of several perovskites [111]. HRTEM images of LaNiO_3 , LaCoO_3 , LaFeO_3 , and LaMnO_3 were prepared using the microwave-assisted citrate technique Fig (8). Images of LaFeO_3 taken using HRTEM revealed a crystallinity-rich orthorhombic phase, whereas LaNiO_3 , LaCoO_3 , and LaMnO_3 HRTEM photos revealed hexagonally deformed rhombohedral phases. For the different perovskites, the HRTEM diffraction patterns were similar to the XRD data [109].

c. FTIR

The perovskites' chemical bonding and chemical structure that has been generated may be investigated using FTIR. In the same way that XRD may provide structural evidence, the FTIR can as well. Biniwale et al. [113] synthesized LaFeO_3 using various methods, including sol-gel, combustion, and co-precipitation. In the FTIR of LaFeO_3 , the stretching vibration mode of Fe-O was detected as an absorption band at 558cm^{-1} Fig (9). The O-Fe-O vibration mode was discovered to be linked to the 430cm^{-1} band. In LaFeO_3 , which is connected to La-O in lanthanum oxide, co-precipitation produced a strong band at 3609cm^{-1} . The band at 3600cm^{-1} simply vanished in the other two methods, suggesting the production of a somewhat pure perovskite phase. Additional bands occurred at 1360 and 1480cm^{-1} in the co-precipitation technique, indicating future stages. Consequently, the absorption peak of about 558cm^{-1} was connected to metallic oxygen bond stretching modes, as described in the literature [109].

d. XPS

The surface compositions of the individual components of the developed perovskites may be examined utilizing XPS. Lee et al. [114] prepared $\text{La}_{0.9}\text{FeO}_3$ and LaFeO_3 samples and investigated their structural composition using XPS analysis. Fig (10) exhibits the XPS spectra of La (3d), Fe (2p), and O (1s) in $\text{La}_{0.9}\text{FeO}_3$ and LaFeO_3 samples. The binding energy of La (3d_{5/2}) in LaFeO_3 and $\text{La}_{0.9}\text{FeO}_3$ was 833.5eV and 833.8eV, respectively, corresponding to the La^{+3} ions in the oxide state. In both samples, however, the bandgap of Fe (2p_{3/2}) was 710.2 eV. This signifies Fe^{3+} ions in the form of oxide. The Fe (2p) XPS signal can't understand the difference between Fe^{3+} and

Fe^{4+} . The XPS signal of O (1s) was split into two peaks at 529.9 and 532.1 eV in the case of $\text{La}_{0.9}\text{FeO}_3$. The O (1s) XPS signal for LaFeO_3 contained three peaks: 529.4, 531.9, and 534.4 eV. The binding energies of O (1s) at lattice oxygen species are 529.9 and 529.4 eV in both experiments. The chemisorbed oxygen species OH or O are important for the peaks at 532.1 and 531.9 eV. The binding energy of chemisorbed oxygen species is 2.1– 2.5eV bigger than even lattice oxygen species. In the instance of LaFeO_3 , the peak at 534.4eV was ascribed to adsorbed water species related to the particularly hygroscopic surface lanthanum oxide [114,109].

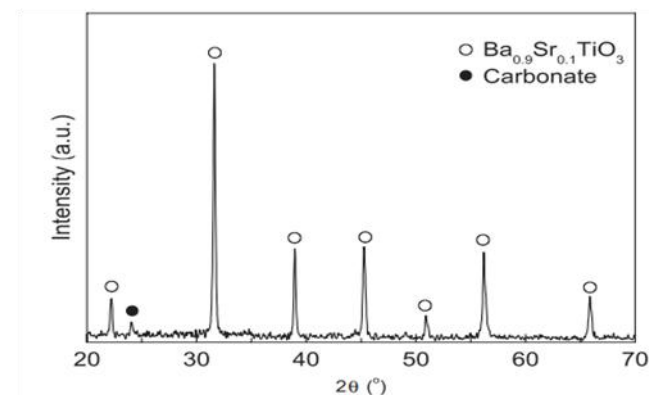


Fig. 11 $(\text{Ba}_{0.9}\text{Sr}_{0.1})\text{TiO}_3$ nanoparticles X-ray diffraction pattern. Reproduced with permission from ref. 115. Copyright 2005 Journal of solid state chemistry

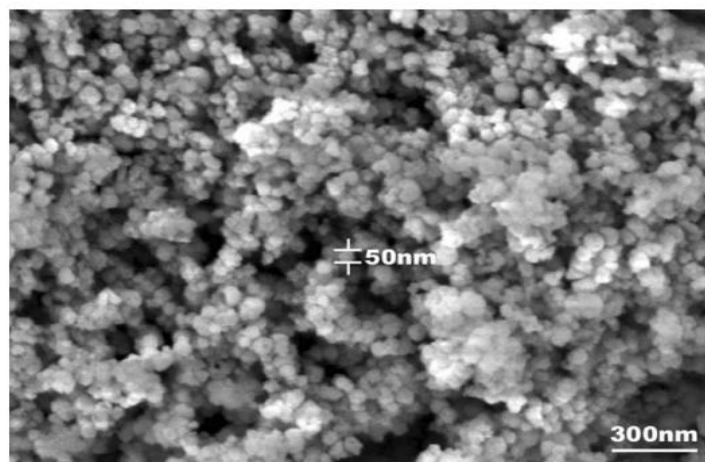


Figure 12: Using field-emission scanning electron microscopy, BST nanoparticles were observed (FE-SEM). With permission from ref. 115. This article has been reprinted. Copyright 2005 Journal of solid state chemistry

7.2. [(Ba, Sr) TiO₃] Perovskite barium strontium titanate**nanoparticles****a. XRD**

Jian Quan qi et al. [115] used wet chemical synthesis at room temperature and ambient pressure to make perovskite barium strontium titanate nanoparticles (BST). Starting ingredients include titanium alkoxide and alkali earth hydroxides, which are processed using very simple methods. Changing the processing conditions can change particle size and crystallinity. The crystallinity and phase of the Ba, Sr) TiO₃ nanoparticles were determined using X-ray diffraction. Fig (11). In the XRD pattern, at 24° barium carbonate appears as a peak. The interactions between carbon dioxide dissolved into solutions from the air and alkaline earth hydroxides are proposed to be the reason for barium carbonate manufacturing. Finishing the production in a protected climate (such as argon or nitrogen) or scrubbing the powders with dilute acids can prevent the impure phase [115].

b. SEM, TEM

The microstructure of as-produced particles of BST was further described using SEM and TEM shows a typical SEM picture of the synthesized BST nanoparticles. The particles are homogeneous in size and have a diameter of 50 nm as shown in Fig (12) [115].

The findings of the TEM observation are shown in (The size of the particle found by TEM was 50nm diameter, Fig (13a) which was consistent with the SEM findings. SAED pattern having atom planes of indexed shown in the inset of HR image of TEM is shown in Fig (13b). The image's darker half shows well-organized patterns, indicating that the particles under investigation have solidified. The structural information of the nanoparticles was obtained using a rapid Fourier transform technique, as illustrated in the Fast Fourier Transform (FFT). The material's lattice parameter was discovered to be 0.398 nm Fig (13c). In the FFT image, dislocations were also discovered in Fig (13 d). The production of dislocations is caused by the low synthesis temperature [115].

7.3. Perovskite oxide Ba_x Mn_{1-x} O₃**a. XRD**

Ba_xMn_{1-x}O₃ oxide of perovskite is a good material for producing electrochemical instruments or devices because of its attractive chemical and physical features. Using a hydrothermal technique, Muhammad Rafique et al. [116] synthesized Ba-doped MnO₃ (BaMnO₃) with variable Ba concentrations. X-ray diffraction was used to characterize the generated material.

Fig (14) exhibits XRD patterns of Ba_xMn_{1-x}O₃ (x = 0.1, 0.15, 0.2), which reveal angles with miller indices of 27.20 (101), 31.60 (110), 380 (002), 41.280 (201), 50.450, 52.90 (211), 560 (300), 65.50 (220), 710 (203), 72.20 (311), and 78.90 (222), respectively. With a = 5.6720, b = 5.6720, and c = 4.7100, hexagonal crystalline structure is discovered. Peaks blue-shift as doping levels rise, with the full width at half maximum (FWHM) increasing and peak strength dropping, reflecting a drop in crystallinity. Doping raises the cell volume and material density to 131.23 cm⁻² and 6.06 g/cm⁻³, respectively, after doping. The EDX results reveal that the samples are pure because there are no impurity peaks in the spectra. The crystallite size was calculated using Debye Scherer's formula based on the obtained data [116].

$$D = \frac{K\lambda}{\beta \cos \theta}$$

CLK = 0.15418nm is the X-ray wavelength, is the FWHM, and is the diffraction angle. K is the form factor (0.9 for hexagonal structures), D is the crystallite size, and CuK = 0.15418nm is the X-ray wavelength. The crystallite size in pure material is 22.1nm. However, when the number of dopants increases, it shrinks. The crystallite diameters of 10wt percent, 15wt percent, and 20wt percent doped BaMnO₃ are 21.2, 16.5, and 11.3 nm, respectively. Lattice distortion is caused by a mismatch in the radius of the matrix and the dopant element, which causes crystallite size to decrease. A stress or strain field is created due to this occurrence, disrupting crystal formation in one direction. Because the dopant (Ba) is big, compression forces produce blue shifting of the diffraction peaks. Tensile strains, on the other hand, move the peaks toward larger angles

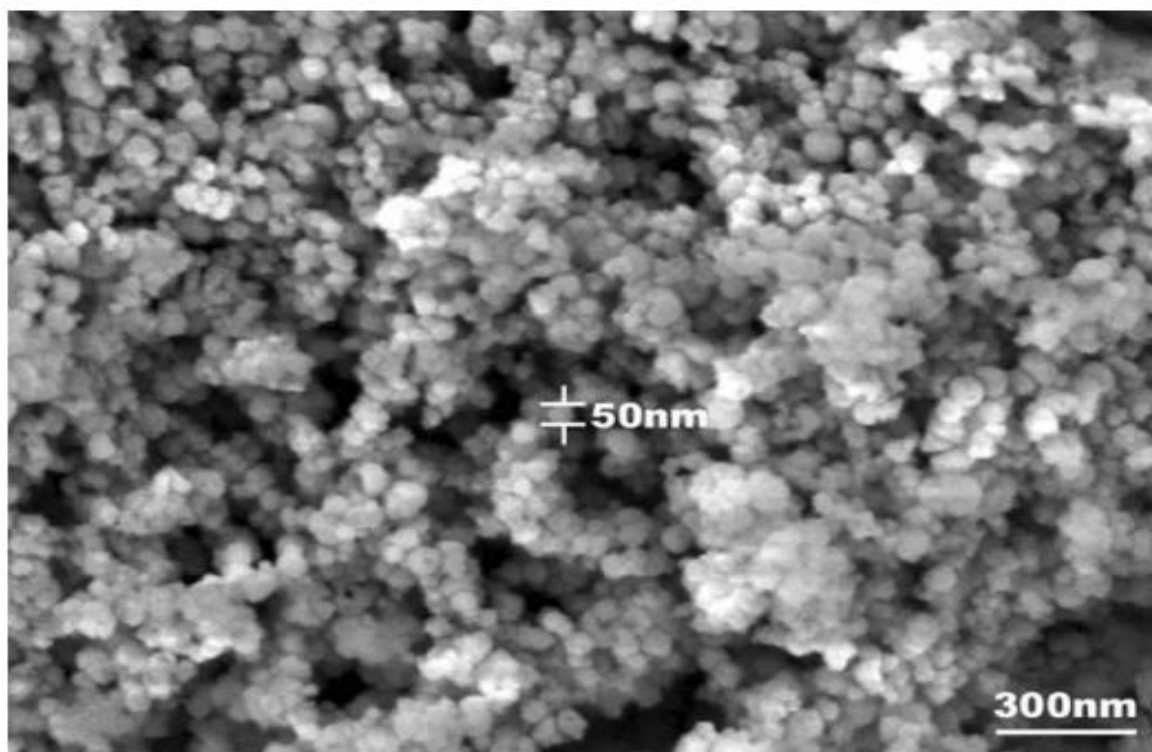


Figure 12: Using field-emission scanning electron microscopy, BST nanoparticles were observed (FE-SEM). With permission from ref. 115. This article has been reprinted. Copyright 2005 Journal of solid state chemistry

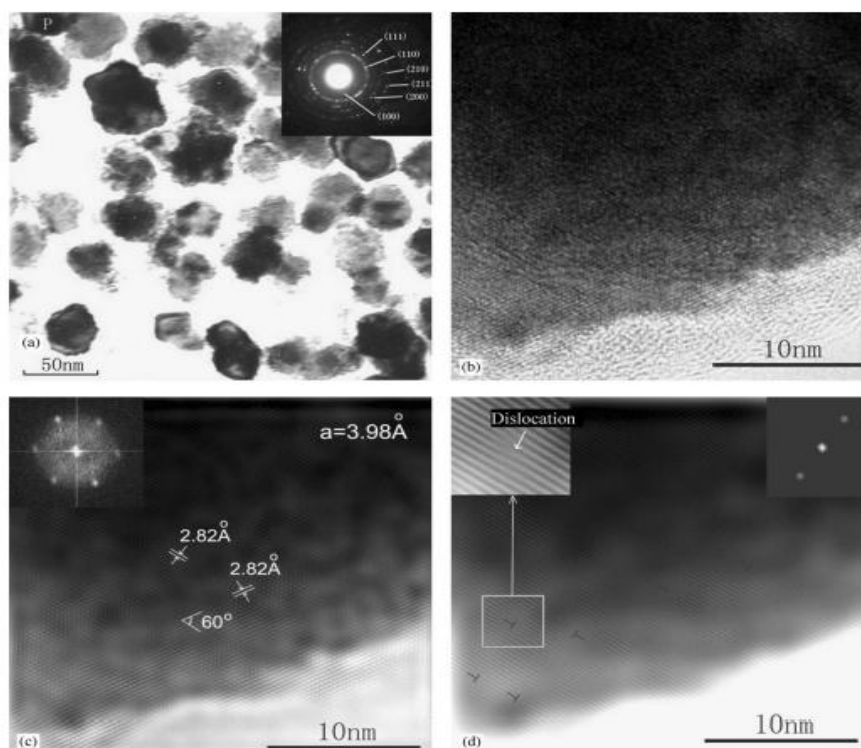


Fig. 13 TEM images of BST nanoparticles: **(a)** 'morphologies', **(b)** 'HR image', **(c)** This FFT graphic shows the link between the atom planes and **(d)** The dislocations in the nanostructure are seen in this FFT image. Reproduced with permission from ref.

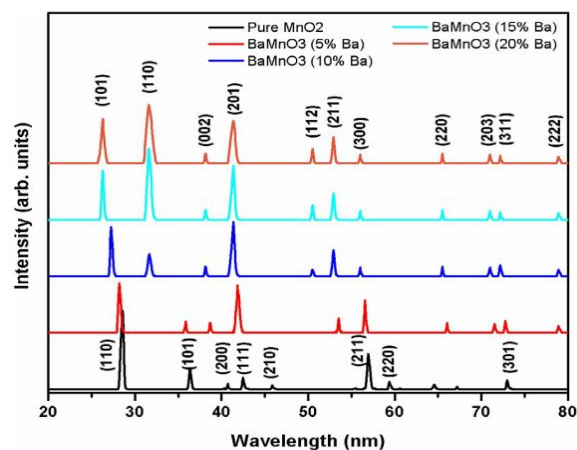


Figure. 14 XRD of pure MnO_2 and 10, 15, and 20wt% doped BaMnO_3 . Reprint with permission from ref. 116. Copyright 2021 International journal of energy research

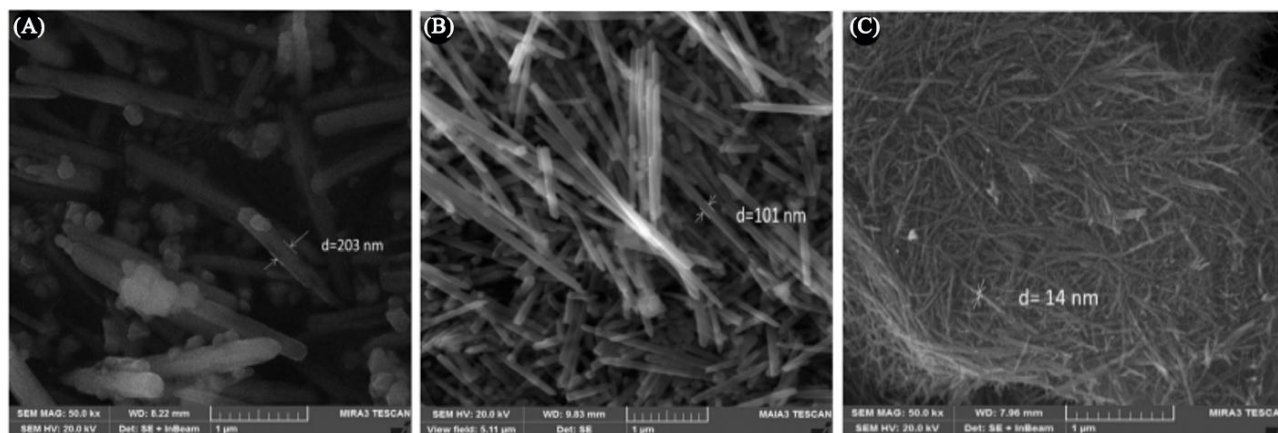


Figure 15: SEM micrographs of Ba_xMnO_3 (A) At 10wt% doped BaMnO_3 , (B) At 15wt% doped BaMnO_3 , and (C) At 20wt% doped BaMnO_3 . Reproduced with permission from ref. 116. Copyright 2021 International journal of energy research

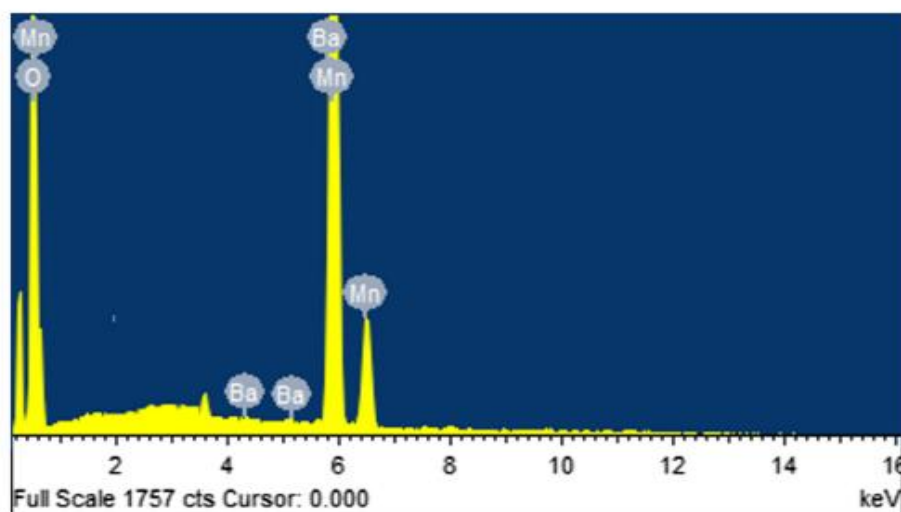


Fig 16: EDX spectra of BaMnO_3 . Reproduced with permission from ref. 116. Copyright 2021 International journal of energy research

Due to a large amount of dopant. Oxygen vacancies have an important role in structural mobility. A cation vacancy is created in this situation by giving dopants (Ba) an excess positive charge. When these vacancies come into contact with oxygen vacancies in MnO_2 , they become less mobile [116].

b. SEM

SEM micrographs of Ba-doped MnO_3 at 10, 15, and 20% by weight are depicted in Fig (15A, B, C). The micrographs for 10, 15, and 20wt percent doped materials reveal nanorods with diameters of 90-110nm, 180-220nm, and 10 to 15nm, respectively [116].

The degree of doping in the nanorods determines their shape and diameter. This is owing to a difference in the materials' ionic radius, which induces bond constriction and, as a result, a size reduction. According to the findings, doping increased the material's surface area, which improved the electrochemical characteristics of MnO_2 by increasing the material's reactive sites [116].

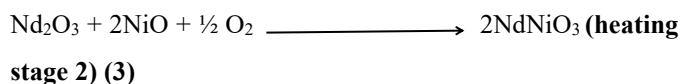
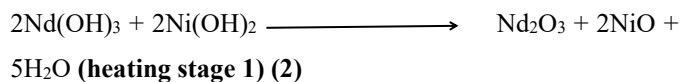
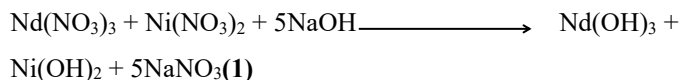
c. EDX

The EDX spectrum of Ba-doped MnO_3 is shown in Fig (16). The spectrum reveals that the samples produced are fully contaminant-free. This spectrum contains only the elements Mn, Ba, and O, contributing 26.45, 7.13, and 65.76 percent by Weight, respectively. As a result, the hydrothermal technique synthesized morphological materials that were both pure and controlled [116].

7.4. NdNiO_3 Perovskite Nanoparticles

a. XRD

To create NdNiO_3 perovskite nanoparticles that were calcined at various temperatures, M. I. Maulana et al. [117] employed sodium hydroxide as a precipitating agent and polyethylene glycol as a surfactant in a co-precipitation approach.



The products are identified using X-ray diffraction Fig (17).

Shows the material's pattern of XRD obtained during manufacturing, calcined at different temperatures. As calculations temperature grew, peaks strength changed. In products of as-synthesis calcined at about 900°C , a crystalline phase of NdNiO_3 nanoparticles, ABO_3 perovskite-type, was identified (P900). Peaks corresponding to novel oxide phases ascribed to extraordinarily strong peaks such as Nd_2O_3 , NiO , and Nd_2NiO_4 were also discovered at that temperature.

The hydroxide and oxide phases coexist in the calcined synthesis result at 700°C , namely $\text{Nd}(\text{OH})_3$, $\text{Ni}(\text{OH})_2$, Nd_2O_3 , NiO , and Nd_2NiO_4 , were formed (P700). The metal hydroxides were expected to not entirely dissolve to oxides during heating step 1 (Reaction 2). However, they can be converted to perovskites at extremely high calcination temperatures. It might be because the first heating stage is just 1 hour long. At temperatures below 900°C , NdNiO_3 nanoparticles do not form. Analysis of XRD indicated that P900 was far superior to P700 due to the development of perovskite and the lack of hydroxide compounds [117].

b. FTIR

The materials were analyzed using FTIR before and after calcination. It was done to see if we successfully eliminated contaminants containing undesirable functional groups. It was also hoped that a wide range of vibrations of Ni–O stretching and O–Ni–O bending would be detected. After calcination, the functional groups OH, CH, and CO in the nitrate ion as precursors, NO, and O–H, C–H, and C–O as a surfactant in PEG 400, OH, CH, and CO, should evaporate. It was considered that the substance was pure since it lacked specific functional groups. The PEG structure is shown in Fig (18) [117].

The spectrum of FTIR of PEG 400 as well as the final product before and after calcination are shown in Fig. (19). The spectra of PEG were given peaks of absorption for OH wide stretched, CH stretched, CO stretched, and CO stretched (primary alcohol) vibrations at 3432 , 2866 , 1092 , and 1066 cm^{-1} , respectively. As the temperature of calcination increased, the OH vibrations of stretching were slowly lost and may not be recognized in spectra of P900, & also as on CH stretched and CO stretched

vibrations [117].

Oxides of metals, like Ni–O, show absorption peaks under 800 cm^{-1} because of interatomic vibrations. Significant absorption is about 6–7 hundred cm^{-1} region because of Ni–O vibration stretching mode [118].

The peak of absorption at 634 cm^{-1} is also caused by the MO, OMO, and M–O–M (M=Ni, Co) [119] vibrations. According to the FTIR spectrum, Ni–O's stretching vibrations were identified before and after calcination in the product. The stretching Ni–O led Ni(OH)₂ to form in the precipitate of the product before calcination. O–H stretching was measured during that time, which supported the idea even more. P700 contains a trace quantity of Ni(OH)₂ as evidenced by mild stretching O–H and NiO₂ vibrations in Nd₂NiO₄ compounds. On the other hand, the O–Ni–O vibration in P900 created NdNiO₃ perovskite nanoparticles. XRD examination verified that all of these assignments gave NdNiO₃ [117].

7.5. LaNiO₃ perovskite oxides

a. XRD and SEM

Harikrishnan and co-presented a co-precipitation technique for synthesizing LaNiO₃ nanoparticles, which were then annealed at various temperatures. Materials' structure and morphology are studied using XRD Fig (20a) [120]. XRD is utilized to identify the structure of the crystal.

The sample that was annealed at 600 degrees had a less crystalline XRD pattern. The crystalline structure of the LaNiO₃ nanoparticles matches 34-1028 which corresponds to a rhombohedral perovskite structure when annealed at temperatures of 700, 800 and 900 degrees Celsius, as illustrated in (Fig. 21) (a) peaks at 23.42° , 33.02° , 40.88° , 41.33° , 47.04° , 53.72° , 54.04° , 58.96° , 59.72° , 68.8° , 69.17° , 74.52° , 78.67° , 79.49° correspond to (101), (110), (021), (003), (020), (211), (113), (122), (220), (029), (303), (312), (214). No other peaks at 700oC, 800oC, or 900oC could be attributed to La₂O₃ or other phases indicating the presence of single-phase LaNiO₃ in the sample. The powerful diffraction patterns confirm the material's crystalline structure [120]. The surface morphology of the generated different LaNiO₃ (LNO) nano-particles ie LNO1, LNO2, LNO3, LNO4, and LNO5 is

investigated using SEM. Fig. (20 b,c,d) depicts the SEM images of the samples. The diverse morphologies of the particles for various calcination temperatures are readily seen in these SEM images [120]. Typically, they appear as a clump of deformed sphere-like particles. Additionally, as the calcination temperature rises, so does the degree of particle agglomeration. Particle grain growth during high-temperature calcination might cause the degree of agglomeration [120].

8. Catalytic Applications of Perovskite Oxides

Oxides based on perovskite having common formula ABO₃ have effectively ammonia oxidation, methane combustion, catalyzed hydrogenation, and CO oxidation, among other reactions. We used examples from previous research that revealed catalytic behavior in numerous conversions to show case the catalytic applicability of perovskite oxides.

8.1. Comparison of Catalytic Activity of GdAlO₃, SrMnO₃, SrCoO₃, and MnFeO₃ Perovskite Oxides

Perovskite oxides, which appear to be potential catalysts, appear to enhance VOC combustion. During the combustion method of Propane, benzene, acetone, and gasoline (Pb-free), Nicolae Rezlescu et al. [121] compare the catalysis activity of several ordinary perovskites having variable cationic concentrations. Nanometer particles with nominal compositions of SrMnO₃, GdAlO₃, MnFeO₃, and SrCoO₃ were created using the self-combustion sol-gel process and subsequently heat treated in the air at 1000°C. As for catalytic studies, the catalytic activity level varied significantly depending on the perovskite content. SrMnO₃ is the most active of the four perovskites when the weather is cold only in the conversion of acetone did catalysts MnFeO₃ and SrCoO_{3-x} exhibit considerable activity as catalysts [121].

(a) Perovskites' Catalytic Activity

Perovskites catalytic capabilities in the combustion of investigated (distinct VOCs) at temperatures ranging from 20 to 550°C. For each perovskite composition, Fig. (21) displays the gas conversion as a parameter of reactive temperature. The following considerations should be taken into account: [121]

- The catalytic activity of the perovskite catalyst is affected by the reaction temperature. Raising the reaction

temperature aids gas combustion.

- Perovskites of diverse compositions have dramatically different catalytic activity, which is consistent with Seyfi et al findings [122]. Strontium manganite catalyst has higher catalytic activity than gadolinium aluminate catalyst Fig. (21 a,b) The activity differential between the two samples cannot be explained by their different surface areas. The surface area of GdAlO_3 is $10 \text{ m}^2/\text{g}$, while the surface area of SrMnO_3 is $2.2 \text{ m}^2/\text{g}$.
- Gas combustion over the SrMnO_3 catalyst began at substantially lower temperatures (about 100°C) than over other perovskites. The SrMnO_3 catalyst's increased VOC conversion activity reflects the existence of reactive oxygen species on the catalyst surface. Because of the high concentration of Mn^{4+} ions on the perovskite surface, oxygen may be less anchored and thus more available for VOC oxidation.
- An interesting result was found for manganese ferrate (MnFeO_3) Fig. (21c) and strontium cobaltite (SrCoO_{3-x}) Fig. (21d). Regardless of chemical composition, the two catalysts only demonstrated high catalytic activity for acetone conversion and low catalytic activity for propane, benzene, and gasoline catalytic combustion. The reasons for such a restricted catalytic activity are unknown. This behavior could be explained by a rearrangement of their lattice structure, which controls their catalytic properties, and, as a result, the active site configuration. It's worth noting that temperature significantly impacts acetone conversion over the MnFeO_3 catalyst. The acetone conversion started at a low temperature (150°C), and when the temperature increased from 200 to 300°C , the conversion rate increased substantially from 10% to 80% . (Fig.22c) This effect was not observed with the other perovskites. Unlike the MnFeO_3 catalyst, the SrCoO_{3-x} catalyst started converting acetone at about 200°C and reached an acetone conversion rate of 80% percent around 450°C . The four gases were converted more efficiently using the GdAlO_3 and SrMnO_3 catalysts [121].

Table 2 shows the data gathered in flame-less combustion of

VOC on the four perovskite catalysts. The conversion against temperature graph can be used to calculate T_{10} and T_{50} , which are the temperatures required to convert a gas by 10% and 50% , respectively. T_{50} is a common metric for assessing the catalytic activity of a catalyst [121].

The catalytic activity for complete gas oxidation is sufficient at T_{50} temperature, and there is substantial contact between the catalyst surface and the reactants. The catalyst is more active if this number is lower. SrMnO_3 appears to be more active than the other catalysts. It has much lower T_{10} and T_{50} temperatures than the other catalysts [121].

a Reaction rate for VOC concentration at low conversion per unit surface area of catalyst.

b Apparent activation energy for low conversions

The chemical composition of catalysts of perovskite, as well as the kind of used gas, have a very much impact on the performance of the catalyst in the combustion of VOC, as shown in Fig (22). On the other hand, SrCoO_3 and MnFeO_3 catalysts favor acetone oxidation alone. At 500 degrees Celsius, catalysts can convert 85% of acetone, but only 30% percent of the other gases. In light of the contrast, despite the little surface area, the most preferred catalyst among the four perovskite samples, SrMnO_3 , has the greatest catalytic activity at low temperatures. This catalyst converted 95% percent of propane, 83% lead-free gasoline, and 75% percent acetone at 500°C . SrMnO_3 less specific area perovskite does not appear to play a role in the catalyst's greater activity. The greater activity of the catalyst to SrMnO_3 might be attributable to the increased oxygen mobility generated by vacancies of oxygen caused by the manganese ions' presence of varied valence. The different activity of catalysts of the four perovskites is not able to be described by distinct surfaces. No indication that activity and surface area were linked. Factors like structural flaws and oxygen mobility are likely to affect the catalytic efficacy of these perovskite catalysts [121].

8.2. Methane Oxidative coupling, ABO_3 perovskites are used

Yujin Sim et al. [123] investigated the active-sites behavior of catalysts of perovskite in the coupling that is oxidative

coupling/reaction of methane (OCM) utilizing 10 different ABO₃ types catalysts of perovskite) with different structural features based on their A and B site components. In addition to being the structure definite and simple having the stability of heat, these materials offer remarkable activity of the catalyst in a range of conversion of CH₄ activities. According to findings, the surface lattice of catalyst species of oxygen is required for targeted methane conversion. Oxygen species of the surface lattice with lesser binding energies were used to purposefully speed the generation of hydrocarbons of C₂ from the OCM. Oxygen-adsorbed of surface and mixed oxygen lattice species were used to fill oxygen surface gaps created by the interaction of oxygen lattice with CH₄. The oxygen ion conductivity of perovskites is significantly related to this oxygen cycle, which can be predicted using structural features tolerance factor and particular free volume are two examples. The simple oxygen cycle converted a considerable amount of CH₄ during this reaction. Finally, they discovered that the oxygen lattice characteristics and for the systematic design of effective catalysts OCM, the conductivity of ion of oxygen of perovskite catalysts is a major component that influences catalytic activity and must be carefully managed [123].

According to the researchers, the conductivity of oxygen-ion of catalysts of perovskite might be utilized to forecast CH₄ conversion during the OCM process. Higher binding energies lattice oxygen species aided CO generation. Furthermore, the oxygen surface adsorbed species formed by gas-phase oxygen adsorption changed CO₂ to CO. As a result, the electrical characteristics of the oxygen species lattice and the conductivity of oxygen ions are essential determinants in the determination of the OCM activity of the catalyst of perovskites. Under the specified reaction conditions, the catalyst CaZrO₃ having strong conversion CH₄ and C₂ selectivity produced the maximum yield of C₂ (14.2 percent) [123].

8.3. BaCe_{1-x}Mn_xO_{3-δ} perovskite for methane combustion

The Manganese doped in BaCeO₃ catalyst oxides of the series

composite were synthesized using a sol-gel methodology. According to Xihan Tan et al. [124] methane as catalyst activity of combustion of BaCe_{1-x}Mn_xO_{3-δ} catalytic oxide of the series composite was investigated on lesser temperatures using a reactor of fixed bed (200-600 °C). Physically catalyst parameters are described using SEM, size of particle analysis, XRD, and measurement of a surface-specific area, while sample conductivity is determined using the impedance of AC spectroscopy [124].

According to the findings, the catalyst oxide of the perovskite phase composite constructed using the sol-gel catalyst phase of perovskite created has excellent catalyst performance and great thermal stability. Catalyst catalytic performance is affected by its conduciveness, which has a proportion in connection. According to the findings, the catalyst oxide of the perovskite phase composite is effectively manufactured using the sol-gel method. The catalyst phase of perovskite generated has better performance and great thermal stability. Catalyst catalytic performance is affected by its conduciveness, and there is a proportional relationship between the two. When the temperature is below 650°C, Mn doping considerably increases the activity of catalysis of the catalyst BaCeO₃ for the combustion of methane. As the quantity of Mn-doped rises, the catalytic activity increases at first, then decreases [124].

They also observed that when the sintering temperature climbed, sample conductivity increased firstly then decreased, grew continuously while increasing temperature test, and rose first and then plummeted as the Mn percentage increased. A BaCe_{0.6}Mn_{0.4}O_{3-δ} catalyst sample sintered at 1250°C had the maximum conductivity at 800°C, 0.4975scm⁻¹. They observed that the conductivity change rule is precisely opposite that of the activation energy in the diagram of Arrhenius of Mn sample conductivity. The activation energy is lowest when the catalyst sample reaches its maximum conductivity. The result of the activity of catalytic oxidation of CH₄ tests explains adding a catalyst considerably enhances methane catalytic oxidation efficiency when compared to doing so without one, and that

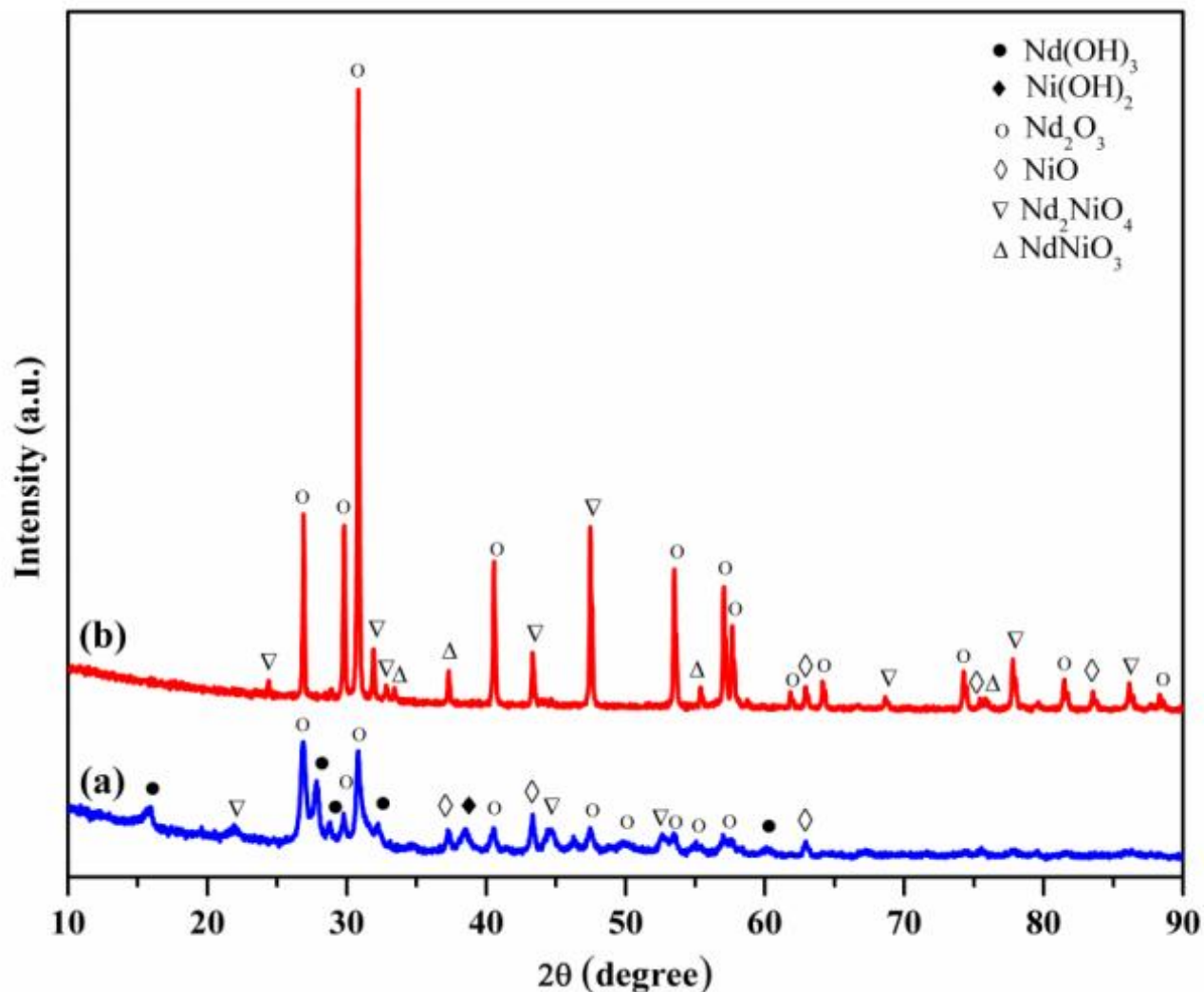


Fig.

17: XRD pattern of calcined materials $\text{Nd}(\text{OH})_3$, $\text{Ni}(\text{OH})_2$, Nd_2O_3 , NiO , and Nd_2NiO_4 during synthesis. Reproduced with permission from ref. [117]. Copyright 2020 Nano Express

CH_4 after doping has a better catalytic oxidation efficiency than BaCeO_3 . When the element $\text{Mn}=0.4$ is doped, sample catalytic activity peaks of CH_4 . The initial temperature of methane is 249.7 degrees Celsius, which is 400.3 degrees Celsius lesser than the experiment of blank, 95.3 degrees Celsius lesser to BaCeO_3 [124].

8.4. $\text{Co}_x\text{Fe}_{1-x}\text{O}_y$ catalyst for CO_2 hydrogenation

The study of $\text{CoO}_x\text{-FeO}_x$ catalysts reveals a lot about how multi-transition metal oxide catalysts are made and used. Minshan Meng et al. [125] stated that an efficient and solid-state mechanochemical redox process for obtaining $\text{Co}_x\text{Fe}_{1-x}\text{O}_y$ from $\text{CoCl}_2 \cdot 6\text{H}_2\text{O}$ and KMnO_4 was established with just two rounds of ball milling (BM). The transition metal oxide

$\text{Co}_x\text{Fe}_{1-x}\text{O}_y$ generated in the RWGS method may be used as a high-activity catalyst as well as a CO selectivity catalyst. Over the whole temperature range, selectivity is greater than 80%. At 500 degrees Celsius, it converted CO_2 at a rate of 43 percent, compared to 15.6 percent for $\text{Co}_x\text{Fe}_{1-x}\text{O}_y$ -CP and 15.8 percent for $\text{Co}_x\text{Fe}_{1-x}\text{O}_y$ -SG [125].

During 120 hours of high ambient temperature, the conversion rate of $\text{Co}_x\text{Fe}_{1-x}\text{O}_y$ -BM increased, suggesting that adding Fe to the Co element improved thermal stability. In the future, such a breakthrough is predicted to be the road to a greater and more efficient system of industries for synthesizing multi-transition metal oxides that are solvent-free and have outstanding catalytic performance [125].

8.5. $\text{La}_{1-x}\text{Sr}_x\text{CuO}$, CO_2 hydrogenation to methanol

catalysts

Because it is a cost-effective solution to the environmental greenhouse gas problem, CO_2 catalytic hydrogenation of the methanol process has become a popular CO_2 consumption technique. Structured materials of perovskite have come as very attractive other possible standard catalysts supports for this process because of their mobility of oxygen feature and feasibility of structural increasing adsorption CO_2 capacity by easy having metal oxides of alkali doping. The impact of the adsorption strength of CO_2 on hydrogenation of CO_2 on the activity of methanol in $\text{La}_x\text{Sr}_{1-x}\text{Cu}_{1.0}\text{O}$ materials with a perovskite structure was investigated and published by Antonius Jeffry Poerjoto et al. [126] $\text{La}_{0.9}\text{Sr}_{0.1}\text{CuO}$ beat all other Sr-modified catalysts in terms of conversion of CO_2 (8.59%), selectivity of methanol on 300°C , 3.0MPa pressure (49 percent). Moreover, $\text{La}_{0.9}\text{Sr}_{0.1}\text{CuO}$ demonstrated sustained catalytic activity over 24 hours with no carbon generation throughout the CO_2 hydrogenation cycle. XRD analysis revealed the forming structures of perovskite in catalysts of calcined. According to XPS research, $\text{La}_{0.9}\text{Sr}_{0.1}\text{CuO}$ has a larger number of lattice oxygen species than the others. Furthermore, because there is a relationship between lattice oxygen concentration and methanol yields, lattice oxygen species are significant for improving methanol selectivity during CO_2 hydrogenation. $\text{La}_{1-x}\text{Sr}_x\text{CuO}$ catalysts of perovskite having catalytic concentration $\text{La}_{0.9}\text{Sr}_{0.1}\text{CuO}$ outperformed another catalysis for hydrogenation of CO_2 in methanol [126].

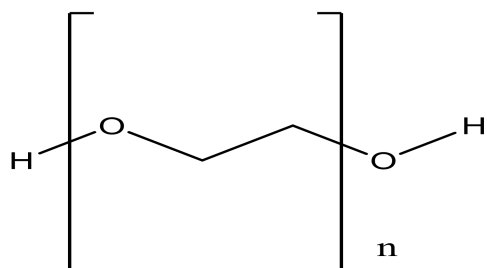


Fig. 18: Polyethylene glycol's chemical structure

8.6. Metal Catalysis on Perovskite-Type Oxides

Rojas Cervantes and colleagues investigated the use of

catalysts of perovskite oxide-based oxidation for wastewater treatment using various oxidants and so UV-visible irradiation producing photocatalysis [127]. The researchers investigate the physicochemical aspects of perovskite oxides like lattice oxygen vacancy and mobility formation as well as maintaining distinct states of oxidation of component elements which may be used to increase AOP employing radicals [128].

Using X-ray absorption spectroscopy, Kim et al. [129] show how Fe drives the oxygen evolution process (OER) in the $\text{PrBaCo}_{2(1-x)}\text{Fe}_{2x}\text{O}_{6-\delta}$ layer double perovskite used as a catalyst under alkaline circumstances. In $\text{PrBaCo}_2\text{O}_{6-\delta}$, Fe leads Cobalt to enter a lesser oxidation state that allows for charge compensation. In reaction circumstances, it prevents Cobalt and the layer doubled perovskites from melting, enabling active surface Co oxy-hydroxide layer to form [128].

Guo et al. [130] show that employing $\text{LaCo}_y\text{Ga}_{1-y}\text{O}_3$ mixed oxides as catalysts, alcohols (mostly methanol/ethanol) may be synthesized from syngas. The precursor of segregated cobalt nanoparticles in the LaGaO composite oxide is $\text{La}_{1-x}\text{K}_x\text{Co}_{0.65}\text{Ga}_{0.35}\text{O}_3$, which boosts its stability in a reactive environment. The impact of K on boosting the dispersion (atomic) of Cobalt and improving the coking composites resistance catalysts is identified by synthesizing La_2O_3 [128].

Steiger et al. [131] examine sulfur tolerance in solid oxide fuel cells and employ segregation reversible Ni to be an element active for the aqueous gas shift process and the second metal transition. Compared to Mn, Mo, Cr, and Fe, only Fe enhances the sulfur tolerance of $\text{La}_{0.3}\text{Sr}_{0.55}\text{Ti}_{0.95}\text{Ni}_{0.05}\text{O}_3$. Segregation simultaneously of iron and nickel in higher temperatures has little effect on the to and fro segregation reintegration of a couple of metals inside the mixed oxide of perovskite during oxidations, enabling greater time high-temperature uses [128].

Wark and colleagues [132] explain how LaFeO_3 works as a photocatalyst in the breakdown of Rhodamine-B and look at the best circumstances for getting the best results. Photoelectrochemical analysis was employed in addition to textural evaluation to explain variations in behavior as a function of calcination temperature. The results indicated lower temperatures boosted separation efficiency with photo-induced

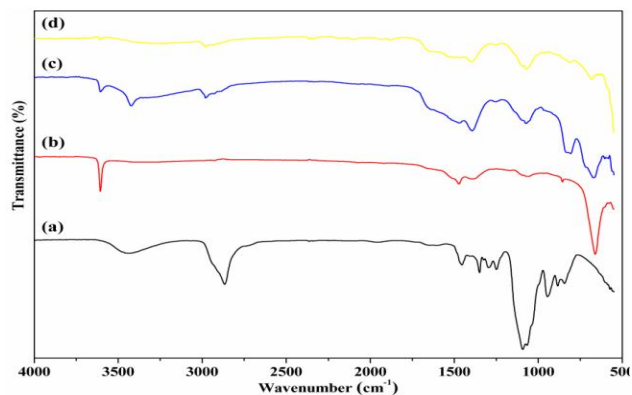


Fig 19: FTIR spectrum of (a) 'PEG 400', (b) 'product before it is calcined', (c) 'P700', and (d) 'P900'. Reproduced with permission from ref. [117]. Copyright 2020 Nano Express

With DFT research by Glisenti et al. [133], replacing La with Sr at the A-site of LaCoO_3 decreases the energy required to create oxygen vacancies, which is helpful in three-way catalysts for CO oxidation. Similar results can be produced by switching Co for Cu at the B-site. Effects of substitution appear as higher in SrTiO_3 [128].

The impact of some Ti substituting BaTiO_3 utilized as lean NO_x catalyst trap on NO_x storage capacity is investigated by Aldridge et al. [134] Cu is beneficial because it helps to separate Ba_2TiO_4 storage from NO_x storage. Among highly active noble metal-based catalysts, $\text{BaTi}_{0.8}\text{Cu}_{0.2}\text{O}_3$ has the most oxygen vacancies and the maximum storage capacity [128].

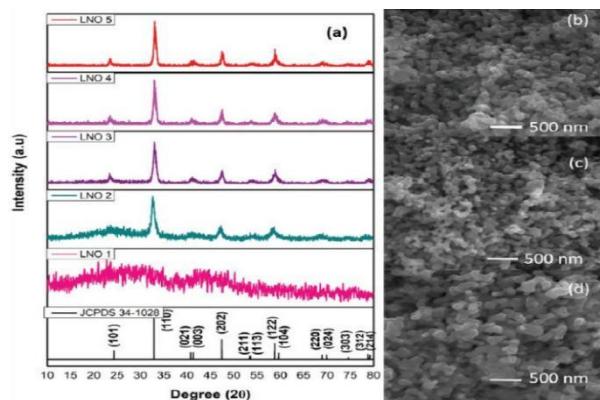


Fig. 20(a) 'XRD spectrum images of LNO1, LNO2, LNO3, LNO4, and LNO5' (b) 'Images showing SEM analysis of LNO3', (c) 'LNO4' and (d) 'LNO5' respectively. Reproduced with permission from ref. 120. Copyright 2019 In AIP

conference proceedings

Roning and colleagues looked at various $\text{LaCo}_{1-x}\text{Mn}_x\text{O}_3$ and $\text{LaCo}_{1-y}\text{Ni}_y\text{O}_3$ catalysts for NO oxidation to NO_2 . [138] While LaCoO_3 has the maximum activity among un-doped perovskites, $\text{LaCo}_{0.75}\text{Ni}_{0.25}\text{O}_3$ and $\text{LaCo}_{0.75}\text{Ni}_{0.25}\text{O}_3$ have the highest activity in substituted catalysts, suggesting that perovskites could be used as NO oxidation catalysts in the industry [128].

Heidinger et al. [136] used 3 stages of crushing: a reactive approach that includes high-energy wet ball milling, solid-state synthesis, and low-energy wet ball milling, all of which were subsequently calcined at 400°C . The catalytic efficiency for toluene oxidation improves in both cases after each synthesis phase, per the gain in surface-specific area, which marks about nineteen m^2g^{-1} to LaFeO_3 [128].

9. Conclusions and Future Perspective

This review has covered how to manufacture various morphologies of perovskite materials, define perovskite oxides, and employ perovskite oxides in catalysis. Because the sum of oxide needs a higher temperature and a large period of calcination, perovskite oxides are composed of some simple oxides and have a very small surface area. The area and properties of the surface of perovskite oxides must be increased to be used in heterogeneous catalysis or surface reactions. This study demonstrates how to make perovskite oxides in a variety of bulk, nanoscaled, supported, porous, and hollow morphologies, to maximize surface area and surface properties while adhering to reaction conditions. Several methods have been developed to understand perovskite oxides better to analyze their structure and physicochemical characteristics. Perovskite oxides' catalytic properties have been examined regarding their usage in catalysis.

We've already discussed nanoporous perovskite oxides, which can be made using soft and hard templates and colloidal crystal templates. Similarly, template-free and template-assisted synthesis of 1D perovskite oxide nanostructures, as well as thin sheets or multilayers of perovskite oxide and PLD of 2D perovskite oxide nanostructures, have been reported. Chemical solution deposition, CVD and MOCVD, & MBE are also

included in PLD (MBE). Top-down and bottom-up methods can be used to make planar perovskite oxide nanostructures in two dimensions. The synthesis of a 3D perovskite oxide nanostructure is also briefly explored.

In characterization, we have reported the characterization of various perovskite oxides namely SrPdO_3 by XRD, SEM, TEM, FTIR, XPS, and $[(\text{Ba}, \text{Sr}) \text{TiO}_3]$ by XRD, SEM, TEM, and $\text{Ba}_x\text{Mn}_{1-x}\text{O}_3$ by XRD, SEM, EDX and NdNiO_3 by XRD, FTIR and LaNiO_3 by XRD, SEM respectively.

We compared the catalytic activity of GdAlO_3 , SrMnO_3 , SrCoO_3 , and MnFeO_3 to overview the catalytic uses of

perovskite oxides. SrMnO_3 at low temperatures that appearing as a catalyst that is active in most of the four perovskites, according to the findings. Only in the conversion of acetone did MnFeO_3 and SrCoO_{3-x} catalysts exhibit strong catalytic activity. We have also reported ABO_3 perovskite in oxidative coupling of methane, $\text{BaCe}_{1-x}\text{Mn}_x\text{O}_{3-\delta}$ perovskite for methane combustion, $\text{Co}_x\text{Fe}_{1-x}\text{O}_y$ catalyst for carbon dioxide hydrogenation, $\text{La}_{1-x}\text{Sr}_x\text{CuO}$ catalyst for carbon dioxide hydrogenation to methanol, and metal catalysis on perovskite oxides from recent studies.

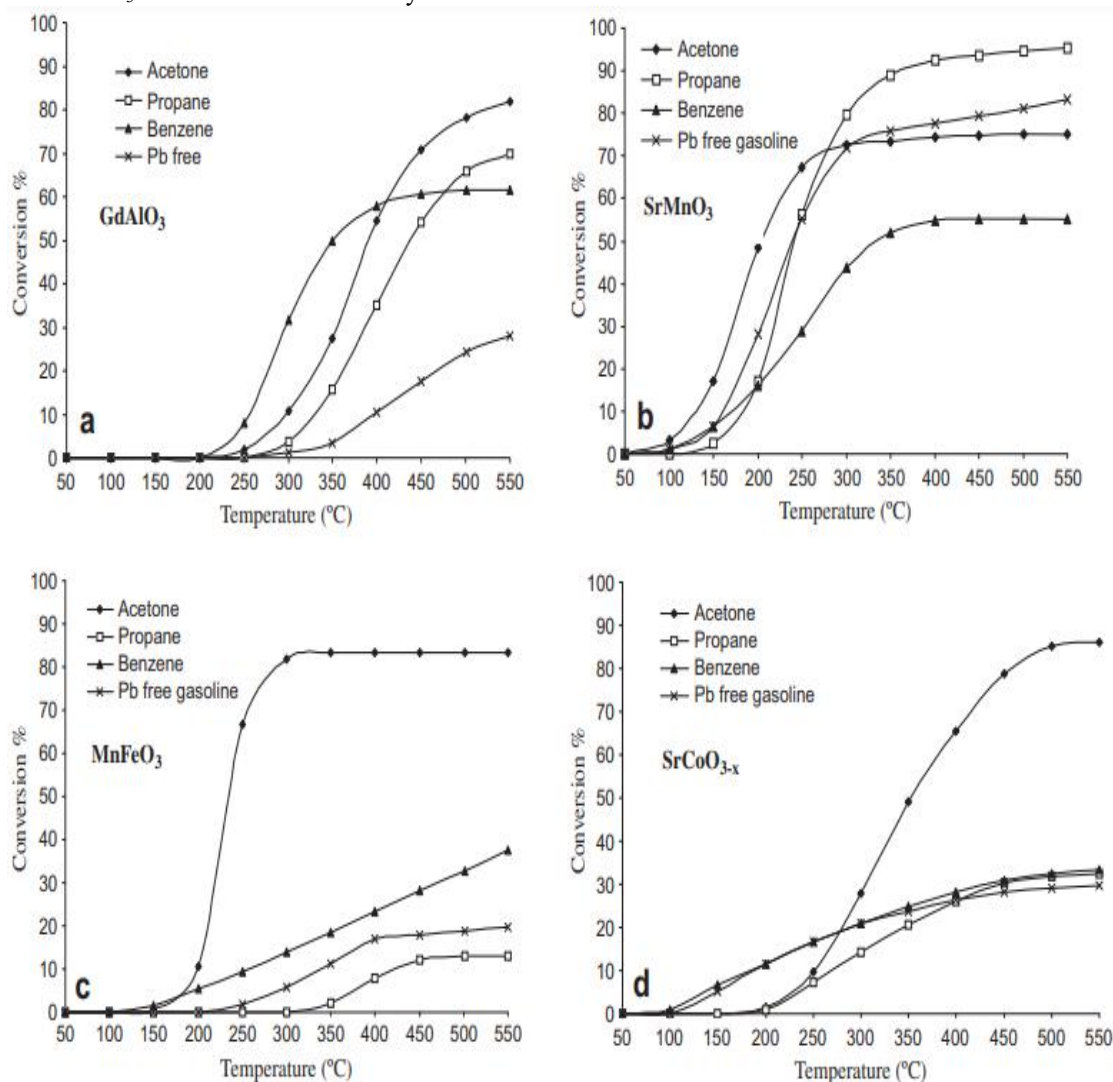


Fig 21: Temperature vs. benzene, propane, acetone, and gasoline of Pb-free conversion by catalytic flameless combustion (a) “ GdAlO_3 ”, (b) “ SrMnO_3 ”, (c) “ MnFeO_3 ” and (d) “ SrCoO_{3-x} ” perovskites. Reproduced with permission from ref. [121].

Copyright 2014 Composites Part B: Engineering

Table 2. T₁₀ T₅₀ and Kinetic parameters (reaction and rate^a and activation energy^b) for perovskite catalysts: Reproduced with permission from ref. [121]

VOCs	GdAlO ₃				SrMnO ₃			
	T ₁₀ (°C)	T ₅₀ (°C)	Reaction Rate (μmol s ⁻¹ m ⁻²)	Activation energy (KJ / mol)	T ₁₀ (°C)	T ₅₀ (°C)	Reaction Rate (μmol s ⁻¹ m ⁻²)	Activation energy (KJ / mol)
Acetone	295	390	6.7 x 10 ⁻²	89	130	200	140 x 10 ⁻²	37
Propane	330	440	7.8 x 10 ⁻²	71	180	240	9.8 x 10 ⁻²	31
Benzene	260	350	6.5 x 10 ⁻²	68	175	325	26 x 10 ⁻²	35
Pb free gasoline	390	-	4.2 x 10 ⁻¹	62	160	240	55 x 10 ⁻²	36

	MnFeO ₃				SrCoO _{3-x}			
	T ₁₀ (°C)	T ₅₀ (°C)	Reaction Rate (μmol s ⁻¹ m ⁻²)	Activation energy (kJ/ mol)	T ₁₀ (°C)	T ₅₀ (°C)	Reaction Rate (μmol s ⁻¹ m ⁻²)	Activation energy (KJ /mol)
Acetone	200	230	65 x 10 ⁻²	98	250	325	16 x 10 ⁻²	41
Propane	400	-	6.1 x 10 ⁻²	80	270	-	3.8 x 10 ⁻²	48
Benzene	255	-	17 x 10 ⁻²	45	190	-	56 x 10 ⁻²	44
Pb free gasoline	340	-	12 x 10 ⁻²	47	190	-	11 x 10 ⁻²	40

Despite major academic advances over the years, perovskite oxides have failed to find commercial applications as a catalyst. Their limited catalytic efficacy and sensitivity to pollutants like sulfur dioxide could be part of the problem. To commercialize these materials for industrial use, researchers should continue to work on developing a more efficient catalyst and learn more about how toxins interact with the surface of perovskite oxides.

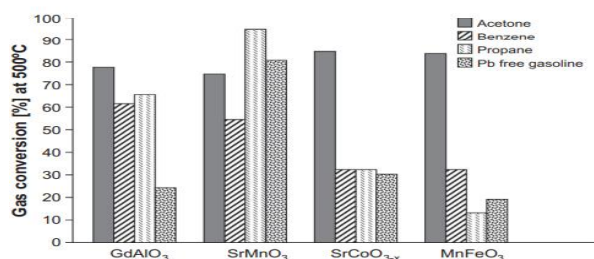


Fig 22: The effect of perovskite catalyst chemical composition on gas conversion at 500°C. Reproduced with permission from ref. [121]. Copyright 2014 Composites Part B: Engineering

Acknowledgment

This work is financially supported by Chemistry Department, University of Wah.

Conflict of interest

The authors reported no potential conflict of interest.

Authors Contribution

F. A and S.Y.B convinced the main idea and wrote the manuscript. K.e.K, S.F revised the manuscript and prepared figures and references.

References

1. Zhu, J., et al., Perovskite oxides: preparation, characterizations, and applications in heterogeneous catalysis. ACS Catalysis, 2014. 4(9): p. 2917-2940. DOI: <https://doi.org/10.1021/cs500606g>.
2. Rojas, M., et al., Preparation and characterization of LaMn1-xCuxO3+ λ perovskite oxides. Journal of Catalysis, 1990. 124(1): p. 41-51. DOI: [https://doi.org/10.1016/0021-9517\(90\)90102-P](https://doi.org/10.1016/0021-9517(90)90102-P).
3. Labhasetwar, N., et al., Perovskite-type catalytic materials for environmental applications. Science and technology of advanced materials, 2015. DOI: <https://doi.org/10.1088/1468-6996/16/3/036002>.
4. Sun, C., J.A. Alonso, and J. Bian, Recent advances in perovskite-type oxides for energy conversion and storage applications. Advanced Energy Materials, 2021. 11(2): p. 2000459. DOI: <https://doi.org/10.1002/aenm.202000459>.
5. Pena, M. and J. Fierro, Chemical structures and

- performance of perovskite oxides. *Chemical reviews*, 2001. 101(7): p. 1981-2018.
DOI: <https://doi.org/10.1021/cr980129f>.
6. Nagai, T., et al., Synthesis of nano-sized perovskite-type oxide with the use of polyvinyl pyrrolidone. *Journal of Asian Ceramic Societies*, 2014. 2(4): p. 329-332.
DOI: <https://doi.org/10.1016/j.jascer.2014.08.004>.
7. Siemons, M., et al., Preparation of Nanosized Perovskite-type Oxides via Polyol Method. *Zeitschrift für anorganische und allgemeine Chemie*, 2004. 630(12): p. 2083-2089.
DOI: <https://doi.org/10.1002/zaac.200400300>.
8. Shao, Z., W. Zhou, and Z. Zhu, Advanced synthesis of materials for intermediate-temperature solid oxide fuel cells. *Progress in Materials Science*, 2012. 57(4): p. 804-874.
DOI: <https://doi.org/10.1016/j.pmatsci.2011.08.002>.
9. Shen, Z., et al., BaTiO₃-BiYbO₃ perovskite materials for energy storage applications. *Journal of Materials Chemistry A*, 2015. 3(35): p. 18146-18153.
DOI: <https://doi.org/10.1039/C5TA03614C>
10. Zhu, Y., et al., Phosphorus-doped perovskite oxide as highly efficient water oxidation electrocatalyst in alkaline solution. *Advanced Functional Materials*, 2016. 26(32): p. 5862-5872.
DOI: <https://doi.org/10.1002/adfm.201601902>.
11. Zhang, Z., et al., Tin-doped perovskite mixed conducting membrane for efficient air separation. *Journal of Materials Chemistry A*, 2014. 2(25): p. 9666-9674.
DOI: <https://doi.org/10.1039/C4TA00926F>
12. Pramana, S.S., et al., Crystal structure and surface characteristics of Sr-doped GdBaCo₂O_{6-δ} double perovskites: oxygen evolution reaction and conductivity. *Journal of Materials Chemistry A*, 2018. 6(13): p. 5335-5345.
DOI: 10.1039/C7TA06817D.
13. Chen, Y., et al., Exceptionally active iridium evolved from a pseudo-cubic perovskite for oxygen evolution in acid. *Nature communications*, 2019. 10(1): p. 1-10.
DOI: <https://doi.org/10.1038/s41467-019-08532-3>
14. Yu, J., et al., Advances in porous perovskites: synthesis and electrocatalytic performance in fuel cells and metal-air batteries. *Energy & Environmental Materials*, 2020. 3(2): p. 121-145.
DOI: <https://doi.org/10.1002/eem2.12064>.
15. Zhu, Y., et al., SrNb_{0.1}Co_{0.7}Fe_{0.2}O_{3-δ} perovskite as a next-generation electrocatalyst for oxygen evolution in alkaline solution. *Angewandte Chemie*, 2015. 127(13): p. 3969-3973.
DOI: <https://doi.org/10.1002/ange.201408998>.
16. Bai, S., et al., High-power Li-metal anode enabled by metal-organic framework modified electrolyte. *Joule*, 2018. 2(10): p. 2117-2132.
DOI: <https://doi.org/10.1016/j.joule.2018.07.010>.
17. Liu, H., et al., Cation deficiency design: A simple and efficient strategy for promoting oxygen evolution reaction activity of perovskite electrocatalyst. *Electrochimica Acta*, 2018. 259: p. 1004-1010.
DOI: <https://doi.org/10.1016/j.electacta.2017.10.172>.
18. Tien-Thao, N., et al., Effect of alkali additives over nanocrystalline Co-Cu-based perovskites as catalysts for higher-alcohol synthesis. *Journal of Catalysis*, 2007. 245(2): p. 348-357.
DOI: <https://doi.org/10.1016/j.jcat.2006.10.026>.
19. Li, R., et al., Realizing fourfold enhancement in conductivity of perovskite Li_{0.33}La_{0.55}Ti_{0.33}O₃ electrolyte membrane via a Sr and Ta co-doping strategy. *Journal of Membrane Science*, 2019. 582: p. 194-202.
DOI: <https://doi.org/10.1016/j.memsci.2019.03.074>.
20. Yu, R., et al., Synthesis and characterization of perovskite-type (Li, Sr)(Zr, Nb) O₃ quaternary solid electrolyte for all-solid-state batteries. *Journal of Power Sources*, 2016. 306: p. 623-629. DOI: <https://doi.org/10.1016/j.jpowsour.2015.12.065>.
21. Song, S., et al., Molten-salt synthesis of porous La_{0.6}Sr_{0.4}Co_{0.2}Fe_{0.8}O₂ perovskite as an efficient electrocatalyst for oxygen evolution. *Nano Res.*, 2018. 11(9): p. 4796-4805.
DOI: <https://doi.org/10.1007/s12274-018-2065-1>
22. Mendoza-Mendoza, E., et al., Molten salts synthesis and electrical properties of Sr-and/or Mg-doped perovskite-type LaAlO₃ powders. *Journal of Materials Science*, 2012. 47(16): p. 6076-6085.
DOI: <https://doi.org/10.1007/s10853-012-6520-1>
23. Huang, X., et al., Facile synthesis of porous spherical La_{0.8}Sr_{0.2}Mn_{1-x}Cu_xO₃ (0 ≤ x ≤ 0.4) and nanocubic La_{0.8}Sr_{0.2}MnO₃ with high catalytic activity for CO. *CrystEngComm*, 2018. 20(43): p. 7020-7029.
DOI: <https://doi.org/10.1039/C8CE01000E>.
24. Wang, Y., et al., Morphologically controlled synthesis of porous spherical and cubic LaMnO₃ with high activity for the catalytic removal of toluene. *ACS applied materials &*

- interfaces, 2014. 6(20): p. 17394-17401.
DOI: <https://doi.org/10.1021/am500489x>.
25. Song, Z., et al., Recent progress on MOF-derived nanomaterials as advanced electrocatalysts in fuel cells. *Catalysts*, 2016. 6(8): p. 116.
DOI: <https://doi.org/10.3390/catal6080116>.
26. Shin, J.F., et al., Self-assembled dynamic perovskite composite cathodes for intermediate temperature solid oxide fuel cells. *Nature Energy*, 2017. 2(3): p. 1-7.
DOI: <https://doi.org/10.1038/nenergy.2016.214>
27. Sun, H., et al., Multi-active sites derived from a single/double perovskite hybrid for highly efficient water oxidation. *Electrochimica Acta*, 2019. 299: p. 926-932.
DOI: <https://doi.org/10.1016/j.electacta.2019.01.067>.
28. Yang, G., et al., Enhancing electrode performance by exsolved nanoparticles: a superior cobalt-free perovskite electrocatalyst for solid oxide fuel cells. *ACS applied materials & interfaces*, 2016. 8(51): p. 35308-35314.
DOI: <https://doi.org/10.1021/acsami.6b12157>
29. Zahrani, E.M. and M. Fathi, The effect of high-energy ball milling parameters on the preparation and characterization of fluorapatite nanocrystalline powder. *Ceramics International*, 2009. 35(6): p. 2311-2323.
DOI: <https://doi.org/10.1016/j.ceramint.2009.01.012>.
30. Zhang, R., H. Alamdari, and S. Kaliaguine, SO₂ poisoning of LaFeO₃- δ CuO₂ perovskite prepared by reactive grinding during NO reduction by C₃H₆. *Applied Catalysis A: General*, 2008. 340(1): p. 140-151.
DOI: <https://doi.org/10.1016/j.apcata.2008.02.028>.
31. Tien-Thao, N., et al., LaCo_{1-x}Cu_xO_{3- δ} perovskite catalysts for higher alcohol synthesis. *Applied Catalysis A: General*, 2006. 311: p. 204-212.
DOI: <https://doi.org/10.1016/j.apcata.2006.06.029>.
32. Li, L., et al., Topochemical molten salt synthesis for functional perovskite compounds. *Chemical science*, 2016. 7(2): p. 855-865.
DOI: [10.1039/C5SC03521J](https://doi.org/10.1039/C5SC03521J).
33. Song, Y.-L., et al., Molten salt synthesis and supercapacitor properties of oxygen-vacancy LaMnO₃- δ . *Journal of Energy Chemistry*, 2020. 43: p. 173-181.
DOI: <https://doi.org/10.1016/j.jechem.2019.09.007>.
34. Liu, X., et al., Enhanced microwave absorption properties by tuning cation deficiency of perovskite oxides of two-dimensional LaFeO₃/C composite in X-band. *ACS applied materials & interfaces*, 2017. 9(8): p. 7601-7610.
DOI: <https://doi.org/10.1021/acsami.6b15379>
35. Fechler, N., T.P. Feller, and M. Antonietti, "Salt templating": a simple and sustainable pathway toward highly porous functional carbons from ionic liquids. *Advanced Materials*, 2013. 25(1): p. 75-79.
DOI: <https://doi.org/10.1002/adma.201203422>.
36. Liu, X. and M. Antonietti, Moderating black powder chemistry for the synthesis of doped and highly porous graphene nanoplatelets and their use in electrocatalysis. *Advanced Materials*, 2013. 25(43): p. 6284-6290.
DOI: <https://doi.org/10.1002/adma.201302034>.
37. Mao, Y., S. Banerjee, and S.S. Wong, Large-scale synthesis of single-crystalline perovskite nanostructures. *Journal of the American Chemical Society*, 2003. 125(51): p. 15718-15719.
DOI: <https://doi.org/10.1021/ja038192w>
38. Kačanka, M., et al., The magnetic and neutron diffraction studies of La_{1-x}Sr_xMnO₃ nanoparticles prepared via molten salt synthesis. *Journal of Solid State Chemistry*, 2015. 221: p. 364-372.
DOI: <https://doi.org/10.1016/j.jssc.2014.10.024>.
39. Li, F., et al., Solid-State Synthesis of LaCoO₃ Perovskite Nanocrystals. *Journal of the American Ceramic Society*, 2002. 85(9): p. 2177-2180.
DOI: <https://doi.org/10.1111/j.1151-2916.2002.tb00431.x>.
40. Deng, X., et al., Molten salt synthesis of nitrogen-doped carbon with hierarchical pore structures for use as high-performance electrodes in supercapacitors. *Carbon*, 2015. 93: p. 48-58.
DOI: <https://doi.org/10.1016/j.carbon.2015.05.031>.
41. Zhou, H., Y. Mao, and S.S. Wong, Probing structure-parameter correlations in the molten salt synthesis of BaZrO₃ perovskite submicrometer-sized particles. *Chemistry of Materials*, 2007. 19(22): p. 5238-5249.
DOI: <https://doi.org/10.1021/cm071456j>.
42. Sun, Y.-F., et al., Smart tuning of 3D ordered electrocatalysts for enhanced oxygen reduction reaction. *Applied Catalysis B: Environmental*, 2017. 219: p. 640-644.
DOI: <https://doi.org/10.1016/j.apcatb.2017.08.017>.
43. Yang, Y., et al., In Situ Tetraethoxysilane-Templated Porous BaO. 5SrO. 5CoO. 8FeO. 2O_{3- δ} Perovskite for the Oxygen Evolution Reaction. *ChemElectroChem*, 2015. 2(2): p. 200-203.
DOI: <https://doi.org/10.1002/celec.201402279>.

44. Xu, Y., et al., Carbon-coated perovskite BaMnO₃ porous nanorods with enhanced electrocatalytic perporites for oxygen reduction and oxygen evolution. *Electrochimica Acta*, 2015. 174: p. 551-556.
DOI: <https://doi.org/10.1016/j.electacta.2015.05.184>.
45. Sennu, P., et al., Exceptional catalytic activity of hollow structured La_{0.6}Sr_{0.4}CoO_{3-δ} perovskite spheres in aqueous media and aprotic LiO₂ batteries. *Journal of Materials Chemistry A*, 2017. 5(34): p. 18029-18037.
DOI: <https://doi.org/10.1039/C7TA04189F>.
46. Han, X., et al., Porous perovskite CaMnO₃ as an electrocatalyst for rechargeable LiO₂ batteries. *Chemical Communications*, 2014. 50(12): p. 1497-1499.
DOI: <https://doi.org/10.1039/C3CC48207C>.
47. Bu, Y., et al., A highly efficient and robust cation ordered perovskite oxide as a bifunctional catalyst for rechargeable zinc-air batteries. *Acs Nano*, 2017. 11(11): p. 11594-11601.
DOI: <https://doi.org/10.1021/acsnano.7b06595>.
48. Ashok, A., et al., Combustion synthesis of bifunctional LaMO₃ (M= Cr, Mn, Fe, Co, Ni) perovskites for oxygen reduction and oxygen evolution reaction in alkaline media. *Journal of Electroanalytical Chemistry*, 2018. 809: p. 22-30.
DOI: <https://doi.org/10.1016/j.jelechem.2017.12.043>.
49. Zhu, Y., et al., A perovskite nanorod as bifunctional electrocatalyst for overall water splitting. *Advanced Energy Materials*, 2017. 7(8): p. 1602122.
DOI: <https://doi.org/10.1002/aenm.201602122>.
50. Zhao, Y., et al., Hierarchical mesoporous perovskite La_{0.5}Sr_{0.5}CoO₂ nanowires with ultrahigh capacity for Li-air batteries. *Proceedings of the National Academy of Sciences*, 2012. 109(48): p. 19569-19574.
DOI: <https://doi.org/10.1073/pnas.121031510>.
51. Liu, L., et al., In situ fabrication of highly active γ-MnO₂/SmMnO₃ catalyst for deep catalytic oxidation of gaseous benzene, ethylbenzene, toluene, and o-xylene. *Journal of hazardous materials*, 2019. 362: p. 178-186.
DOI: <https://doi.org/10.1016/j.jhazmat.2018.09.012>.
52. Jiang, S., et al., Hierarchical porous cobalt-free perovskite electrode for highly efficient oxygen reduction. *Journal of Materials Chemistry*, 2012. 22(32): p. 16214-16218.
DOI: <https://doi.org/10.1039/C2JM33311B>.
53. He, J., et al., 3D ordered macroporous SmCoO₃ perovskite for highly active and selective hydrogen peroxide detection. *Electrochimica Acta*, 2018. 260: p. 372-383.
DOI: <https://doi.org/10.1016/j.electacta.2017.12.084>.
54. Zhuang, S., et al., Preparation of homogeneous nanoporous LaO. 6CaO. 4CoO₃ for bi-functional catalysis in an alkaline electrolyte. *Electrochemistry communications*, 2011. 13(4): p. 321-324. DOI: <https://doi.org/10.1016/j.elecom.2011.01.014>.
55. Zhen, D., et al., Electrospun porous perovskite La_{0.6}Sr_{0.4}Co_{1-x}Fe_xO_{3-δ} nanofibers for efficient oxygen evolution reaction. *Advanced Materials Interfaces*, 2017. 4(13): p. 1700146.
DOI: <https://doi.org/10.1002/admi.201700146>.
56. Jin, C., et al., Electrochemical study of Ba_{0.5}Sr_{0.5}Co_{0.8}Fe_{0.2}O₃ perovskite as bifunctional catalyst in alkaline media. *international journal of hydrogen energy*, 2013. 38(25): p. 10389-10393.
DOI: <https://doi.org/10.1016/j.ijhydene.2013.06.047>.
57. Gosavi, P.V. and R.B. Biniwale, Pure phase LaFeO₃ perovskite with improved surface area synthesized using different routes and its characterization. *Materials Chemistry and Physics*, 2010. 119(1-2): p. 324-329.
DOI: <https://doi.org/10.1016/j.matchemphys.2009.09.005>.
58. Pham, T.V., et al., Carbon-and binder-free 3D porous perovskite oxide air electrode for rechargeable lithium-oxygen batteries. *Journal of Materials Chemistry A*, 2017. 5(11): p. 5283-5289. DOI: <https://doi.org/10.1039/C6TA10751F>.
59. Hua, B., et al., All-in-one perovskite catalyst: smart controls of architecture and composition toward enhanced oxygen/hydrogen evolution reactions. *Advanced Energy Materials*, 2017. 7(20): p. 1700666.
DOI: <https://doi.org/10.1002/aenm.201700666>.
60. Pinna, N. and M. Niederberger, Surfactant-free nonaqueous synthesis of metal oxide nanostructures. *Angewandte Chemie International Edition*, 2008. 47(29): p. 5292-5304.
DOI: <https://doi.org/10.1002/anie.200704541>.
61. Fu, S., et al., Low temperature synthesis and photocatalytic property of perovskite-type LaCoO₃ hollow spheres. *Journal of Alloys and Compounds*, 2013. 576: p. 5-12.
DOI: <https://doi.org/10.1016/j.jallcom.2013.04.092>.
62. Ji, K., et al., One-pot hydrothermal preparation and catalytic performance of porous strontium ferrite hollow spheres for the combustion of toluene. *Journal of Molecular Catalysis A: Chemical*, 2013. 370: p. 189-196. DOI: <https://doi.org/10.1016/j.molcata.2013.01.013>.

63. Gao, P., et al., Perovskite LaMnO₃ hollow nanospheres: The synthesis and the application in catalytic wet air oxidation of phenol. *Materials Letters*, 2013. 92: p. 173-176.
DOI: <https://doi.org/10.1016/j.matlet.2012.10.091>.
64. Kim, Y., et al., Ferromagnetic nanospheres of perovskite manganite La_{0.7}Ca_{0.3}MnO₃ prepared by template replication in porous carbon framework. *Journal of applied physics*, 2004. 95(11): p. 7088-7090.
DOI: <https://doi.org/10.1063/1.1687634>.
65. Ko, Y., C.L. Cahill, and J. Parise, Novel layered sulfides of tin: synthesis and structural characterization of Cs₄Sn₅S₁₂·2H₂O and Sn₅S₁₂ (N₂C₄H₁₁)₂ (N₄C₁₀H₂₄). *Journal of the Chemical Society, Chemical Communications*, 1994(1): p. 69-70
DOI: <https://doi.org/10.1039/C39940000069>
66. Kresge, a.C., et al., Ordered mesoporous molecular sieves synthesized by a liquid-crystal template. *mechanism. nature*, 1992. 359(6397): p. 710-712.
DOI: <https://doi.org/10.1038/359710a0>
67. Zhao, D., et al., Triblock copolymer syntheses of mesoporous silica with periodic 50 to 300 angstrom pores. *science*, 1998. 279(5350): p. 548-552.
DOI: 10.1126/science.279.5350.548.
68. Grosso, C., B.S. Boissiere, and N.P. T Brezesinski, P. Albouy, H. Amenitsch, M. Antonietti, and C. Sanchez, "Periodically Ordered Nanoscale Islands and Mesoporous Films Composed of Nanocrystalline Multimetallic Oxides,". *Nat. Mater*, 2004. 3(11): p. 787-92.
DOI: <https://doi.org/10.1038/nmat1206>
69. Reitz, C., et al., Nanocrystalline NaTaO₃ thin film materials with ordered 3D mesoporous and nanopillar-like structures through PIB-b-PEO polymer templating: Towards high-performance UV-light photocatalysts. *RSC advances*, 2012. 2(12): p. 5130-5133.
DOI: 10.1039/C2RA20203D.
70. Lertpanyapornchai, B., T. Yokoi, and C. Ngamcharussrivichai, Citric acid as complexing agent in synthesis of mesoporous strontium titanate via neutral-templated self-assembly sol-gel combustion method. *Microporous and Mesoporous Materials*, 2016. 226: p. 505-509.
DOI: <https://doi.org/10.1016/j.micromeso.2016.02.020>.
71. Suzuki, N., et al., Synthesis of highly strained mesostructured SrTiO₃/BaTiO₃ composite films with robust ferroelectricity. *Chemistry—A European Journal*, 2013. 19(14): p. 4446-4450.
DOI: <https://doi.org/10.1002/chem.201203421>.
72. Hou, R., P. Ferreira, and P. Vilarinho, A facile route for synthesis of mesoporous barium titanate crystallites. *Microporous and mesoporous materials*, 2008. 110(2-3): p. 392-396.
DOI: <https://doi.org/10.1016/j.micromeso.2007.06.051>.
73. Huang, X., et al., Synthesis and applications of nanoporous perovskite metal oxides. *Chemical science*, 2018. 9(15): p. 3623-3637.
DOI: 10.1039/C7SC03920D.
74. Gu, D. and F. Schüth, Synthesis of non-siliceous mesoporous oxides. *Chemical Society Reviews*, 2014. 43(1): p. 313-344.
DOI: 10.1039/C3CS60155B.
75. Ren, Y., Z. Ma, and P.G. Bruce, Ordered mesoporous metal oxides: synthesis and applications. *Chemical Society Reviews*, 2012. 41(14): p. 4909-4927.
DOI: <https://doi.org/10.1039/C2CS35086F>
76. Wang, Y., et al., Nanocasted synthesis of mesoporous LaCoO₃ perovskite with extremely high surface area and excellent activity in methane combustion. *The Journal of Physical Chemistry C*, 2008. 112(39): p. 15293-15298.
DOI: <https://doi.org/10.1021/jp8048394>.
77. Nair, M.M., F. Kleitz, and S. Kaliaguine, Kinetics of methanol oxidation over mesoporous perovskite catalysts. *ChemCatChem*, 2012. 4(3): p. 387-394.
DOI: <https://doi.org/10.1002/cctc.201100356>.
78. De Lima, R., et al., High specific surface area LaFeCo perovskites—Synthesis by nanocasting and catalytic behavior in the reduction of NO with CO. *Applied Catalysis B: Environmental*, 2009. 90(3-4): p. 441-450.
DOI: <https://doi.org/10.1016/j.apcatb.2009.04.004>.
79. Huang, X., et al., Effect of metal species on the morphology of metal (oxides) within mesochannels of SBA-15 via a double-solvent method. *Microporous and Mesoporous Materials*, 2015. 207: p. 105-110.
DOI: <https://doi.org/10.1016/j.micromeso.2015.01.008>.
80. Huang, X., et al., Effect of surface properties of SBA-15 on confined Ag nanomaterials via double solvent technique. *Microporous and mesoporous materials*, 2011. 144(1-3): p. 171-175.
DOI: <https://doi.org/10.1016/j.micromeso.2011.04.012>.
81. Stein, A., F. Li, and N.R. Denny, Morphological control in colloidal crystal templating of inverse opals, hierarchical structures, and shaped particles. *Chemistry of*

- Materials, 2008. 20(3): p. 649-666.
DOI: <https://doi.org/10.1021/cm702107n>.
82. Chi, E.O., et al., A macroporous perovskite manganite from colloidal templates with a Curie temperature of 320 K. *Chemistry of materials*, 2003. 15(10): p. 1929-1931.
DOI: <https://doi.org/10.1021/cm034031f>.
83. Xu, J., et al., Three-dimensionally ordered macroporous $\text{LaCoFe}_{1-x}\text{O}_3$ perovskite-type complex oxide catalysts for diesel soot combustion. *Catalysis Today*, 2010. 153(3-4): p. 136-142.
DOI: <https://doi.org/10.1016/j.cattod.2010.01.063>.
84. Zhao, Z., et al., Three-dimensionally ordered macroporous $\text{La}_{0.6}\text{Sr}_{0.4}\text{FeO}_{3-\delta}$: High-efficiency catalysts for the oxidative removal of toluene. *Microporous and mesoporous materials*, 2012. 163: p. 131-139.
DOI: <https://doi.org/10.1016/j.micromeso.2012.07.006>.
85. Arandiyana, H., et al., Three-dimensionally ordered macroporous $\text{La}_{0.6}\text{Sr}_{0.4}\text{MnO}_3$ with high surface areas: active catalysts for the combustion of methane. *Journal of Catalysis*, 2013. 307: p. 327-339.
DOI: <https://doi.org/10.1016/j.jcat.2013.07.013>.
86. Arandiyana, H., et al., Three-dimensionally ordered macroporous $\text{La}_{0.6}\text{Sr}_{0.4}\text{MnO}_3$ supported Ag nanoparticles for the combustion of methane. *The Journal of Physical Chemistry C*, 2014. 118(27): p. 14913-14928.
DOI: <https://doi.org/10.1021/jp502256t>.
87. Guo, G., et al., Three dimensionally ordered macroporous Pd-LaMnO_3 self-regeneration catalysts for methane combustion. *Chemical Communications*, 2014. 50(88): p. 13575-13577.
DOI: <https://doi.org/10.1039/C4CC05966B>.
88. Joshi, U.A., et al., Surfactant-free hydrothermal synthesis of highly tetragonal barium titanate nanowires: a structural investigation. *The Journal of Physical Chemistry B*, 2006. 110(25): p. 12249-12256.
DOI: <https://doi.org/10.1021/jp0600110>.
89. Wang, J., et al., Mechanism of hydrothermal growth of ferroelectric PZT nanowires. *Journal of crystal growth*, 2012. 347(1): p. 1-6.
DOI: <https://doi.org/10.1016/j.jcrysgro.2012.03.022>.
90. Chen, X., et al., 1.6 V nanogenerator for mechanical energy harvesting using PZT nanofibers. *Nano letters*, 2010. 10(6): p. 2133-2137.
DOI: <https://doi.org/10.1021/nl100812k>.
91. Rao, S., et al., Weakening of charge order and antiferromagnetic to ferromagnetic switch over in $\text{Pr}_{0.5}\text{Ca}_{0.5}\text{MnO}_3$ nanowires. *Applied Physics Letters*, 2005. 87(18): p. 182503.
DOI: <https://doi.org/10.1063/1.2125129>.
92. McQuaid, R., et al., Domain wall propagation in meso- and nanoscale ferroelectrics. *Journal of Physics: Condensed Matter*, 2011. 24(2): p. 024204.
DOI: <https://doi.org/10.1088/0953-8984/24/2/024204>.
93. Mao, Y., S. Banerjee, and S.S. Wong, Hydrothermal synthesis of perovskite nanotubes. *Chemical communications*, 2003(3): p. 408-409.
DOI: <https://doi.org/10.1039/B210633G>.
94. Fu, L., et al., Magnetic, electronic, and optical properties of perovskite materials, in *Revolution of Perovskite*. 2020, Springer. p. 43-59.
DOI: 10.1039/D1RA08185C.
95. Xia, W., Y. Lu, and X. Zhu, Preparation Methods of Perovskite-Type Oxide Materials, in *Revolution of Perovskite*. 2020, Springer. p. 61-93.
DOI: https://doi.org/10.1007/978-981-15-1267-4_3.
96. Shankar, K.S. and A. Raychaudhuri, Growth of an ordered array of oriented manganite nanowires in alumina templates. *Nanotechnology*, 2004. 15(9): p. 1312.
DOI: <https://doi.org/10.1088/0957-4484/15/9/034>.
97. Chen, F., et al., Synthesis and characterization of $\text{La}_{0.825}\text{Sr}_{0.175}\text{MnO}_3$ nanowires. *Journal of Physics: Condensed Matter*, 2005. 17(44): p. L467.
DOI: <https://doi.org/10.1088/0953-8984/17/44/L02>.
98. Hernandez, B.A., et al., Sol-gel template synthesis and characterization of BaTiO_3 and PbTiO_3 nanotubes. *Chemistry of Materials*, 2002. 14(2): p. 480-482.
DOI: <https://doi.org/10.1021/cm010998c>.
99. Sousa, C., et al., Rapid synthesis of ordered manganite nanotubes by microwave irradiation in alumina templates. *Journal of nanoscience and nanotechnology*, 2009. 9(10): p. 6084-6088.
DOI: <https://doi.org/10.1166/jnn.2009.1572>.
100. Tagliazucchi, M., et al., Synthesis of lanthanum nickelate perovskite nanotubes by using a template-inorganic precursor. *Solid state communications*, 2006. 137(4): p. 212-215.
DOI: <https://doi.org/10.1016/j.ssc.2005.11.022>.
101. Bassiri-Gharb, N., Y. Bastani, and A. Bernal, Chemical solution growth of ferroelectric oxide thin films and nanostructures. *Chemical Society Reviews*, 2014. 43(7): p. 2125-2140.

- DOI: <https://doi.org/10.1039/C3CS60250H>.
102. Schwartz, R.W., Chemical solution deposition of perovskite thin films. *Chemistry of materials*, 1997. 9(11): p. 2325-2340.
DOI: <https://doi.org/10.1021/cm970286f>.
103. Zhang, Q., D. Sando, and V. Nagarajan, Chemical route derived bismuth ferrite thin films and nanomaterials. *Journal of Materials Chemistry C*, 2016. 4(19): p. 4092-4124.
DOI: <https://doi.org/10.1039/C6TC00243A>.
104. Wang, H., G. Meng, and D. Peng, Aerosol and plasma assisted chemical vapor deposition process for multi-component oxide La_{0.8}Sr_{0.2}MnO₃ thin film. *Thin Solid Films*, 2000. 368(2): p. 275-278.
DOI: [https://doi.org/10.1016/S0040-6090\(00\)00781-1](https://doi.org/10.1016/S0040-6090(00)00781-1).
105. Weiss, F., et al., Multifunctional oxide nanostructures by metal-organic chemical vapor deposition (MOCVD). *Pure and Applied Chemistry*, 2009. 81(8): p. 1523-1534.
DOI: <https://doi.org/10.1351/PAC-CON-08-08-10>.
106. Ahluwalia, R., et al., Manipulating ferroelectric domains in nanostructures under electron beams. *Physical review letters*, 2013. 111(16): p. 165702.
DOI: <https://doi.org/10.1103/PhysRevLett.111.165702>
107. Lee, W., et al., Individually addressable epitaxial ferroelectric nanocapacitor arrays with near Tb inch⁻² density. *Nature Nanotechnology*, 2008. 3(7): p. 402-407.
DOI: <https://doi.org/10.1038/nnano.2008.161>
108. Li, Y., et al., Physical processes-aided periodic micro/nanostructured arrays by colloidal template technique: fabrication and applications. *Chemical Society Reviews*, 2013. 42(8): p. 3614-3627.
DOI: <https://doi.org/10.1039/C3CS35482B>.
109. Atta, N.F., A. Galal, and E.H. El-Ads, Perovskite nanomaterials—synthesis, characterization, and applications. *Perovskite Materials—Synthesis, Characterisation, Properties, and Applications*; Pan, L., Ed, 2016: p. 107-151.
DOI: <http://dx.doi.org/10.5772/61280>
110. Atta, N.F., et al., Nano-perovskite carbon paste composite electrode for the simultaneous determination of dopamine, ascorbic acid and uric acid. *Electrochimica Acta*, 2014. 128: p. 16-24.
DOI: <https://doi.org/10.1016/j.electacta.2013.09.101>.
111. Srivastava, A., et al., Effect of cation doping on low-temperature specific heat of LaMnO₃ manganite. *Journal of Magnetism and Magnetic Materials*, 2008. 320(21): p. 2596-2601
DOI: <https://doi.org/10.1016/j.jmmm.2008.05.042>
112. Maroneze, C.M., et al., Electroactive properties of 1-propyl-3-methylimidazolium ionic liquid covalently bonded on mesoporous silica surface: development of an electrochemical sensor probed for NADH, dopamine and uric acid detection. *Electrochimica Acta*, 2014. 123: p. 435-440.
DOI: <https://doi.org/10.1016/j.electacta.2014.01.071>.
113. Vijayakumar, C., et al., Synthesis, characterization, sintering and dielectric properties of nanostructured perovskite-type oxide, Ba₂GdSbO₆. *Bulletin of Materials Science*, 2008. 31(5): p. 719-722
DOI: <https://doi.org/10.1007/s12034-008-0113-2>
114. Cho, Y.-G., et al., Characterization and catalytic properties of surface La-rich LaFeO₃ perovskite. *Bulletin of the Korean Chemical Society*, 2009. 30(6): p. 1368-1372.
DOI: <https://doi.org/10.5012/bkcs.2009.30.6.1368>
115. Qi, J.Q., et al., Direct large-scale synthesis of perovskite barium strontium titanate nano-particles from solutions. *Journal of Solid State Chemistry*, 2005. 178(1): p. 279-284.
DOI: <https://doi.org/10.1016/j.jssc.2004.12.003>.
116. Rafique, M., et al., Fabrication of novel perovskite oxide BaxMn1-xO₃ electrode for supercapacitors. *International Journal of Energy Research*, 2021. 45(3): p. 4145-4154.
DOI: <https://doi.org/10.1002/er.6075>.
117. Medina, M., et al., Low oxygen pressure synthesis of NdNiO_{3-δ} nanowires by electrospinning. *Nano Express*, 2020. 1(1): p. 010028
DOI: <https://doi.org/10.1088/2632-959X/ab8a77>
118. Qiao, H., et al., Preparation and characterization of NiO nanoparticles by anodic arc plasma method. *Journal of Nanomaterials*, 2009. 2009.
DOI: <https://doi.org/10.1155/2009/795928>.
119. Li, R., et al., Large scale synthesis of NiCo layered double hydroxides for superior asymmetric electrochemical capacitor. *Scientific reports*, 2016. 6(1): p. 1-9.
DOI: <https://doi.org/10.1038/srep18737>
120. Harikrishnan, M. and A.C. Bose. LaNiO₃ perovskite oxides by co-precipitation method as electrode for high performance supercapacitor. in *AIP Conference Proceedings*. 2019. AIP Publishing LLC.
DOI: <https://doi.org/10.1063/1.5112968>.
121. Rezlescu, N., et al., Characterization and catalytic properties of some perovskites. *Composites Part B*: 53

- Engineering, 2014. 60: p. 515-522.
DOI: <https://doi.org/10.1016/j.compositesb.2014.01.006>.
122. Seyfi, B., M. Baghalha, and H. Kazemian, Modified LaCoO₃ nano-perovskite catalysts for the environmental application of automotive CO oxidation. Chemical Engineering Journal, 2009. 148(2-3): p. 306-311.
DOI: <https://doi.org/10.1016/j.cej.2008.08.041>.
123. Sim, Y., et al., Catalytic behavior of ABO₃ perovskites in the oxidative coupling of methane. Molecular Catalysis, 2020. 489: p. 110925.
DOI: <https://doi.org/10.1016/j.mcat.2020.110925>.
124. Tan, X., et al., Investigation of perovskite BaCe_{1-x}Mn_xO_{3-δ} for methane combustion. Ceramics International, 2021. 47(7): p. 8762-8768.
DOI: <https://doi.org/10.1016/j.ceramint.2020.11.141>.
125. Meng, M., et al., Mechanochemical redox synthesis of interstitial mesoporous Co_xFe_{1-x}O_y catalyst for CO₂ hydrogenation. Greenhouse Gases: Science and Technology, 2021.
DOI: <https://doi.org/10.1002/ghg.2108>.
126. Poerjoto, A.J., et al., The role of lattice oxygen in CO₂ hydrogenation to methanol over La_{1-x}Sr_xCuO catalysts. Journal of CO₂ Utilization, 2021. 47: p. 101498.
DOI: <https://doi.org/10.1016/j.jcou.2021.101498>.
127. Rojas-Cervantes, M.L. and E. Castillejos, Perovskites as catalysts in advanced oxidation processes for wastewater treatment. Catalysts, 2019. 9(3): p. 230.
DOI: <https://doi.org/10.3390/catal9030230>.
128. Ferri, D., Catalysis by Metals on Perovskite-Type Oxides. 2020, Multidisciplinary Digital Publishing Institute.
DOI: <https://doi.org/10.3390/catal10091062>.
129. Kim, B.-J., et al., Fe-Doping in Double Perovskite PrBaCo₂ (1-x) Fe_{2x}O_{6-δ}: Insights into Structural and Electronic Effects to Enhance Oxygen Evolution Catalyst Stability. Catalysts, 2019. 9(3): p. 263.
DOI: <https://doi.org/10.3390/catal9030263>.
130. Guo, S., et al., K-Modulated Co nanoparticles trapped in La-Ga-O as superior catalysts for higher alcohols synthesis from syngas. Catalysts, 2019. 9(3): p. 218.
DOI: <https://doi.org/10.3390/catal9030218>.
131. Steiger, P., et al., Segregation of Nickel/Iron Bimetallic Particles from Lanthanum Doped Strontium Titanates to Improve Sulfur Stability of Solid Oxide Fuel Cell Anodes. Catalysts, 2019. 9(4): p. 332.
DOI: <https://doi.org/10.3390/catal9040332>.
132. Ismael, M. and M. Wark, Perovskite-type LaFeO₃: photoelectrochemical properties and photocatalytic degradation of organic pollutants under visible light irradiation. Catalysts, 2019. 9(4): p. 342.
DOI: <https://doi.org/10.3390/catal9040342>.
133. Glisenti, A. and A. Vittadini, On the Effects of Doping on the Catalytic Performance of (La, Sr) CoO₃. A DFT Study of CO Oxidation. Catalysts, 2019. 9(4): p. 312.
DOI: <https://doi.org/10.3390/catal9040312>.
134. Aldridge, C., et al., BaTi_{0.8}B_{0.2}O₃ (B= Mn, Fe, Co, Cu) LNT Catalysts: Effect of Partial Ti Substitution on NO_x Storage Capacity. Catalysts, 2019. 9(4): p. 365.
DOI: <https://doi.org/10.3390/catal9040365>.
135. Hyrve, S.M., et al., Catalytic Oxidation of NO over LaCo_{1-x}B_xO₃ (B= Mn, Ni) Perovskites for Nitric Acid Production. Catalysts, 2019. 9(5): p. 429.
DOI: <https://doi.org/10.3390/catal9050429>.
136. Heidinger, B., et al., Reactive grinding synthesis of LaBo₃ (B: Mn, Fe) perovskite; properties for toluene total oxidation. Catalysts, 2019. 9(8): p. 633.
DOI: <https://doi.org/10.3390/catal9080633>.

How to cite this article: Batool SM, Kainat KE, Fazal S, Ahmad F. (2022). Comprehensive review on synthesis of abox material and its catalytic applications. Journal of Chemistry and Environment. 1(1).p.16-55.
<https://doi.org/10.56946/jce.v1i01.49>

Authors Bibliography

Dr. Fawad Ahmad received his Ph.D. degree in physical chemistry in 2018 from University of Science and Technology of China (USTC) under the supervision of Professor Jie Zeng Group at Hefei National Laboratory for Physical Sciences at Microscale USTC. He moved back to his homeland and join University of Wah, Wah-Cantt, Pakistan as assistant professor of chemistry in august 2019. His work is focused on synthesis of nanomaterials and its catalytic application for fuel cell and water decontamination.





Syeda Mehak Batool earned her MSc degree in chemistry from university of Wah in 2019. Currently she is pursuing MS in inorganic chemistry from the same university under the supervision of Dr. Fawad Ahmad, her research interest is synthesis of nano materials

and its catalytic applications.



Khushboo E kainat earned her BS degree in chemistry from university of Wah in 2019. Currently she is pursuing MS in inorganic chemistry from the same university under the supervision of Dr. Fawad Ahmad, her research interest is

synthesis of nanomaterial based novel catalyst.



Suqqyana Fazal earned her MSc degree in chemistry from university of Wah in 2021. Currently she is pursuing MS in inorganic chemistry from the same university under the supervision of Dr. Fawad Ahmad, her research interest is synthesis of nanomaterials and its

application in catalysis, degradation and adsorption.



ARTICLE

Fractionation and Characterization of the Bioactive Compounds of the Extracts of Buds of *Syzygium aromaticum*

Agu Chukwuemeka Leonard*, Omeje Nelson Osita

Department of Chemistry Education
Federal College of Education, Eha-Amufu
Enugu State Nigeria.

Correspondence:
aguemeka45@gmail.com

Abstract

This research focused on the separation and identification of bioactive components of the methanolic extracts of the buds of *Syzygium aromaticum*. A bioassay and phytochemical screening were performed on the various solvent fractions, and the most active fraction was subjected to spectroscopic analysis using infrared, mass spectroscopy, and nuclear magnetic resonance to determine the structure of the active compounds present. The methodology involved extracting the flower buds of *Syzygium aromaticum* using methanol, fractionating the plant extract using three solvents—n-hexane, ethylacetate, and methanol, and performing a bio Using the agar well diffusion method, the antibacterial properties of the three solvent fractions were ascertained. The analysis' findings revealed that each of the three solvent fractions had tannins, alkaloids, flavonoids, and reducing sugars; the only fraction to contain saponins was the ethylacetate fraction, and the only fraction to have glycosides. The results of the study further showed that the ethylacetate fraction had the strongest antimicrobial activity against the test organisms, inhibiting the growth of bacteria such as *Escherichia coli*, *Salmonella typhi*, *Staphylococcus aureus*, *Bacillus subtilis*, and *Candida albicans* at concentrations of 200 mg/mL. The structural elucidation of the active compounds responsible for the antimicrobial was done through spectroscopic analysis using infrared, nuclear magnetic resonance and mass spectroscopy. The antimicrobial activities of this plant highlighted the significance of the extracts in traditional drug preparations, according to the study's findings, which suggested that the antimicrobial properties of the flower buds of *Syzygium aromaticum* may be due to the synergetic or individual effects of the phytoconstituents found.

Keywords: Antimicrobial, characterization, fractionation, screening, *syzygium aromaticum*

1. Introduction

Numerous chemical substances that plants produce have therapeutic benefits in the treatment of ailments. Different plant parts with beneficial chemical constituents have been extracted and biologically tested to demonstrate their therapeutic potentials [1]. Additionally, the modern medications utilized in conventional treatment have been

derived from plants [2]. Therefore, it is not surprising that medicinal plants are widely used in the treatment of a variety of illnesses, such as measles, hepatitis, arthritis, rheumatism, burns, scalds, abdominal colic, peptic ulcer, diarrhea, and dysentery [3]. Proper bioassays need to be conducted to establish the biological activity shown by plant extracts as simple isolation and elucidation of chemical structures of plant extracts may not be enough to identify the medicinal

importance of the plants [4].

Because of its benefits to healthcare, medicinal plants have been the subject of scientific study in many nations. Exploring methods for collecting the necessary plant materials and analyzing their constituents has been sparked by the ongoing interest and quest for natural plant products that can be used as medications [5]. Many of the commercially successful medications used in contemporary medicine were first employed in undeveloped forms in conventional or folk medicine, or for other uses that revealed potential biological utility. The main advantages of employing plant-derived medicines are that they are generally safer than synthetic equivalents, provide significant therapeutic advantages, and are more cost-effective than other forms of therapy.

Syzygium aromaticum or cloves, is a plant in the Myrtaceae family that are indigenous to Indonesia's Maluku Islands. An evergreen tree with broad leaves and terminal clusters of crimson flowers, *S. aromaticum* can reach heights of 8 to 12 meters. The color of the flower buds changes from pale to gradually green to vivid red when they are ready for harvest. Cloves are picked when they are 1.5 to 2.0 cm long and are made up of four unopened petals that create a compact central ball and a long calyx that ends in four spreading sepals. Traditional healers have employed the plant *Syzygium aromaticum* to treat a variety of illnesses like toothache, a burning sensation in the tissue, pains in the body, and used to improve peristalsis [6].

Clove has been utilized in modern aromatherapy to treat illnesses like anxiety, sadness, sexual dysfunction, and weariness. It also works to balance hormones and tone the nervous system [7]. It is also employed in the flavoring of food and pharmaceutical products [8], as well as an antiseptic [9]. This study is consequently embarked upon with the intention of carrying out fractionation, antimicrobial screening, and characterisation of the bio-active chemicals on the methanolic extract of buds of *Syzygium aromaticum* in order to advance research on the pharmacological significance of the clove plant.

1.1 Statement of the problem

The use of different plant parts to cure illnesses is a global phenomenon that has been more prevalent in recent years as scientific evidence of herbal medicines' efficacy has become more publicly available [10]. In order to defend themselves from antimicrobial treatments, bacterial and fungal pathogens have developed a variety of defensive mechanisms. As a result, resistance to both old and new medications is increasing. The majority of medications, including antibiotics, are no longer effective against the intended pathogens. As a result, we see the development of bacteria that are resistant to antibiotics. The majority of conventional medications also cost a lot of money and have many negative side effects for the consumers. The cost of managing patients is very high, particularly in underdeveloped nations. Discovering and identifying new safe drugs without severe side effects has become an important goal of research in biomedical science.

The plant *Syzygium aromaticum* has been recognized as a potential treatment for human illnesses like toothaches, hormonal imbalances, sexual dysfunction, and exhaustion [7]. It has also been recognized as a significant source for the discovery of novel pharmacologically active compounds, from which many drugs can be derived either directly or indirectly [1]. In order to find the compound(s) responsible for the plant's numerous pharmacological and medicinal activities, it is therefore essential to advance the research on the plant by conducting spectroscopic analyses on the plant with reference to its methanolic extract, which is the motivation behind this study.

1.2 Aim and objectives of the study

The study's aim include methanolic extract fractionation, antimicrobial screening, and characterisation of the bioactive components from *Syzygium aromaticum* buds. The study's objectives are as follows:

1. To extract the bioactive components of *Syzygium aromaticum* using methanol
2. To fractionate the plant extract using n-hexane, ethylacetate and methanol
3. To determine the phytochemicals present in the different solvent fractions and to conduct the

antimicrobial screening of the fractions

4. To subject the pure compound of the most active fraction to spectroscopic analysis using infrared, mass spectroscopy and nuclear magnetic resonance with a view to ascertaining the structure of the compounds present.

1.2.1 Scope of the study

1. The fractionation of the methanolic plant extract of *Syzygium aromaticum* using n-hexane, ethylacetate and methanol.
2. The phytochemical screening of the different fractions of the flower buds of *Syzygium aromaticum* to determine the presence of alkaloids, tannin, glycosides, saponins, flavonoids and reducing sugars using standard analytical procedures.
3. Antibacterial screening of the solvent fractions using gram positive *Staphylococcus aureus* and *Bacillus subtilis*, and gram negative *Escherichia coli* and *Salmonella typhi*
4. Antifungal screening of the fungi *Aspergillus niger* and *Candida albicans*
5. Spectroscopic analysis of the pure compound of the most active fraction using Infrared (IR), Mass Spectroscopy and Nuclear Magnetic Resonance (NMR).
6. Identification of the active chemical compounds from the flower buds of *Syzygium aromaticum* that exhibit highest bioassay actions against micro-organisms.

2. Methods

2.1. Plant material:

The *Syzygium aromaticum* flower buds were acquired from the Orie Igbo-Eze Market in the Udenu Local Government Area of Enugu State, Nigeria. A taxonomist from the Department of Plant Science and Biotechnology at the University of Nigeria, Nsukka, Mr. Onyukwu authenticated the flower buds, and the voucher specimen was kept for reference in the departmental herbarium.

2.2 Preparation of plant sample

Syzygium aromaticum flower buds were cleaned before air dried for a week at room temperature. They were ground with a hand grinder. After that, the powder was kept in an airtight container for the remainder of the project.

2.3 Solvent extraction

Methanol was employed in the extraction process. In a 2L sterile bucket, 500g of the powdered plant material was steeped in 1000mL of methanol. Stirred, covered, and left to stand for 48 hours at room temperature. Whatmann No. 1 filter paper was used to filter the mixture, and the filtrate was concentrated using a rotary evaporator before being kept in a refrigerator at 40°C until needed. After extraction, 168.4g of stock extract were obtained.

2.3 Determination of extractive value (percentage yield) of the crude methanol extract

The value of the extract produced by evaporating a solution of the dried flower buds is known as the extractive value of *Syzygium aromaticum* flower buds. To do this, the methanol extract was evaporated in a conical flask with a specified weight, and the difference was measured after the evaporation. The crude methanol extract's extractive value was 33.68%.

2.4 Fractionation of the methanol extract using separating funnel

The methanol extract of the flower buds of *A. Syzygium* was fractionated using ethylacetate, n-hexane, and methanol. The solvents were utilized for the fractionation using separating funnel in the following order of increasing polarity: n-hexane, ethylacetate, and methanol. Following fractionation, the various solvent fractions were gently dried using a rotary evaporator and kept in a refrigerator at 40 degrees Celsius until needed. The stock fractions obtained were 4.93g for the ethylacetate fraction, 5.52g for the n-hexane fraction, and 6.08g for the methanolic fraction.

2.5 Preparation of stock solutions of the different solvent fractions

The stock solvent fractions were used to create the stock solutions for the three solvent fractions, which included 200 mg/mL concentrations of the methanolic, ethylacetate, and n-

hexane fractions. This was accomplished by dissolving 2g of each fraction in 10ml of sterile distilled water. They were clearly labeled and kept at 40°C until needed.

2.6 Preparation of test organisms

The Department of Microbiology, University of Nigeria Nsukka, provided the stock bacterial and fungi isolates that were used in the experiment. The isolate cultures obtained on agar slants were used to create new plates of the test organisms. The isolates were sub-cultured into new, sterile nutritional broth for bacteria and Sabouraud Dextrose Agar SDA for fungus, and incubated for 24 hours at 37°C for bacteria and 25°C for fungi, respectively. By comparing the turbidity to the 0.5 McFarland turbidity standard, they were standardised. To regulate the turbidity of the microbial solution so that the quantity of microorganisms will be within a specific range, the McFarland standard was employed as a guide. The 0.5 McFarland standard was made by continuously swirling 9.95 mL of 0.18M H₂SO₄ with 0.05ml of barium chloride (BaCl₂) (1.17% w/v BaCl₂.2H₂O). The McFarland standard tube was kept in storage with a tight seal to prevent evaporation loss [11, 12, 13].

Colonies of the various isolated bacterial fresh cultures were selected using sterile wire loop, and they were then suspended in 5 mL of nutritional broth in sterile 10 mL bijou bottles with clear labels. They were incubated for 24 hours at 37°C.

2.7. Determination of phytochemical constituents of the fractions

Chemical investigations of the various solvent fractions were conducted for the qualitative assessment of phytochemical contents as described by [14] and [15].

2.8. Determination of saponins

1 mL of the stock solutions (200 mg/mL) of each of the solvent fractions was added to five milliliters of distilled water before being heated. The mixture's soluble portion was heated up and then decanted into a test tube. The solution was used for the following tests:

2.9. Emulsion test

A test tube containing 1mL of the decanted solutions and two

drops of olive oil was thoroughly shaken to see the emulsion.

2.10. Frothing test

A test tube containing 1mL of the filtrates and 3mL of distilled water was violently shaken to observe the presence of stable foam.

2.11. Determination of tannins

Acid test: Into a test tube, 3mL from the stock solution (200mg/mL) of methanol fraction was added to 2mL of 1% hydrogen chloride. The solution was observed for reddish brown ppt. The procedure was repeated for ethylacetate and n-hexane fractions.

Bromine water test: Into a test tube, 2mL from the stock solution (200mg/mL) of methanol fraction was added to 2mL of bromine water. The solution was observed for greenish-red colour. The procedure was repeated for ethylacetate and n-hexane fractions also.

Determination of alkaloids: 5mL of 2% hydrogen chloride acid were added to the methanol fraction (1mL) that was obtained from the stock solution of 200 mg/mL in the test tube. Whatmann No. 1 filter paper was used to filter the combinations after they had been heated in a water bath at 40°C for 10 minutes. The following tests were performed on the filtrate:

Wagner's test: 1mL of Wagner's reagent was added to each filtrate (1mL) in a test tube. The mixture was thoroughly shaken, and a reddish-brown ppt color change revealed the presence of an alkaloid.

Meyer's test: 1 mL of Meyer's reagent was added to 1 mL of each filtrate in a test tube. After thoroughly shaking the combination, an assessment was done for the presence of an alkaloid-indicating cream color. The methanol fraction's alkaloid identification process was repeated for the ethylacetate and n-hexane fractions, respectively.

2.12 Determination of flavonoids

FeCl₃ test: To 1mL of methanol fraction got from 200mg/mL of the stock solution was added 1mL of 10% ferric chloride. The solution was mixed thoroughly and observed for colour change (green/black colour). This procedure was repeated for ethylacetate and n-hexane fractions respectively.

Lead acetate test: To 1mL of methanol fraction (from the stock solution of 200mg/mL) in a test tube was added 1mL of 10% lead acetate. It was mixed thoroughly. The mixture was observed for black colour or ppt, and the procedure repeated for n-hexane and ethylacetate fractions.

2.13 Determination of glycosides

Glycosides were measured by covering the powdered plant bud (1g) with adequate water in a 250mL conical flask. Picrate paper was suspended in the flask by a thread. The flask was heated for one hour at 40°C in a water bath. It was noted that the picrate paper's color changed from yellow to brick-red.

2.14. Determination of reducing sugar

The amount of reducing sugar was determined by adding 7.5mL of Fehling's solution to 1g of powdered plant bud in a test tube. The mixture was heated in a water bath for 5 minutes at 40°C while being watched for a change in color to brick-red.

2.15. Determination of preliminary antimicrobial activity of the different solvent fractions

Using the agar well diffusion technique, the antibacterial activity of the n-hexane, ethylacetate, and methanol fractions was assessed [16]. *Escherichia coli* and *Salmonella typhi* for gram positive bacteria; *Staphylococcus aureus* and *Bacillus subtilis* for gram negative bacteria; *Candida albicans* (yeast) and *Apergillus nigger* (mold) for fungi; and a panel of organisms representing the different classes of microorganisms were used to test the fractions. Each of the bacterial isolates was seeded onto a nutrient agar plate with 0.1 mL of an overnight broth culture, whereas each of the fungal strains was seeded onto a sabouraud dextrose agar plate with a comparable amount. The seeded plates were given time to set before being dried. Eight uniform wells of 8mm in diameter were drilled into the agar's surface using a sterile cork borer.

To each of the agar wells, 0.1mL of each of the solvent fractions of the stock solution (200mg/mL) were added. For the bacterial strains' positive and negative controls, the 7th and 8th wells were filled with 0.1 mL of chloramphenicol (25

mg/mL), while the fungal strains' positive and negative controls were fluconazole (50 mg/mL) and sterile distilled water. For the pre-diffusion step, the plates were left on the bench for 40 minutes. Then, for bacterial isolates, an overnight incubation at 37°C and for fungi isolates, an overnight incubation at 25°C were performed. Each solvent fraction's level of antibacterial activity was quantified by measuring the inhibition zone diameter in millimeters. In triplicates, the sensitivity test was conducted. The zone of inhibition for the specific bacterial and fungal isolates at the given concentration was determined to be the average of the three values.

2.16. Purification of the fraction with the highest anti-microbial activity

Gradient-elution chromatography was used to further purify the solvent fraction with the best anti-microbial activity. For the chromatography, various n-hexane and ethylacetate solvent systems were employed. At the end of use of each solvent system, a thin layer chromatography (TLC) also at a solvent system of 80% n-hexane and 20% ethylacetate was carried out on the eluates to evaluate the presence or lack of compound(s) under a UV light. The Gradient-Elution chromatography process at different solvent systems was carried out until there was no further elution, which was confirmed by subjecting the eluate to UV lamp of the TLC. The eluates that showed identical peaks under the UV lamp were combined together and labelled.

2.17. Spectroscopic analysis of the compound

Spectroscopic analysis was carried out on the fraction with the highest antimicrobial activity to determine the structure of its active component(s). The spectroscopic analysis carried out were Infrared Spectroscopy (IR), Mass Spectroscopy, and Nuclear Magnetic Resonance (NMR).

3. Results and Discussions

3.1. Percentage yield and macroscopic characteristics

Table 1 below shows the extractive yield and macroscopic characteristics of the crude extract of the flower buds of *Syzygium aromaticum*. The percentage yield of the crude extract of the plant was 33.68%, while its macroscopic characteristics showed that it was a solid substance, brown and

sticky in texture.

Table 1. Extraction yield and macroscopic characteristics of the crude methanolic extract

Extract	Percentage yield (%)	Macroscopic characteristics
Crude methanolic extract	33.68	A brown sticky substance

Table 2 below shows the extractive yield and macroscopic characteristics of the three solvent fractions. The % yield of the n-hexane fraction was 32.70%, had a dark green colour with sticky mass texture. The % yield of the methanol fraction was 33.56%. It had a dark brown colour with molten mass texture, while the ethylacetate fraction has a percentage yield of 24.90%. It was an oily mass substance, with greenish colour.

According to the results of the various solvent fractions, the methanol extract of *Syzygium aromaticum* flower buds had the highest extractive value (33.56%), was followed by the n-hexane fraction (32.70%), and had the lowest yield (24.90%). This finding demonstrates that methanol, which is used as the solvent in the fractionation process, has greater extrinsic and fractionating power than n-hexane and ethylacetate.

Table 2. Extraction yield and macroscopic characteristics of the three solvent (n-hexane, methanol and ethylacetate) fractions

Extract	Percentage yield (%)	Macroscopic characteristics
n-hexane fraction	32.70	A dark green colour with sticky mass texture
Methanol fraction	33.56	A dark brown substance with molten mass texture
Ethylacetate fraction	24.90	An oily mass substance, greenish in colour

3.2. Phytochemical screening

The findings of the phytochemical screening of the various fractions of the methanolic extract of *A. syzygium* were displayed in Tables 3, 4, and 5 above. The findings demonstrated that tannins, alkaloids, flavonoids, and reducing sugars were present in all of the fractions. Saponins were only present in the ethylacetate fraction, and glycosides were only found in the n-hexane fraction. Since they extracted all

phytochemicals except for one—glycosides for ethylacetate and saponins for n-hexane—these solvents were discovered to be effective for extracting phytochemicals. Saponins and glycosides were not extracted using methanol.

The chemical makeup of the *Syzygium aromaticum* flower buds' three solvent fractions is revealed by phytochemical screening, which can also be used to look for bioactive substances that could be used to create very beneficial medications [17]. According to the study's phytochemical analysis of *Syzygium aromaticum*'s flower buds, tannins, flavonoids, glycosides, saponins, alkaloids, and reducing sugars are all present. It demonstrates that the solvent fractions of this plant all include tannins, alkaloids, flavonoids, and reducing sugars, whereas only the ethylacetate fraction and n-hexane contain saponins and glycosides, respectively.

The findings, which excluded saponins from the phytochemical content of the methanol and n-hexane fractions, did not accord with the findings of [18], but they did with those of [19]. The geographical locations of the plant may be responsible for this variation. Different phytochemicals have the ability to inhibit microbial growth in various ways; for instance, tannins can work by robbing microbial cells of essential proteins like enzymes, hydrogen bonding, or iron [20, 21].

Tannins are widely known for their diuretic, calming, anti-inflammatory, and anti-microbial activities, as well as their antioxidant and anti-microbial capabilities [22]. Tannin-containing plants are astringent in nature and are used to treat gastrointestinal conditions like diarrhea and dysentery [23]. This could also explain why *Syzygium aromaticum* is used as a traditional treatment for typhoid and digestive problems [24].

Only the ethylacetate fraction, which has the most anti-microbial activity, tested positive for saponins, which are responsible for several pharmacological activities [25]. The majority of the biological effects that have been seen are attributed to saponins, which are regarded as a vital component of traditional Chinese medicine [26]. They reduce cholesterol and have anti-diabetic, anti-carcinogenic, and anti-cancer activities [27]. Additionally, saponins have expectorant, antitussive, and hemolytic properties [15, 28].

The most revered phytochemicals, alkaloids, are thought to be plant material contain alkaloids, which have a characteristic pharmacologically active; they are believed to affect the poisonous nature that boosts their biological capabilities and autonomic nervous system, blood vessels, respiratory system, their activities against cells of foreign species [21]. gastrointestinal tract, uterus, malignant illnesses, infections, Additionally, flavonoids are said to be a key antibacterial and malaria [27]. Alkaloids also have antibacterial, analgesic, component [29, 30], and are potent polyphenolic antioxidants and antispasmodic properties [22]. All solvent fractions of [19].

Table 3. Phytochemical properties of methanolic fraction of flower buds of *Syzygium aromaticum*.

	Phytochemical test	Observation	Methanolic fraction
1.	Tannins		
	Acid test	Reddish brown precipitate observed	+
	Bromine water test	Greenish red colour observed	+
2.	Saponins		
	Frothing test	No thick persistent froth observed	-
	Emulsion test	No emulsion observed	-
3.	Alkaloids		
	Wagner's test	Reddish-brown precipitate observed	+
	Meyer's test	Cream colour precipitate observed	+
4.	Flavonoids		
	Lead acetate test	Black colour or precipitate observed	+
	FeCl ₂ test	Green/black colour observed	+
5.	Glycosides		
	Picrate paper test	No brick red colour observed	-
6.	Reducing sugars		
	Fehling's test	Brick-red precipitate observed	+

+ = Present

- = Absent

Table 4. Phytochemical properties of n-hexane fraction of flower buds of *Syzygium aromaticum*.

	Phytochemical test	Observation	n-hexane fraction
1.	Tannins		
	Acid test	Reddish brown precipitate observed	+
	Bromine water test	Greenish red colour observed	+
2.	Saponins		
	Frothing test	No thick persistent froth observed	-
	Emulsion test	No emulsion observed	-
3.	Alkaloids		
	Wagner's test	Reddish-brown precipitate observed	+
	Meyer's test	Cream colour precipitate observed	+
4.	Flavonoids		
	Lead acetate test	Black colour or precipitate observed	+
	FeCl ₂ test	Green/black colour observed	+
5.	Glycosides		
	Picrate paper test	Brick red colour observed	+
6.	Reducing sugars		
	Fehling's test	Brick-red precipitate observed	+

+ = Present

- = Absent

Table 5. Phytochemical properties of ethylacetate fraction of flower buds of *Syzygium aromaticum*.

	Phytochemical test	Observation	Ethylacetate fraction
1.	Tannins		
	Acid test	Reddish brown precipitate observed	+
	Bromine water test	Greenish red colour observed	
2.	Saponins		
	Frothing test	Thick persistent froth observed	+
	Emulsion test	Emulsion observed	
3.	Alkaloids		
	Wagner's test	Reddish-brown precipitate observed	+
	Meyer's test	Cream colour precipitate observed	
4.	Flavonoids		
	Lead acetate test	Black colour or precipitate observed	+
	FeCl ₂ test	Green/black colour observed	
5.	Glycosides		
	Picrate paper test	No brick red colour observed	-
6.	Reducing sugars		
	Fehling's test	Brick-red precipitate observed	+

+ = Present

- = Absent

Table 6. Sensitivity analysis of the solvent fractions at concentration of 200mg/mL.

Test organisms	Inhibition Zone Diameter, IZD (mm)			Standards	
	Methanolic fraction	n-hexane fraction	Ethylacetate fraction	Fluconazole (50mg/mL)	Chloramphenicol (25mg/mL)
1. <i>Escherichia coli</i>	--	7	17		27
2. <i>Salmonella typhi</i>	--	7	15		21
3. <i>Staphylococcus aureus</i>	--	--	--		19
4. <i>Bacillus subtilis</i>	11	15	7		13
5. <i>Candida albicans</i>	--	20	24	22	
6. <i>Aspergillus niger</i>	--	--	--	19	

Key: -- = No inhibition

Flavonoids have been proven to prevent the peroxidation of polyunsaturated fatty acids in cell membranes by studies of [31, 32]. Additionally, research has demonstrated that flavonoids from the *Syzygium* genus prevent the production of hydroxyl radicals and superoxide ions, two potent peroxidation agents [33]. While heated caramels made of reducing sugars have astringent and poisonous effects, the glycoside works on the heart muscles and increases renal flow (diuresis) [34].

3.3 Anti-microbial screening of the fractions

The findings of the preliminary/sensitivity study of the fractions at concentrations of 200 mg/mL were displayed in Table 6 below. The outcome demonstrated that only *Bacillus subtilis*, with an inhibition zone diameter (IZD) of 11mm, was sensitive to the methanolic fraction. With IZDs of 7 mm, 7 mm, 15 mm, and 20 mm, respectively, the n-hexane fraction

was sensitive to *Escherichia coli*, *Salmonella typhi*, *Bacillus subtilis*, and *Candida albicans*. Further analysis revealed that the ethylacetate fraction had IZDs of 17 mm, 15 mm, 7 mm, and 24 mm for *Escherichia coli*, *Salmonella typhi*, *Bacillus subtilis*, and *Candida albicans*, respectively. The findings indicated that none of the fractions were sensitive to the development of the bacterium *Staphylococcus aureus* and the fungus *Aspergillus niger*.

Comparing the results of the antibacterial activities of the different solvent fractions to that of the standards (Fluconazole for fungi and Chloramphenicol for bacteria), it could be observed that methanolic (11mm) and n-hexane (15mm) fractions exhibited antibacterial activities against *Bacillus subtilis* that could be related to the antibacterial activity of Chloramphenicol (13mm) against *Bacillus subtilis*, while n-hexane (20mm) and ethylacetate (24mm) fractions exhibited

anti-fungal activities similar to Fluconazole (22mm) against *Candida albicans*. From the above result, the three solvent fractions could be compared to the standards (Chloramphenicol and Fluconazole) as their inhibition zone diameter (in mm) is almost the same as that of the standards.

3.4. Antimicrobial activity of the ethylacetate fraction

The ethylacetate fraction's antibacterial activity was displayed in Table 7 below at concentrations ranging from 200 mg/mL to 6.25 mg/mL. According to the results, the fraction exhibited antimicrobial effects on *Escherichia coli* at doses of 200 mg/mL, 100 mg/mL, 50 mg/mL, 25 mg/mL, and 12.5 mg/mL, respectively. The inhibition zone diameters, or IZDs, of the fraction were 17 mm, 14 mm, 10 mm, 6 mm, and 4 mm. Additionally, the fraction inhibits *Salmonella typhi* at 200 mg/mL, 100 mg/mL, 50 mg/mL, and 25 mg/mL, respectively, with IZDs of 15 mm, 11 mm, 9 mm, and 3 mm. Additionally, the ethylacetate fraction inhibited the growth of *Bacillus subtilis*, but only at high concentrations of 200 mg/mL and 100 mg/mL with IZDs of 7 mm and 5 mm, respectively. Conversely, the ethylacetate fraction had the highest inhibition against *Candida albicans*, with IZDs of 24 mm, 20 mm, 18 mm, 11 mm, 7 mm, and 5 mm at concentrations of 200mg/mL.

3.5. Antimicrobial activity of the n-hexane fraction

The antibacterial performance of the n-hexane fraction at concentrations ranging from 20 mg/ml to 6.25 mg/mL is shown in Table 8 below. The results revealed that the fraction had inhibitory effects against *Salmonella typhi* with IZDs of 7mm and 3mm at concentrations of 200mg/mL and 100mg/mL, respectively, but only at high concentrations of 200mg/mL and 100mg/mL with IZDs of 7mm and 4mm. With IZDs of 15mm, 11mm, 9mm, 5mm, and 3mm at concentrations of 200mg/mL, 100mg/mL, 50mg/mL, 25mg/mL, and 12.5mg/mL, respectively, the n-hexane fraction likewise shown a significant inhibitory activity against *Bacillus subtilis*. With IZDs of 20mm, 17mm, 11mm, 9mm, 5mm, and 4mm at doses of 200mg/mL, 100mg/mL, 50mg/mL, 25mg/mL, 12.5mg/mL, and 6.25mg/mL, respectively, the fraction showed the most inhibitory activity

against *Candida albicans*.

3.6. Antimicrobial activity of the methanolic fraction

Table 9 below showed the antimicrobial result of the methanolic fraction. The result showed that the fraction had the lowest inhibition activity against the microorganisms with IZDs of 11mm, 8mm and 3mm at concentrations of 200mg/mL, 100mg/mL and 50mg/mL respectively against *Bacillus subtilis* only. From these results, it could be ascertained that the ethylacetate fraction had the highest antimicrobial activity, followed by n-hexane fraction and the least was methanolic fraction.

The ethylacetate fraction which has the highest anti-microbial activity was further purified using solvent system of 80% n-hexane and 20% ethylacetate. The resulting fraction was again tested against the test microorganisms and the result is shown in table 10 below.

3.7. Antimicrobial activity of the purified ethylacetate fraction

Table 10 below showed the antimicrobial activity of the purified ethylacetate fraction at 100mg/mL to 6.25mg/mL. The outcome demonstrates that the unpurified fraction and the purified fraction almost had the same activity. The antimicrobial results revealed that the fraction had inhibitory activities against *Salmonella typhi* with IZDs of 12mm, 11mm, and 4mm at concentrations of 100mg/mL, 50mg/mL, and 12.5mg/mL, respectively, while inhibiting the growth of *Escherichia coli* with IZDs of 15mm, 12mm, 8mm, and 4mm at concentrations of 100mg/mL, 50mg/mL. The purified ethylacetate fraction demonstrated significant inhibitory activity against *Bacillus subtilis* with IZDs of 9 mm, 7 mm, and 3 mm at concentrations of 100 mg/mL, 50 mg/mL, and 25 mg/mL, respectively. Conversely, it demonstrated its greatest inhibitory activity against *Candida albicans* with IZDs of 22 mm, 19 mm, 13 mm, 10 mm, and 5 mm at concentrations of 100mg/mL, 50mg/mL, 25mg/mL, 12.5mg/mL and 6.25mg/mL respectively.

The n-hexane and ethylacetate fractions of the *Syzygium aromaticum* flower buds evaluated for antibacterial activity against disease-causing organisms showed substantial activity,

but the methanol fraction showed very little activity and exclusively against *Bacillus subtilis*.

Of the three solvent fractions, result showed that both n-hexane and ethylacetate fractions of *Syzygium aromaticum* had antimicrobial activity against all the microorganisms except *Aspergillus niger* while the methanol fraction exhibited very little activity, and only against *Bacillus subtilis*.

The *Syzygium aromaticum* flower buds of n-hexane and ethylacetate fractions had little effect on *Aspergillus niger* but had the strongest effect on *Candida albicans*, with zones of inhibition at 20 and 24 mm, respectively. The zone of inhibition for the methanol fraction's activity against *Bacillus subtilis* was barely 10 mm, and it had no effect on other microbes. This outcome relates to research on the effectiveness of *Syzygium aromaticum* flower buds against yeast microorganisms [35].

From the antimicrobial activity conducted, the ethylacetate fraction had the most inhibitory activity against the microorganisms used for the study, and thus the spectroscopic analysis and Gas Chromatography-Mass Spectroscopy (GC-MS) were carried out on it to determine the active compounds present.

3.8. Spectroscopic analysis of the purified ethyl acetate fraction

The result of the spectroscopic analysis of the ethylacetate fraction was interpreted as follows:

3.8.1. Infrared analysis

The IR result (Table 11) suggested that the isolated compound contains a carbonyl of ketone or aldehyde; a hydroxyl (OH) group band, an NH₂ band probably of an amide given the appearance of C = O band of amide at 1638cm⁻¹. The fraction also contains an aromatic ring and aliphatic chains.

3.8.2. Proton Nuclear Magnetic Resonance (¹H NMR) analysis

Table 12 showed the results of the ¹H NMR of the isolated compounds. From the spectra obtained, signal at 1.29ppm indicated the presence of one hydrogen (1H, CH) singlet, while signal at 2.32ppm showed 3H of CH₃ singlet. Also,

signals at 3.40-3.33ppm showed 6H of CH₃ multiplet; 3.84ppm showed 3H of CH₃ singlet; 3.88ppm showed 4H of 2CH₂ singlet which were hydrogen of cycloalkanes, while 5.15-5.06ppm depicted 12H of 4CH₃ multiplet.

Signals at 5.58ppm showed hydrogen of NH₃ which is singlet and broad, while signals at 5.92 – 6.02ppm showed 5H multiplet which could be aromatic hydrogen; peaks at 6.72 – 6.07ppm depicted 2H multiplet of aromatic hydrogen and peaks at 6.81 – 6.77ppm and 6.88 – 6.86ppm showed 1H multiplet and 2H multiplet respectively, both of which were aromatic hydrogen, while signals at 6.98 – 6.96ppm depicted 1H doublet which could be aromatic hydrogen.

Furthermore, the Correlation Spectroscopy (COSY) result showed that the protons at 3.40 – 3.83ppm were coupled to protons at 6.72 – 6.70ppm, 6.02 – 5.92ppm, and 5.15 – 5.06ppm, while the protons at 6.72 – 6.70ppm were coupled to protons at 3.83ppm. Also, the protons at 6.02 – 5.92ppm were coupled to the protons at 5.15 – 5.06ppm, while the rest of the protons were not coupled.

3.8.3. ¹³C - Nuclear Magnetic Resonance (¹³C – NMR) analysis

Table 13 below showed the results of ¹³C-NMR of the isolated compound. From the spectra obtained, peaks at 169.01 showed the presence of carbonyl (C=O) group; peaks at 151.20, 146.46, 143.91, 139.02, 137.84, 137.05, 131.91, 122.52, 121.18, 120.67, 116.15, 115.51, 114.29, 112.73, 111.14 showed the presence of 15 aromatic, alkenyl or quaternary carbons, signals at 77.39 – 76.76 indicated the solvent peak, while signals at 55.85, 40.09, 39.89, and 20.67 showed the presence of four aliphatic carbons.

3.8.4. Gas Chromatography - Mass Spectroscopy (GC-MS)

The GCMS data revealed compounds which were identified following their fragmentation patterns. The fragmentation pattern of 2-methoxy-4-(prop-2-enyl) phenyl ethanoate is shown in figure 1.

The DEPT result further simplified the ¹³C-NMR result as it showed that there were six quaternary carbons with signals at 169.01, 151.20, 146.46, 143.91, 139.02, and 131.91. The result further showed that there were eight C-H carbons with signals at 137.84, 137.05, 122.52, 121.18, 120.67, 114.29, 112.73,

111.14, while signals at 116.15, 115.51, 40.09, 39.89 indicated the presence of four CH₂ carbons and signals at 55.83 and 20.67 indicated the presence of two CH₃ carbons.

3.8.5. Structure Elucidation

Investigation of the pure ethylacetate fraction was done by the purification of the ethylacetate fraction over polyamide column and elution with solvent system of 80% n-hexane and 20% ethylacetate. The structure of the compounds present in the purified ethylacetate fraction were confirmed by interpretation and comparison of their spectral data. Also, the fragmentation pattern of 4[-5-methylhex-1,4-dienyl]-2-methylidenecyclohexanol is shown in figure 2.

Table 7. Antimicrobial activity of ethylacetate fraction.

Microorganisms	Inhibition Zone Diameters(mm)					
	200mg/mL	100mg/mL	50mg/mL	25mg/mL	12.5mg/mL	6.25mg/mL
<i>Escherichia coli</i>	17	14	10	6	4	--
<i>Salmonella typhi</i>	15	11	9	3	--	--
<i>Bacillus subtilis</i>	7	5	--	--	--	--
<i>Candida albicans</i>	24	20	18	11	7	5

Key: -- = No inhibition

Table 8. Antimicrobial activity of n-hexane fraction.

Microorganisms	Inhibition Zone Diameters(mm)					
	200mg/mL	100mg/mL	50mg/mL	25mg/mL	12.5mg/mL	6.25mg/mL
<i>Escherichia coli</i>	7	4	--	--	--	--
<i>Salmonella typhi</i>	7	3	--	--	--	--
<i>Bacillus subtilis</i>	15	11	9	5	3	--
<i>Candida albicans</i>	20	17	14	11	8	6

Key: -- = No inhibition

Table 9. Antimicrobial activity of methanolic fraction.

Microorganisms	Inhibition Zone Diameters(mm)					
	200mg/mL	100mg/mL	50mg/mL	25mg/mL	12.5mg/mL	6.25mg/mL
<i>Bacillus subtilis</i>	11	8	3	3	--	--

Key: -- = No inhibition

Table 10. Antimicrobial activity of the purified ethylacetate fraction (at 100mg/mL concentration).

Microorganisms	Inhibition Zone Diameters (mm)				
	100mg/mL	50mg/mL	25mg/mL	12.5mg/mL	6.25mg/mL
<i>Escherichia coli</i>	15	12	8	4	--
<i>Salmonella typhi</i>	12	11	4	--	--
<i>Bacillus subtilis</i>	9	7	3	--	--
<i>Candida albicans</i>	22	19	13	10	5

Key: -- = No inhibition

Table 11. Infrared spectroscopy interpretation of the purified ethylacetate fraction.

Infrared Spectroscopy bands (cm ⁻¹)	Possible functional groups
3516, 3455	OH, NH ₂
3177, 3077, 3003	C-H of aromatic ring
2842	C-H of aliphatic ring
1764	C=O of a ketone or aldehyde
1638	C=O of amide
1231, 1196, 1148, 1120, 1032	C-N, C-O

Table 12. Proton NMR (¹H NMR) (δ or ppm) interpretation of isolated compound.

¹ H NMR (δ or ppm)	Interpretations
1.29	s, 1H, CH
2.32	s, 3H, CH ₃
3.40 – 3.33	m, 6H, CH ₃
3.84	s, 3H, CH ₃
3.88	s, 4H, 2CH ₂ of cyclo alkanes
5.15 – 5.06	m, 12H, 4CH ₃
5.58	s, broad, NH ₃
6.02 – 5.92	m, 5H, ArH
6.72 – 6.70	m, 2H, ArH
6.81 – 6.77	m, 1H, ArH
6.88 – 6.86	m, 2H, ArH
6.98 – 6.96	d, J = 8.0 Hz, 1H, ArH

Table 13: ¹³C - NMR interpretation of the isolated compound.

¹³ C – NMR	Interpretations
169.01	C = O
151.20, 146.46, 143.91, 139.02, 137.84, 137.05, 131.91, 122.52, 121.18, 120.67, 116.15, 115.51, 114.29, 112.73, 111.14	15 Aromatic, alkenyl or quaternary carbons
77.39 – 76.76	Solvent peak (CDCl ₃)
55.85, 40.09, 39.89, 20.67	Four aliphatic carbons
DEPT Interpretation	
169.01, 151.20, 146.46, 143.91, 139.02, 131.91	Six Quaternary carbons
137.84, 137.05, 122.52, 121.18, 120.67, 114.29, 112.73, 111.14	Eight C – H carbons
116.15, 115.51, 40.09, 39.89	Four CH ₂ carbons
55.83 and 20.67	Two CH ₃ carbons

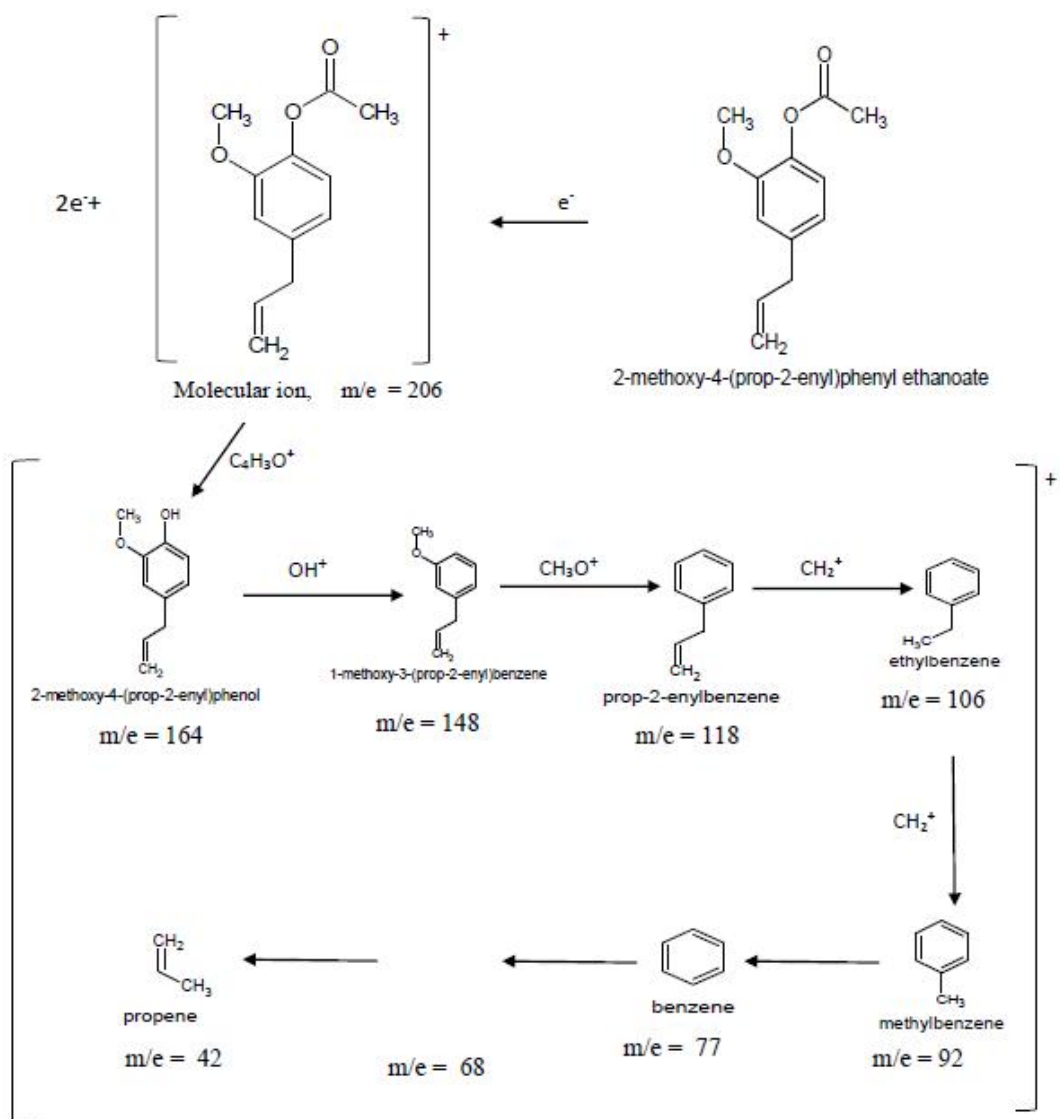


Figure 1. The GCMS fragmentation pattern of 2-methoxy-4-(prop-2-enyl) phenyl ethanoate

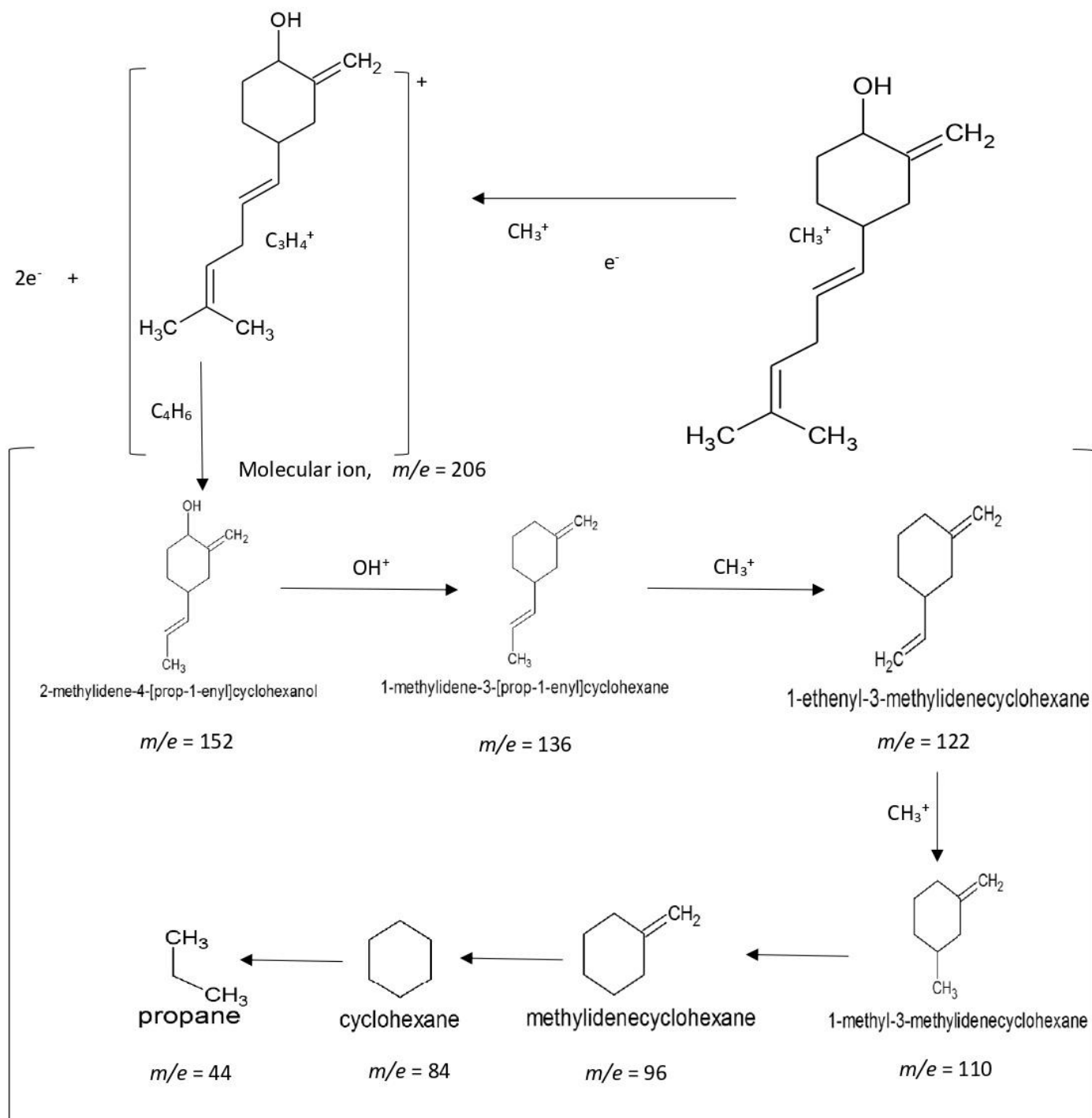


Figure 2. The GCMS fragmentation pattern of 4[-5-methylhex-1,4-dienyl]-2-methylenecyclohexanol

After analyzing the spectral data of the purified ethylacetate fraction, the compounds present were Aceteugenol with IUPAC name of 2-methoxy-4-(prop-2-enyl)phenylethanoate and 4[-5-methylhex-1,4-dienyl]-2-methylidenecyclohexanol. These compounds were authenticated using their fragmentation pattern which agrees with their structures as was revealed by the Gas-Chromatography-Mass Spectroscopy carried out on them. Based on the total spectral analyses done, the structures of the compound are as shown in figure 3.

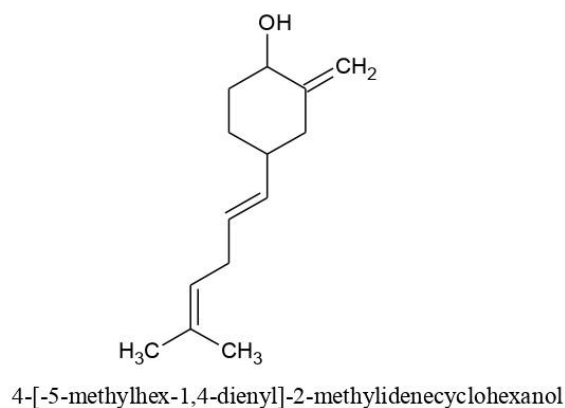
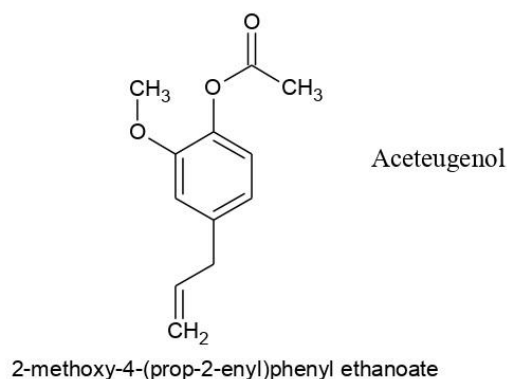


Figure 3. Structures of 2-methoxy-4-(prop-2-enyl)phenyl ethanoate and 4[-5-methylhex-1,4-dienyl]-2-methylidenecyclohexanol

The discovery of these compounds, 2-methoxy-4-(prop-2-enyl)phenyl ethanoate and 4[-5-methylhex-1,4-dienyl]-2-methylidenecyclohexanol, as well as their inhibitory activities against microorganisms, support previous research on the benefits of *Syzygium aromaticum* cloves for oral health by

authors like [36]. Their research showed that *Syzygium aromaticum* extracts had analgesic, anti-inflammatory, and biocidal properties against *A. albopictus* (tiger mosquitos), which aid in the prevention and treatment of malaria. The study's findings also agree with those of [6], which claimed that eugenol, which is present in clove oil from *Syzygium aromaticum* and has antioxidant properties, prevents cancer.

The study's finding is also in line with the study on the antibacterial properties of spices and herbs done by [37]. The research showed that *S. aureus*, *L. monocytogenes*, and *C. albicans* are all inhibited by *Syzygium aromaticum* extract, particularly clove oil. Additionally, eugenol, which has antibacterial, antifungal, anti-inflammatory, insecticidal, and antioxidant properties, is highly concentrated in *Syzygium aromaticum* flower buds, according to a study by [38] on the constituents of the essential oil from the plant's leaves and buds, and it is traditionally used as a flavoring agent and an antimicrobial.

This study therefore supports and justifies the traditional uses of *Syzygium aromaticum* flower buds for treating a variety of diseases. This is in line with the finding made by [38] who investigated the antibacterial activity of *Syzygium aromaticum* flower buds and came to the conclusion that the main ingredient in clove oil, eugenol, is widely used in folk medicine as an analgesic, anti-vomiting, antispasmodic, kidney-enhancer, antiseptic, diuretic, and aromatic agent [39].

4. Conclusion

The natural world contains herbs in abundance. Natural elements found in plants have the potential to improve health. According to the results of the current investigations, the antimicrobial properties of *Syzygium aromaticum* flower buds may result from the combined or individual effects of the phytoconstituents identified. This conclusion is further supported by extensive studies, the findings of which revealed that the phytochemicals present in the various solvent fractions of the plant include tannins, alkaloids, flavonoids, reducing sugars, saponins, and glycosides. As it inhibited the growth of

Escherichia coli, *Salmonella typhi*, *Staphylococcus aureus*, *Bacillus subtilis*, and *Candida albicans* at a concentration of 200 mg/mL, the plant's ethylacetate fraction exhibited the highest antimicrobial activity against the test organisms. Its spectroscopic analysis using infrared spectroscopy, nuclear magnetic resonance, and mass spectroscopy for structural elucidation of the active compounds responsible for the antimicrobial inhibition revealed the presence of two compounds; 2-methoxy-4-(prop-2-enyl) phenylethanoate and

4[-5-methylhex-1,4-dienyl]-2-methylidenecyclohexanol.

The antibacterial properties of this plant brought to light the significance of the extracts in conventional medication formulations. Further investigation should be done to determine how the two compounds obtained from the ethylacetate fractions can be produced in large quantities without incurring much cost for their efficient integration into precursors used for drug production. This is because they inhibited the growth of some microorganisms.

Conflict of Interest

The authors declare no conflict of interest.

Authors' credit statement

Agu, C.L. conducted the research work, wrote the manuscript and has the main idea. Omeje N.O. revised the manuscript and provided suggestions.

Acknowledgement

Profound gratitude goes to Professor I.O. Okerulu of the Department of Pure and Industrial Chemistry, Nnamdi Azikiwe University, Awka, Anambra State, Nigeria for providing guidance and intellectual instructions needed to carry out this research.

Data Availability Statement

The data presented in this study are available on request from the corresponding author.

REFERENCES

1. Cordell, G.A. (2000). Biodiversity and drug discovery: A symbiotic relationship. *Phytochemistry*, 55: 463 – 480.
2. Sofowora, A. (2008). *Medicinal plants and traditional medicine in Africa* (3rd ed). Spectrum Books Limited,

Ibadan.

3. Esuoso, K.O., & Odetoun, S.M. (1995). Proximate chemical composition and possible industrial utilization of *Blighia sapida* seed and oils. *L. Riv. Ital. Grasse*, 72(7): 311 – 313.
4. Ekong, D.E. (1986). Medicinal plants research in Nigeria; Retrospect and prospects. *Medicinal Plant Resources*, 10: 1 – 12.
5. Ilhami, G., Mahfuz, E. & Hassan, Y.A. (2012), Antioxidant activity of clove oil – A powerful antioxidant source. *Arabian Journal of Chemistry*, 5: 489–499.
6. Encyclopedia of Spices (2012). *Cloves: The epicentre*, Retrieved from http://www.encyclopediaofspices.html_30
7. Lehrner, J, Marwinski, G., Hehr, S., Johron, P., & Deecke, L. (2005). Immunological and Psychological Benefits of Aromatherapy Massage. *Evidence Based Complementary Alternative Medicine*, 2(2): 74-92.
8. Cai, L. & Wu, C.D. (1996). Compounds from *Syzygium aromaticum* possessing growth inhibitory activity against oral pathogens. *Journal of Natural Products*, 59(10): 987-990.
9. Seenivasan P., Manickkam, J. & Savarimuthu, I. (2006). *In Vitro* Antibacterial activity of some plant essential oils. *BMC Complement Alternative Medicine*, 6(39), 1–8.
10. Atherden L. M. (1945). *Bentley and drivers text book of pharmaceutical chemistry*, 8th. New York University Press.
11. Cheesbrough, M. (2006). *District laboratory practice in tropical Countries. Part 2*. Cambridge University Press, London.
12. Collins, C.H., Lyne, P.M. & Grange, J.M. (1995). *Microbiological methods*. 7th Edition. Hodder Education Publishers.
13. Baker, F.J., Silverstone, R.E., Pallister, C.J. (1998). *Introduction to medical laboratory technology*. 7th Edition. Reed Educational and Publishing Ltd.
14. Harbone, J.B. (1973), “Essential oils”, In: *Phytochemical methods: A guide to modern techniques in plant analysis*, 3rd ed. Chapman & Hall, PA., USA.

15. Sofowora, A.E. (1993). *Medicinal plants and traditional medicines in Africa*. 2nd Ed. Spectrum Books Limited, Ibadan, Nigeria.
16. Adeniyi, B.A., Odelola, H.A. & Oso, B.A. (1996). Antimicrobial potentials of *Diospyros mespiliformis* (Ebenaceae). *African Journal of Medicines and Medical Sciences*, 25(3): 221-224.
17. Sundaram, M.M., Karthikeyan, K., Sudarsanam, D. & Brindha, P. (2010). Antimicrobial and anticancer studies on *Euphorbia heterophylla*. *Journal of Pharmacy Research*, 3(9): 2332-2333.
18. Ogunkunle, A.T.J. & Ladejobi, T. A. (2006). Ethnobotanical and phytochemical studies on some species of *Senna* in Nigeria. *African Journal of Biotechnology*, 5(21), 2020-2023.
19. Nuhu, A.A. & Aliyu, R. (2008), Effects of *Cassia occidentalis* aqueous leaf extract on biochemical markers of tissue damage in rats. *Tropical Journal of Pharmaceutical Research*, 7(4), 1137-1142.
20. Scalbert, A. (1991), Antimicrobial properties of tannins. *Phytochemistry*, 30, 3875-3883.
21. Akinpelu, D.A., Adegboye, M.F., Adeloye, O.A. & Okoh, A.I. (2008). Biocidal activities of partially purified fractions from methanolic extract of *Garcinia Kola* (Heckel) seeds on bacterial isolates. *Biology Research*, 41, 277-287.
22. Okwu, D.E. & Okwu, M.E. (2004), Chemical composition of *Spondias mombin* Linn plant parts. *Journal of Sustainable Agriculture and Environment*, 6(2), 140-147.
23. Dharnananda, S. G. (2003). "The uses of tannins in Chinese medicine". In: *Proceedings of Institute for Traditional Medicine*, Portland, Oregon.
24. Anthonia, O. & Olumide, O. (2010), *In vitro* antibacterial potential and synergistic effect of South Western Nigerian plant parts used in folklore remedy for *Salmonella typhi* Infection. *Nature and Science*, 8(9), 52-59.
25. Estrada, A., Katselis, G.S., Laarveid, B. & Bari, B. (2000). Isolation and evaluation of immunological adjuvant activities of Saponins from *Polygala senega* L. comparative immunology. *Microbial Infectious Diseases*, 23: 27-43.
26. Liu, J. & Henkel, T. (2002), Traditional Chinese medicine (TCM): Are polyphenols and saponins the key ingredients triggering biological activities? *Current Medical Chemistry*, 9: 1483-1483.
27. Trease, G.E & Evans, W.C. (1996) *Pharmacognosy*. 14th ed, W.B. Saunders Co., London.
28. Okwu, D. E. & Ekeke O. (2005). Phytochemical screening and mineral composition of chewing sticks in South Eastern Nigeria. *Global Journal of Pure and Applied Sciences*, 9(2), 235-238.
29. Chung, K.T., Wong, T.Y., Huang, Y.W & Lin, Y. (1998). Tannins and human health: A review. *Critical Review of Food Science and Nutrition*, 38: 421-464.
30. Karou, D., Dicko, H.M., Simpore, J. & Traore, S.A. (2005), Antioxidant and antibacterial activities of polyphenols from ethnomedical plants from Burkina Faso. *African Journal of Biotechnology*, 4(8), 823-828.
31. Torell, J., Cillard, J. & Cillard, P. (1986), Antioxidant activity of flavonoids and reactivity with peroxy radical. *Biochemistry*, 25(2): 383-385.
32. Faure, P., Roussel, M.A. & Richard, M.J. (1991). Effect of acute zinc depletion on rat lipoprotein distribution and peroxidation. *Biological Trace Element Research*, 28, 135-146.
33. Facino, M.R., Carini, M., Franzoi, L. & Pirola, O. (1990). Phytochemical characterization and radical scavenger activity of flavonoids from *Helichrysum italicum* G. Don (Compositae). *Pharmacology Research*, 22: 709-721.
34. Omotayo, F.O. & Borokini, T.I. (2012), Comparative phytochemical and ethnomedicinal survey of selected medicinal plants in Nigeria. *Scientific Research and Essays*, 7(9): 989-999.
35. Prashar, A.I., Locke, I.C. & Evans, C.S. (2006). Cytotoxicity of clove (*Syzygium aromaticum*) oil and its

- major components to human skin cells. *Cell Prolif.* 39: 241-248.
36. Aishawarya, J., Harini, N. & Kathikeyan, M. (2014). Clove oil and its role in oral health: A review. *International Journal of Pharmaceutical Science and Health Care*, 4(3): 155-168.
37. Snyder, O.P. (2013). *Antimicrobial effects of spices and herbs*. Retrieved 12 August, 2017.
38. Nazrul, P. & Mittal, G.C. (1982). Clinical evaluation of a traditional herbal practice in Nigeria: A Preliminary. *Reproductive Journal of Ethnopharmacology*, 6(3), 355-359.
39. Anand, K.S., Sunil S.D, & Mohammed A. (2009). *Anti-stress activity of hydro alcoholic extracts of Eugenia caryophyllus bud (clove)*. *Indian Journal of Pharmacology*, 41(1), 28-31.

How to cite this article:

Leonard AC, Osita OM. (2022). Fractionation and Characterization of the Bioactive Compounds of the Extracts of Buds of *Syzygium Aromaticum*. 1 (1). p.56-73
<https://doi.org/10.56946/jce.v1i01.28>

**ARTICLE**

Evaluation of Heavy Metals in Drinking Water of Tribal Districts Ex-FATA Pakistan

Rahim Ullah¹, Muhammad Suleman¹, Hina Fazal², Zafar Ali Shah¹, Muhammad Nauman Ahmad¹, Yaseen Ahmed¹, Naik Nawaz¹, Aiman Niaz¹, Kashif Ahmed¹, Kalsoom Bashir¹

¹Department of Agricultural Chemistry and Biochemistry, Agriculture University Peshawar KPK Pakistan, 25000,

² Pakistan council for scientific and industrial research, PCSIR LABS COMPLEX Peshawar 25000

Correspondence: rahim@aup.edu.pk

Abstract

This study was conducted to evaluate the heavy metals such as zinc (Zn), iron (Fe), copper (Cu), nickel (Ni), chromium (Cr), and cadmium (Cd) in seven water samples which were collected from Ex-FATA Pakistan (Bajaur, Mohmand, Khyber, Orakzai, Kurram, South Waziristan and North Waziristan). All samples were digested using the wet digestion method and the digested samples were analyzed for heavy metals using an atomic absorption spectrophotometer. The results of water samples from seven districts were compared to the recommended standard value from the World Health Organization and the Environmental Protection Agency. The results obtained from the analysis for nickel (Ni) showed that the highest concentration (0.093 mg/l) was reported in the water of the Khyber district, while the lowest concentration (0.011 mg/l) was found in the water of the Orakzai district. Iron (Fe) highest concentration (0.86 mg/l) was found in the water of the district Mohmand which was slightly high than the WHO recommended value. The highest concentration (0.19 mg/L) of chromium (Cr) was reported in the water of the Orakzai district. furthermore, the result showed that the highest concentration (0.87 mg/l) of zinc (Zn) was in the Orakzai district, the highest concentration (1.92 mg/l) of copper (Cu) in Khyber and Mohmand districts (1.92 mg/l), while the highest concentration (0.0029 mg/l) of cadmium (Cd) was measured in the water of Orakzai district. After the comparison of all these values to WHO and EPA standard values, this study shows that the water of all these districts is safe for drinking water purposes

Keywords: Drinking water, water quality, heavy metals, human health, environment

1. Introduction

Water is one of the naturally available resources that play a key role in the sustainability of life[1]. Pollutant-free water is a basic need for healthy human life. Toxic heavy metals present in water are very harmful to human health and all living organisms. Some of the heavy metals are required by the human body in small amounts, while their excess leads to dangerous effects on human life. The presence of some heavy metals is very toxic even in very small amounts[2]. Increasing

environmental pollution from pollutants is a major concern for local users. Numerous pollutants are regularly introduced into the aquatic environment, mainly as a result of increasing industrialization, technological advances, population growth, resource depletion, and runoff of household and agricultural waste[3]. Increasing environmental pollution from pollutants is a major concern for local users. Numerous pollutants are regularly introduced into the aquatic environment, mainly as a result of increasing industrialization, technological advances, population growth, resource depletion, and runoff of household

and agricultural waste[4]. Increasing environmental pollution from pollutants is a major concern for local users. Numerous pollutants are regularly introduced into the aquatic environment, mainly as a result of increasing industrialization, technological advances, population growth, resource depletion, and runoff of household and agricultural waste[5].

Historically, there have been reports of heavy metals in drinking water covering their types and amounts, as well as origins, human exposure, hazard, and distance. Despite enormous progress, research is still needed to obtain clean drinking water[6]. Due to their limited economic capacity, many low- and middle-income countries are particularly concerned about the problem of reducing small numbers of heavy metals below the proposed limits[7]. A region's medical problems can be found by routinely evaluating the drinking water quality. Because heavy metals are toxic, persistent, and bio accumulative, heavy metal contamination of drinking water and food has become a major concern for environmental professionals worldwide[8].

The drinking water contaminated with heavy metals has not yet been investigated in the study region. To determine heavy metal concentrations in drinking water from seven EX-FATA districts, this study was designed with population, geology, and anthropogenic inputs in mind, the heavy metal concentrations were examined for potential health risks.

2. Materials and Methods

2.1 Samples Collection

Drinking water samples were collected from seven districts of the Ex-FATA. Two water samples were collected at different points from each district and were mixed. The samples were stored in polythene bottles. The samples were collected in the districts showing in figure 1 and table 1.

2.2 Preparation Sample

The samples were taken to the laboratory where they were later digested. 10 ml of the sample, 5 ml of concentrated HNO₃ and 5 ml of concentrated HCl were used for the digestion. This combination was left at room temperature for almost an hour after being gently stirred and covered with a watch glass. Then the samples were heated on a hot plate until yellow fumes were generated, and the solution became clear.

After cooling, a Millipore filter (0.4 μ) was used to filter the acid solution and deionized water was used to bring the volume to 50 mL[9].

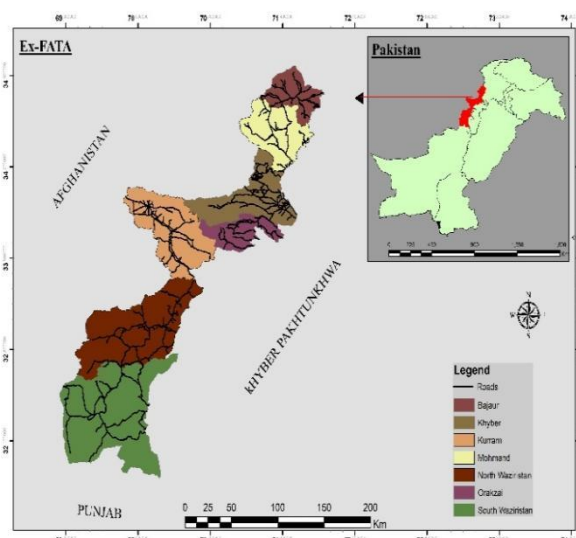


Figure 1. Map representing the districts where samples were collected.

Table 1. Districts and Locations of collected samples.

S.No	District	Location
1	Bajaur	Tehsil Salarzai
2	Mohmand	Tehsil Safi
3	Orakzai	Lower Orakzai
4	North Waziristan	Tehsil Miranshah
5	Khybar	Tehsil Bara
6	Kurram	Lower Kurram
7	South Waziristan	Tehsil Wana

2.3 Preparation of standards

Deionized water was used to dilute several prepared standards of each element (0.1g/100ml; Fisher Chemicals, U.K). Ultra-pure chemicals were used for the analytical analysis. Overall process of research are presented in figure 2.

2.4 Analysis of Heavy metals

Atomic absorption spectrometer (PerkinAnalyst 800 JAPAN) was used for the analysis of heavy metals such as copper (Cu), Iron (Fe), Cadmium (Cd), Chromium (Cr), Zinc (Zn), and Nickle (Ni).

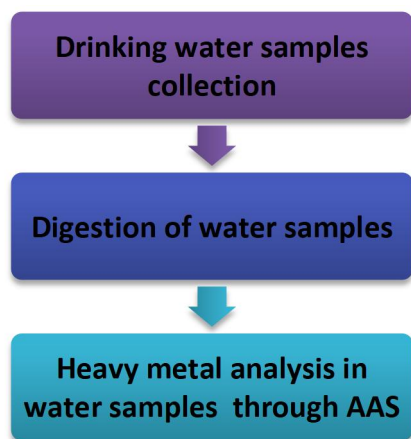


Figure 2. Overall process of research.

3. Results and Discussion

3.1 Concentration of Nickel (Ni):

Nickel is a heavy metal found in the environment such as water, air, and soil. The main sources that generate nickel are the various industries, municipalities, fuels, and industrial effluents[10]. Excessive nickel consumption can cause various diseases in humans such as pulmonary fibrosis, lung cancer, cardiovascular disease, and kidney disease[11]. Figure 3 shows the total concentration of nickel in each water sample, ranging from 0.011 to 0.093 mg/L. The water sample from Khyber district showed the highest concentration with 0.093 mg/L, followed by the water from North Waziristan district and the water from South Waziristan with 0.09 and 0.07 mg/L nickel, which were below that from the WHO recommended value (0.1 mg/L). The lowest concentration of 0.011 mg/L was found in the water of Orakzai district, followed by Bajaur, Mohmand, and Kurram with 0.017, 0.019 and 0.049 mg/L.

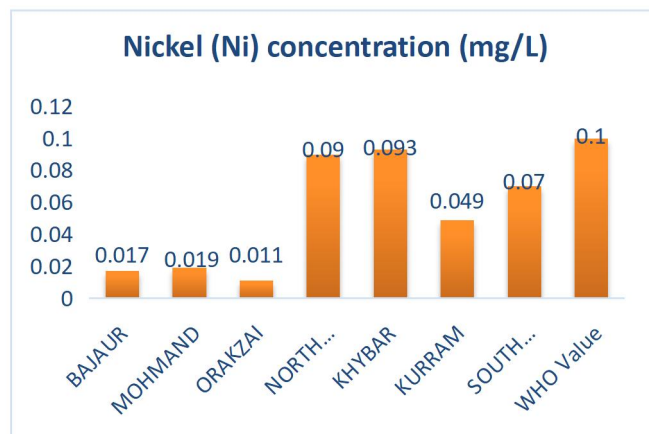


Figure 3. Concentration of Nickel (Ni) in each district water

samples.

3.2 Concentration of Iron (Fe):

In the human body, iron is one of the main elements that play a very important role in various reactions in the human body, such as intracellular and oxygen transport[13]. Iron deficiency can cause various types of diseases in humans, including anemia or iron deficiency, although the high levels of iron in water also have adverse effects on humans, leading to heart problems, liver disease, and diabetes[14]. The availability of iron in the soil is also important for plants as it plays an important role in the process of photosynthesis and chlorophyll[15], while the excess/lower iron content in the soil can cause direct damage to plants, including low-fat or protein content, disruption of root viability and cell damage[16]. The level of iron (Fe) in drinking water recommended by the World Health Organization is 0.3 mg/l[17]. The results of Fig. 4 shows that all fifteen samples have Fe values ranging from 0.07 mg/L to 0.86 mg/L. The highest concentration, above the WHO recommended level (0.3 mg/L), was found in the drinking water of the Mohmand district (0.86 mg/L) and Orakzai district at 0.32 mg/L, while the lowest concentrations were found in the water of the district Khyber (0.07 mg/L).

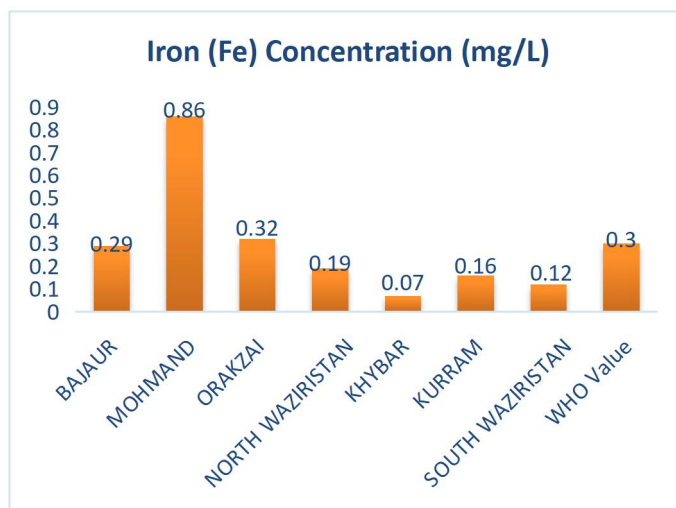


Figure 4. Concentration of Iron (Fe) in each district water samples.

3.3 Concentration of Chromium (Cr)

Chromium is one of the important heavy metals that play an important role in enhancing the action of insulin and lowering the level of glucose in the human body[18], although its excess intake of chromium can lead to irregular heartbeats, headaches,

allergic reactions, kidney and liver damage[19]. The excess amount of chromium in the soil/water also has adverse effects on plant growth and other important metabolic processes that make plants toxic such as oxidative stress[20]. The WHO recommended level of chromium in water is 0.1 mg/L[21]. The results in Fig. 5 show that all of the water samples from the Orakzai district have a high value of 0.19 mg/l, followed by the water sample from the Mohmand district with 0.16 mg/l, which is slightly above the recommended standard value (0.1 mg/l). The lowest concentration was recorded in Khyber District (0.07 mg/L), South Waziristan Water District (0.08 mg/L), Bajaur District (0.09 mg/L), and Kurram District (0.1 mg/L) detected.

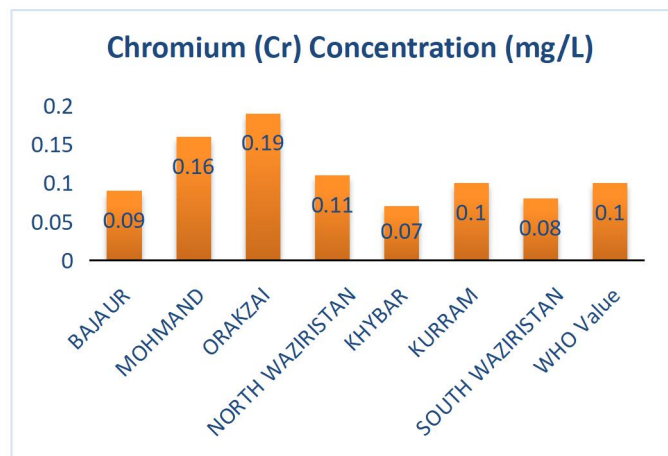


Figure 5. Concentration of chromium (Cr) in each district water samples.

3.4 Concentration of Zinc (Zn):

Zinc is one of the vital heavy metals that play a key role in both humans and plants[22]. Zinc is most abundant in foods that are primarily of animal origin[23]. Low zinc intake can lead to various types of diseases such as wound healing disorders and hypogonadal dwarfism. After taking zinc, it accumulates very quickly in different parts of the body[24]. Excessive intake of zinc has negative effects on humans and plants[25]. The recommended standard value for zinc is 3 mg/L, this standard value is the same for both surface water and groundwater[26]. The results in Fig. 6 show that the concentration value in all water samples is below the recommended standard value, which is between 0.018 mg/L and 0.087 mg/L. The lowest concentration was found in the water of the Bajaur district (0.018 mg/l), while the highest concentration was reported in the water of the Orakzai district

(0.087 mg/l).

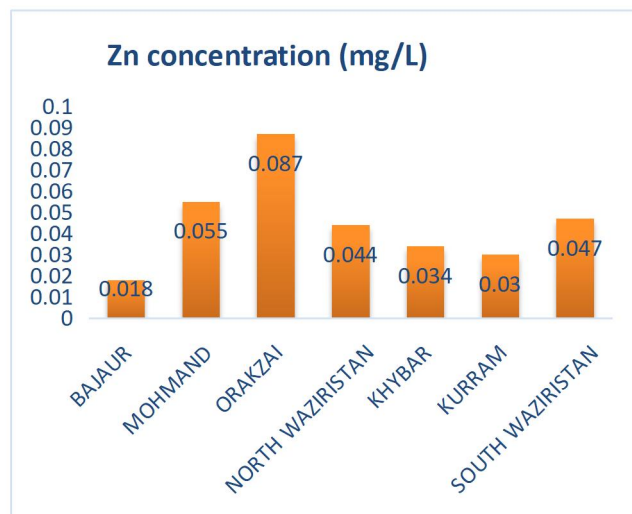


Figure 6. Concentration of Zinc (Zn) in each district water samples.

3.5 Concentration of Copper (Cu):

Copper is one of the most important essential trace elements that play a vital role in the human body[27]. In humans, copper plays an important role in the absorption of iron, the formation of red blood cells, and the maintenance of the immune system and nerve cells[28], while too high or too low levels of copper can cause severe damage to the brain, heart, and kidneys in humans[29]. According to the WHO, the recommended standard range for copper water is 2 mg/L. The result in Fig. 7 shows that the copper concentration in all water samples was below the recommended standard value.

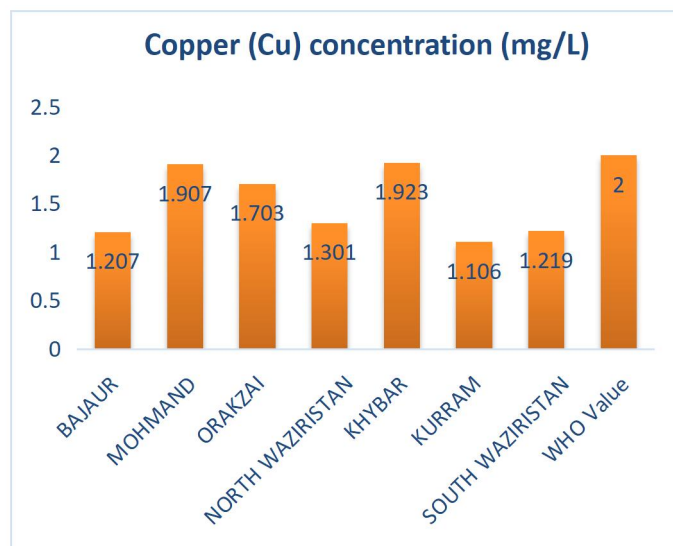


Figure 7. Concentration of Copper (Cu) in each district water samples.

3.6 Concentration of Cadmium (Cd):

Cadmium is one of the toxic heavy metals that are toxic to humans in the long and short term[30]. Intake of cadmium in food and water can cause severe harmful effects on humans like intestinal diseases and kidney damage [31]. According to the world health organization, the recommended safe level of cadmium in water is 0.003 mg/L [32]. The results in Fig. 8 show that the cadmium levels in all water samples are below the WHO-recommended standard level of safe drinking water.

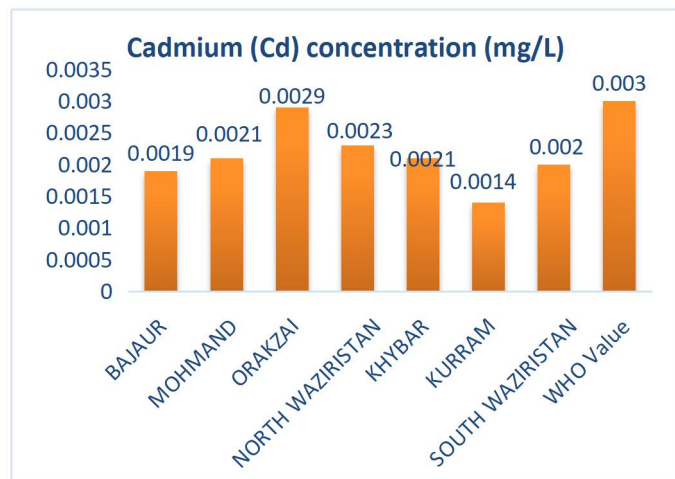


Figure 8. Concentration of Cadmium (Cd) in each district water samples.

4. Conclusion

This study was conducted to evaluate the concentration of six heavy metals in drinking water from Ex-FATA seven districts (Bajaur, Mohmand, Orakzai, Kurram, Khyber, South Waziristan, and North Waziristan). Drinking water samples from the groundwater of the tested sites, after careful examination and comparison with the recommended WHO standard values, the results of this study show that the water in these areas is not carcinogenic and is suitable for both drinking and agricultural use.

Authors Contribution

R.U and M.S supervised the research work, wrote the Manuscript, and has the main idea and NN, AN, KA and KB helps in lab work and samples collection. HF, ZAS, MNA, YA, revised the manuscript and provided suggestions

Conflicts of Interest

There are no conflicts of interest reported by the writers.

Data Availability statement

The data presented in this study are available on request from the corresponding author.

REFERENCES

1. Mutlu, E. and A. Kurnaz, Determination of seasonal variations of heavy metals and physicochemical parameters in Sakiz Pond (Kastamonu-Turkey). *Fresenius Environmental Bulletin*, 2017. 26(4): p. 2806-2815.
2. Bibi, S., et al., Heavy metals analysis in drinking water of Lakki Marwat District, KPK, Pakistan. *World applied sciences journal*, 2016. 34(3): p. 15-19.
3. Lu, Y., et al., Major threats of pollution and climate change to global coastal ecosystems and enhanced management for sustainability. 2018. 239: p. 670-680.
4. Daud, M., et al., Drinking water quality status and contamination in Pakistan. 2017. 2017.
5. Varma, V.G., Water-efficient technologies for sustainable development, in *Current Directions in Water Scarcity Research*. 2022, Elsevier. p. 101-128.
6. Iordache, A.M., et al., Climate change extreme and seasonal toxic metal occurrence in Romanian freshwaters in the last two decades—Case study and critical review. 2022. 5(1): p. 1-9.
7. Das, D., S. Chakraborty, and J. Ghosh, Climate change mitigation strategies: impacts and obstacles in low-and middle-income countries. 2022.
8. Zhu, M., et al., A review of the application of machine learning in water quality evaluation. 2022.
9. Ojekunle, O.Z., et al., Health risk assessment of heavy metals in drinking water leaching through improperly managed dumpsite waste in Kurata, Ijoko, Sango area of Ogun State, Nigeria. 2022. 18: p. 100792.
10. Patel, N., et al., Contamination and Health Impact of Heavy Metals, in *Water Pollution and Remediation: Heavy Metals*. 2021, Springer. p. 259-280.
11. Begum, W., et al., A comprehensive review on the sources, essentiality and toxicological profile of nickel.

2022. 12(15): p. 9139-9153.
12. Kumar, P., et al., Heavy Metals: Transport in Plants and Their Physiological and Toxicological Effects, in Plant Metal and Metalloid Transporters. 2022, Springer. p. 23-54.
 13. Jansen van Rensburg, Z., et al., Toxic feedback loop involving iron, reactive oxygen species, α -synuclein and neuromelanin in Parkinson's disease and intervention with turmeric. 2021. 58(11): p. 5920-5936.
 14. Riaz, N. and M.L.J.J.o. E.B. Guerinot, All together now: regulation of the iron deficiency response. 2021. 72(6): p. 2045-2055.
 15. Khan, Y., S. Shah, and H.J.A. Tian, The roles of arbuscular mycorrhizal fungi in influencing plant nutrients, photosynthesis, and metabolites of cereal crops—A review. 2022. 12(9): p. 2191.
 16. Rizaludin, M.S., et al., The chemistry of stress: understanding the 'cry for help of plant roots. 2021. 11(6): p. 357.
 17. Nguyen, T.T.Q., et al., Removing arsenate from water using batch and continuous-flow electrocoagulation with diverse power sources. 2021. 41: p. 102028.
 18. Bharti, R. and R.J.M.T.P. Sharma, Effect of heavy metals: An overview. 2021.
 19. Ungureanu, E.L. and G. Mustatea, Toxicity of Heavy Metals. 2022.
 20. Prasad, S., et al., Chromium contamination and effect on environmental health and its remediation: A sustainable approaches. 2021. 285: p. 112174.
 21. Karunanidhi, D., et al., Chromium contamination in groundwater and Sobol sensitivity model-based human health risk evaluation from leather tanning industrial region of South India. 2021. 199: p. 111238.
 22. Gondal, A.H., et al., A detailed review study of zinc involvement in animal, plant and human nutrition. 2021. 9(2): p. 262-271.
 23. Duan, M., et al., Zinc nutrition and dietary zinc supplements. 2021: p. 1-16.
 24. Wessels, I., et al., Zinc deficiency as a possible risk factor for increased susceptibility and severe progression of Corona Virus Disease 19. 2022. 127(2): p. 214-232.
 25. Natasha, N., et al., Zinc in the soil-plant-human system: A data-analysis review. 2022. 808: p. 152024.
 26. Shaibur, M.R. and T.K.J.G.f.S.D. Das, Quantification of potentially toxic element contamination in groundwater using the novel particle-induced X-ray emission (PIXE) technique and human health impacts. 2022. 17: p. 100755.
 27. Domingo, J.L., M.J.F. Marquès, and C. Toxicology, The effects of some essential and toxic metals/metalloids in COVID-19: A review. 2021. 152: p. 112161.
 28. Garg, A.J.C.A.i.S. and T. Vol-II, Role of Metal ions in Biological System. 2022: p. 67.
 29. Burkhead, J.L. and J.F.J.A.i.N. Collins, Nutrition Information Brief—Copper. 2022. 13(2): p. 681-683.
 30. Balali-Mood, M., et al., Toxic mechanisms of five heavy metals: mercury, lead, chromium, cadmium, and arsenic. 2021. 12: p. 643972.
 31. Munir, N., et al., Heavy metal contamination of natural foods is a serious health issue: a review. 2021. 14(1): p. 161.
 32. Nantongo, S., Quantitative analysis of heavy metals in juice and water. 2021, Makerere University.

How to cite this article:

Rahim U, Suleman M, Hina F, Zafar A.S, Ahmad M.N, Yaseen A, Niak N, Aiman N, Kashif A, Kalsoom B. (2022). Evaluation of Heavy Metals in Drinking Water of Tribal Districts Ex-FATA Pakistan. Journal of Chemistry and Environment, 1(01), pp 74-79

**REVIEW**

Advancement and Future Perspectives of Prostate Cancer Treatment by Using Plant Bio-actives: A Review

Hira Zulfikar^{1*}, Hunain Zulfikar², Muhammad Furqan Farooq³, Iqbal Ahmed³, Iqra Rani³, Farman Ullah⁴

¹ University of Bologna, Italy

² University of Chinese Academy of Sciences, China

³ Government College University, Faisalabad, Pakistan

⁴ Quaid-i-Azam University Islamabad, Pakistan

Correspondence:

Email: hirazulfikar646@gmail.com

Abstract

Prostate cancer (PCa) is the world's second most lethal and hateful disease in people. Even while chemotherapy medications have made considerable progress against cancer disease, the body still has to deal with their toxic side effects. In order to produce anticancer medicines with the lowest cost and treatment time, mostly people are using mechanistic techniques. In addition to chemotherapy advanced treatment techniques are also used in clinical practices, and they have an excellent healing results by enhancing patient survival rates. The social care net faces serious challenges because of the lack and high cost of modern therapeutic techniques. The side effects of chemotherapeutic drugs and expensive advance techniques triggered the patient interest towards phytochemicals drugs which indicate that nature always attracts human to fulfill their medical needs at very low cost. The pharmaceutical industries are showing strong interest in recent research, which has led to the addition of a quite large number of phyto-medicines in PCa therapeutic practices. Currently, several experimental epidemiological and clinical research reports confirmed that plant bio-actives play a significant role in PCa prevention by using different mechanistic ways such as suppressing adhesion, anti-angiogenesis, pro-apoptosis, anti-proliferation, invasion and migration. This review systematically highlighted various strategies to treat PCa and advances in research by using different bioactive plant extracts and isolated components that have been tested for PCa therapy along with corresponding clinical and epidemiological studies.

Keywords: Prostate Cancer, Phytochemicals, Bio-actives, Treatment, Radiotherapy.

1. Introduction

The prostate is the glandular organ composed of epithelial cells found under the bladder in a fibro-muscular network [1]. Globally, prostate cancer (PCa) is a common fatal disease in men, and the second lethal disease in western countries. It may be asymptomatic in the early stages of PCa [2, 3]. It is a complex and heterogeneous type of malignancy that can be aggressive or non-aggressive early-onset or indolent, high or low grade PCa [4]. However, in Asian countries the relative ratio of PCa is

less than the western countries, but its occurrence and mortality rate is rapidly increasing by adopting the western life style and the exchange in the socio-cultural life [5]. The PCa treatment includes many different methods such as chemotherapy, radiotherapy and surgery. The chemotherapy is more effective at the early stage of tumor development which induces side effects. When the tumor is spread from their original site to the other body parts, all the treatment is ineffective and form some metastatic tumors in the body. The metastasis stage is highly resistant to treatment tactics as a result death ratio increases among

the patients [6, 7]. However, PCa can be treated via radiotherapy define as the treatment through x-ray's or similar form of radiations and can be applied either external or internal, but ensure that the method is complex and highly expensive [8]. Although, advancement in the radiotherapy leads to many of the targeted radionuclide such as Lutetium 177 (Lu) labelled PSMA peptides (a molecular biomarker) that exhibits the high tolerance in men with prostate-cancer and low toxicity profile [9-11]. Meanwhile, surgery is the only effective method when PCa tumor is localized in early diagnosis.

Epidemiological studies show that cancer can be controlled by intake of more fruits and vegetables. Several reports highlighted that the chances of death occur due to cancer is reduced up to 75% by taking nutrients rich food and drinks (Figure 1). Why fruits and vegetables is essential for the control and treatment of cancer? The fruits and vegetables consists of several biomolecules known as phytochemicals (i.e. polyphenolics, terpenes, carotenoids, alkaloids, anthocyanin's etc), they shows simultaneous targeting multiple neoplastic eventuality by preventing the damage of DNA, inhibiting proliferation of malignant cells, modulation inflammation, so that reducing the overall risk of cancer [6, 12]. Scientific community are now moving towards the herbal or natural treatment strategies for the development of safe and effective treating ways of malignancy, due to the adverse side-effects of the chemotherapy and the other treating methods. Ancient literature studies and current epidemiological review are directed the researchers to focus on the treating ways by using phytochemicals, because these are natural, easily acceptable and have minimum side effects [13]. Further, it is estimated that over 60% anti-cancer agents currently used are extracted from natural sources [14]. The increasing attention for chemoprevention by phytochemicals is just because that they have chemical diversity, essential biological activity, easily available,

affordable, and less toxic effects [15]. Meanwhile, with the development of technology it is estimated that many novel natural components from the medicinal plants will be recognized and developed as anti-cancer agents [16, 17]. This review highlights the advances in PCa treatment by using plant bio-actives as the chemo-preventive and anti-inflammatory agents. We mainly focus and analyzed the past ten years' work that was reported on the treatment of the PCa by bioactive components (i.e. tanshinones, biochanin-A, oleuropein, anthocyanins) from different medicinal plants.

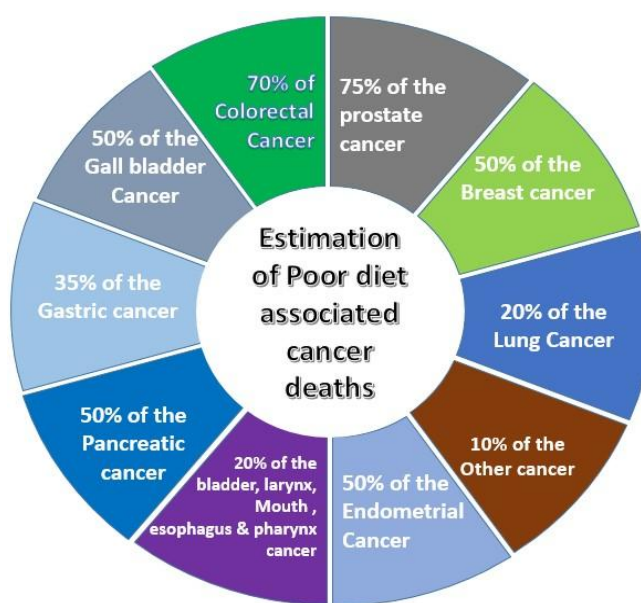


Figure1: Estimation of poor diet associated with cancer deaths. Intake of natural plant based diet (fruits, vegetables etc.) has been proved to significantly reduce the cancer risk. Reproduced with permission: Copyright 2019, MDPI [6].

2. Prostate Cancer (PCa) Treatment

Prostate cancer is the most commonly occurring cancer in men. It is the most lethal malignant disease in people whose symptoms started at the base of the bladder in prostate gland. It surround the proximal part of the urethra that brings the urine from bladder [18]. Geographically, the disease does not show the same symptoms and affects in people across the world, but it shows variation among patients based on their regions or continents. For example,

Asian cancer effected person having less incidence rate of PCa than white and black of Americans. In America and Africa it is reported that 37% of the death occur due to cancer in 2013 [19]. According to UK researchers, approximately and above 40,000 people are effected with this lethal disease every year. National Institute for Health and Care Excellence (NICE) describes PCa as slow growing disease, and hence many of the person may not die due to this disease in their lifespan. In spite of the slow growing localized PCa that is not prove to be fatal, metastatic PCa after multimodal therapy largely remains incurable. About 80% of the newly diagnosed PCa cases are localized, while remaining are the adversely metastatic or advanced. There are various treatment strategies are applying for the treatment of PCa including active surveillance, surgery, radiation therapy, high intensity focused ultrasound, immunotherapy, vaccine treatment, targeted therapy and bone directed treatments etc. [20-23].

2.1 Risk factors of PCa

As PCa is a heterogeneous malignant disease that's why its causality varied from patient to patient even when they have the same type of tumor [24]. Main risk factors that may become the reason of PCa occurrence and associated with treatment, mortality or survival are mainly divided into two categories that is adaptable and non-adaptable risk factors [25]. Some of the main non adaptable risk factors for the PCa to be occur are age, race, ethnicity, geography, positive family history (for example one's first degree relatives) and genetics. Meanwhile, several of other adaptable risk factors such as obesity, smoking, may not the reason of its incidence but may become the booster of PCa mortality. Epigenetic changes i.e. life style ascribe approximately 90%, while somatic or epigenetic changes may attribute 10% or less for the cause of PCa. Similarly, inflammation is the evident process that associates cancer with the main risk factors [26-29]. Physical activities, infectious diseases, external and occupational exposure, endogenous hormones are also

some of the adaptable PCa risk factors[30].

2.1.1 Age

PCa possibly occurs among the older men with the age of about 66 years old. Probability of PCa occurrence is increasing with the age, 5% men with age 60-69 years and 7.69% men with age ≥ 70 years are diagnosed. PCa is the third leading cause of death in men with the age 60-79, and at second with the men age ≥ 80 years [31, 32]. It has been observed that over the age of 50 years risk factors increases in white men with no PCa family history, and in black men over the age of 50 having PCa family history [33].

2.1.2 Race, Ethnicity and Geography

Globally, the occurrence of PCa is vary on the basis of geography. In developed countries of the world such as Western and North Europe, North America and Australia, the rate of PCa is more than the rest of the world. The developed counties have the facilities for its early detection, screening and medical cares. In contrast death rate associated with PCa is highest in ancient African. Based on population it was reported i.e., GLOBOCAN, 2012, Sub-Saharan African (SSA) and Afro-Caribbean (AC) people are suffered from the world highest death rate due to PCa with the rate 18.7-29.3 deaths per 100,000 [29]. Main reason of these differences of PCa between the countries has not clear entirely. It may have attributed to prostate specific antigen (PSA) testing the main reason of the worldwide variations of PCa incidence. Recent research demonstrated that approximately 20-40% of the PCa cases in Europe and USA may because of the over diagnosis via extensive PSA testing [3].

However, race is actually not associated with the survival after local treatment in metastatic PCa patients. The radiotherapy treated patients of Caucasian race are more associated with the higher cancer-specific mortality and overall mortality than that of the African American race. In the study 2004-2014, people with newly diagnosed metastatic PCa 408 (77.2%) Caucasians and 121 (22.8%) Africa-American's were treated with local-therapy: radiotherapy (n=357) or (n=172). When local therapy

includes radical prostatectomy then the Caucasian race patients demonstrates comparatively higher survival vs. African American's: cancer specific mortality free survival 123 vs. 63 months ($p=0.004$) and overall mortality free survival were 108 vs 46 months ($p=0.002$). Thus, it is evident from the foregoing details that when radical prostatectomy is used as local therapy, there will be no racial differences in cancer-specific mortality or total mortality [34].

2.1.3 Family history and Genetics

Family history of PCa is strongly associated with the increased risk of PCa incidence and also the higher mortality rate. A recent analytical study reveals the relationship between the PCa incidence and that of the positive family history of PCa are highly associated with the increased risk of PCa in overall cohort of PCa patients and also the PCa risk in non-screened sub-cohort. From the total 74,781 participants, 5281 participants were having the first degree relative (FDR) positive family history and 69,500 participants was without any positive family history. From the participants having no family history of PCa in FDR, PCa were to be diagnosed in the total of 7540 participants' (10.5%). However, the patients having the family history of PCa in FDR are 889 (16.5%) from the total are diagnosed [35].

Mutations play a major role in PCa carcinogenesis, as family history and race are linked to PCa incidence and mortality. Family history helps identify PCa-prone genes. Many of studies have identified some of the susceptible genes that are RNASEL, ELAC2, MSR1 and HOXB13. Among them HOXB13 found to be the gene play significant role in the PCa development that is actually the homeo-box transcription factor gene [36]. Increased risk factors for PCa has been notably demonstrated by the BRCA2 and HOXB13 mutations and observed more commonly in early onset PCa diagnosis among the patients. It has been shown that HOXB13 recurrent mutation leads to the hereditary PCa [37].

2.1.4 Obesity

Weight gain or obesity is highly associated with the increased risk of fatal and advanced level of PCa. Metabolic changes that are concerned with obesity or weight gain may become the reason for PCa development [38]. Obesity may play its role as a factor that leads to the less likely early stage PCa diagnosis in the obese patients. Physical examination, laboratory test and imaging process may hindered due to the adiposity [39]. A quantitative study on the relationship between obesity and PCa had done. In cohort studies total of the 3,569,926 individuals were selected in 17 studies takes up to the result that obesity was not as such associated with the PCa incidence. However, further analysis provides with the evidences that obesity were significantly associated with the high risk of PCa aggressiveness [40, 41].

2.1.5 Smoking

Smoking increases PCa incidence and death. Cigarettes' mutagens may induce prostate tumorigenesis [42]. Smokers PCa risk factors rise, leading to PCa-related death. Many studies have linked aggressive-violent PCa to smoking at diagnosis [43]. A quantitative cohort study elaborated the PCa specific mortality associated with smoking, leading to the results that PCa patients with current smoking are at high risk of PCa specific mortality compared to non-smokers, and this increased risk was also partially attributable to tumor characteristics [44]. Recent studies also provides with the evidence that smoking at the time of diagnosis enhance the risk for PCa specific and all-cause mortality [45].

3. PCa therapeutic strategies: A brief summary

PCa treatment includes many different methods such as chemotherapy, radiotherapy, immunotherapy, hormone therapy, and surgery. In the following sections we briefly explain all these types of clinically practiced strategies.

3.1 Chemotherapy

Chemotherapy kills cancerous cells by stopping their replication. Chemotherapeutic agents may cause cell death by producing reactive oxygen species, necrosis or apoptosis of malignant cells, or influencing cell proliferation enzymes. Chemotherapeutic agents are

categorized by their chemical structure, mode of action, and interaction with other drugs, such as alkylating, cross-linking, intercalating, DNA cleaving, and anti-tubulin agents. Treatment by chemotherapy has been used by targeting the escalation potential and metastatic ability of the cancerous tumor cells. Present use of chemotherapy involves DNA interactive agents (doxorubicin, cisplatin), anti-tubulin agents (taxanes), antimetabolite (i.e. methotrexate), molecular targeting agents and hormones [46, 47].

In an analytical study exhibits the results that N-acetylated α -linked acidic dipeptides (NAALADase) activity of PSMA expressing cells can be inhibited by the nanoparticle conjugate forming a dendrimer G5 PAMAM while they bind specifically to these cells. In nanoparticle conjugate the drug methotrexate and a small targeting agent molecule glutamate urea conjugated through the serum stable amide links to a dendrimer G5 PAMAM. In vitro study of this target showed the more cytotoxic behavior towards LNCap cells as compared to PC-3 cells. Maximum of the inhibition of cell growth was reached approximately at 300nM that was about 50% for the conjugate and 70% for the free methotrexate [48]. Despite progress in developing strong chemotherapeutic drugs, their toxic effect on normal body cells (such as hair loss) and adverse concomitant in multiple organ systems (i.e. gastrointestinal lesions, neurological dysfunction, bone-marrow suppression) are major impediments to their successful clinical use. Cytotoxic agents decrease the life of cancer patients, resulting in dire complaints and long-term effects on survivors. Toxicity limits the usefulness of anti-cancer agents, which is why patients stop treatment [13, 47].

3.2 Radiotherapy

Radiotherapy is a physical process in which ionizing radiations are used for the destruction of cancerous cells. Energy from the ionizing radiations passing through the cancerous cells in turn alters the genetic structure and hence blocking their ability to proliferate. In radiotherapy

the main goal is to maximally destroy the cancerous cells by the high energy radiation without affecting the adjacent normal cells. Despite of all the development in radiation therapy, the main drawback of it that normal cells are also damaged along with the cancerous cells. Prostate cancerous cells may develop the radiation resistance because of some unknown factors. Hence making radiotherapy an ineffective strategy and causing cancer metastasis. Many of the combination procedures are going through the clinical trials for finding new ways for the effective radiotherapy. Radiotherapy mainly exercised by the two ways describes below.

3.2.1 External beam radiation therapy (EBRT)

External radiotherapy is the grade level strategy which can be opted for the localized PCa. It is the process in which high energy radiation are externally aimed at the location of cancer and destroy them by different way of actions such as apoptosis, autophagy, necrosis or mitotic cell death. Many of the technological advancements in external beam radiation therapy such as 3D conformal radiotherapy, Intensity modulated radiation therapy, and Image guided radiotherapy, stereotactic body radiation therapy are developing in order to decrease the toxic effects of EBRT and making them more effective against PCa [49-51]. External radiation therapy varies in effect as different radiations/particles (photon or proton) and protocols are uses accordingly for the treatment of PCa. Patients recovered from PCa by external beam radiation therapy have 72% increased risk of acquiring second primary bladder cancer than that of the surgical strategy [52].

3.2.2 Internal Radiotherapy

Internal radiotherapy is described as the brachytherapy in which sealed radionuclide (a source of radiation) is introducing into tumor or next to it for treating it directly or by means of catheters. These radionuclides emit a range of radiations including auger electrons, alpha, beta, gamma and x-rays. Most commonly used radionuclides (Yttrium-90, Lutetium-177, and Iodine-131) emits beta rays while others are less common [53-55]. Brachytherapy provides

with a significant good option treatment for the PCa and more advancement in this therapy provides with the marvelous oncological outcomes, limited toxicity rate and also increased life expectancy of PCa patients [56].

Internal radiotherapy is actually the targeted treatment strategy, a lot of development and new radionuclides are formed specifically for the treatment of PCa. An alpha-emitter radionuclide ^{225}Ac complexed with PSMA forms the ligand ^{225}Ac -PSMA-617 for the PCa treatment although still in clinical trials however also demonstrating the strong potential toward the advanced stage PCa. The other most efficient therapeutic radionuclide that are also in practice to label PSMA is β -emitter Lu-177 – which required one or two more cycles of therapy to eradicate the PCa as compared to ^{225}Ac -PSMA [57, 58]. ^{177}Lu labelled PSMA which demonstrating strong efficacy in short period of time due to which patient quickly recover from the PCa [59]. Two main factor are big barrier to adopt this therapy; one is the high cost and second is the establishment of $^{225}\text{Ac}/^{177}\text{Lu}$ -PSMA therapy.

3.3 Immunotherapy

Immunotherapy plays a consequential role in recent years for the PCa treatment by triggering the immune system of patient's to kill the PCa [22]. A noteworthy reduction in T-cells (immune responsive lymphocytes) are detected in the high risk PCa as compared to the benign nodular hyperplasia of the prostate. Several of the immunologic therapies for the castrateresistant PCa includes antibodies, adoptive T cell therapy, vaccines or targeting the immune function by chemical compounds and the most successful immunotherapy from all of them is the vaccinated immunotherapy while others exhibits less activity comparatively. One of the FDA (Food and drug administration) approved vaccine Sipuleucel-T as the first successful vaccine for PCa immune therapy [60-62]. Despite of the extensive research towards the immunotherapeutic treatment of PCa as monotherapy are not exhibiting the satisfying results. Much more of the further researches are needed in this regard as not all PCa

tumors exhibiting the immune-sensitive behavior. For the purpose of more improvements, Combination immunotherapies (immunotherapy with other therapies such as chemotherapy, radiotherapy, hormonal therapy or surgery) shows some positive response, hence paving the way for immunotherapy as a revolutionized PCa treatment strategy [63, 64].

3.4 Hormonal therapy

Hormonal therapy is also regarded as the androgen deprivation therapy. Androgen receptors are the steroidal transcriptional factor for dihydro-testosterone and testosterone PCa growth is triggered by the increased level of androgens, hence provided the basis for androgen deprivation therapy. Androgen deprivation therapy suppresses the androgens and in turn suppresses the growth of PCa. This therapy may also result in the high risk PCa to castrate resistant PCa [65, 66]. Androgen deprivation therapy may also leads to many other diseases involving cerebrovascular disease, cardiovascular disease, Alzheimer's disease and osteoporosis [67, 68].

3.5 Surgery

Surgery is not considered as the only treatment option for the PCa treatment, instead it's the part of multimodal approaches for treatment. Surgery is mostly suggested for the treatment of localized PCa in which tumor is surgically removed from the body and in turn provides with the survival benefits. Surgery may become the protocol for localized PCa treatment and more favorable than watchful waiting of impermanence, risk of metastatic and localized proliferation. Most commonly applicable surgery types for the PCa are pelvic lymphadenectomy and radical prostatectomy (RP). However, RP is generally not preferred for the high risk PCa due to the adverse side effects such as metastasis of lymph nodes, elevated positive surgical margins and PSA recurrence. RP increases the life expectancy of patient with high risk of PCa. While patients having intermediate risk disease gained high benefits by RP, with 24% reduction in PCa specific death, 15% reduction in overall death and 20%

reduction in metastatic disease development. RP may lead to the poorer sexual and urinary function, while leading to the much better execution in bowel domain. However, surgery is not the only and complete treatment option for cancer, as it's just the first mechanistic approach to remove maximum tumor cells/tissues hence surgery is followed by the other treatment options such as radiation therapy or chemotherapy to dead the remaining cancerous cells [69-71].

4. PCa treatment by natural product

Various plant bioactive chemo-preventive compounds target signaling pathways and cellular molecules. These include reactive oxygen species (ROS) formation and signaling, cyclooxygenase-2 (COX-2), xenobiotic metabolizing enzyme (XME), lipo-oxygenase pathways, cell cycle proteins, transcription factors, apoptosis, angiogenesis, invasion, and epigenetic enzyme alterations [15]. PCa treatment with a plant-based extract containing bioactive components reduces the incidence rate of this malignant disease and kills prostate cells through many different pathways (cell cycle arrest, inhibiting cancer cell growth, inducing apoptosis, anti-angiogenesis or anti-proliferation activity, etc.).

In the next sections, we describe all these criteria to update our knowledge of PCa origination, primary risk factors, natural product therapy processes, and screening the remainder of the flora for PCa treatment. Different prostate cell lines (i.e. LNCaP, DU145 or PC-3 cell lines) are used by in vivo, in vitro, or animal model to find the exact pathways of treating PCa by the specific bioactive in specific efficacious concentration from the specific plants, which may be traditional herbal medicine plants or dietary plants etc. These natural chemicals originating from plants are bioactives exhibit their potential anti-cancerous activity within days or months. For better treatment of PCa by plant extracts, more clinical trials and research are needed to obtain viable, less costly, and easily available cancer treatment procedures.

4.1 Plant derived bioactive phytochemicals and PCa

Commonly, it was believed that the chemo-preventive drugs from the last 40 years are used for the treatment of cancer a natural products extracted from plant roots. These natural products are many different types of bioactive components that are present in different parts of the plant i.e. leaves, flowers, fruits, seeds, bark, and roots etc. These bioactive components may have anti-cancer effects used for multiple purposes such as by inducing apoptosis, altering the cell cycle, or inhibiting cancer cell growth and by scavenging free radicals etc. [16].

Researchers have found many plants derivative bioactive components that show the anti-PCa activities in vivo or in vitro, such as *Psoralea corylifolia*, Danshen, American cranberry, olive oil, *Salvia miltiorrhiza* Bunge, black pepper, *O. gratissimum* etc. and many of other plants are describe below (**Table 1**).

Table 1: List of plants from which phytochemicals have been extracted and are used to treat prostate cancer.

Plant	Used phytochemicals	Efficacy	Prostate target cell lines	Analysis time (Hours, days)	Model of PCa	Result of the used model	References
<i>Psoralea corylifolia</i>	Neobava-isoflavone and psoralidin	Cause apoptosis in the PCa cells.	LNCaP cells	48-h	In vivo & In vitro	Causes increased Percentage apoptosis $77.5 \pm 0.5\%$ or $64.4 \pm 0.5\%$,	[2]
Danshen (<i>Salvia miltiorrhiza Bunge</i>)	Diterpene compounds (Cryptotanshinone (CT), Tanshinone IIA (T2A) and Tanshinone I (T1))	Anti-angiogenesis activity, anti-growth, anti-invasion	PC-3, LNCaP, and DU145 cell lines(in vitro) Bax and Bcl-2 proteins(in vivo)	7 days (In vivo), 5h (In vitro),	In vivo (in mice) & in vitro	T1 shows IC ₅₀ 's around 3-6.5 μ M, IC ₅₀ 's of CT and T2A are around 10–25 μ M and 8–15 μ M, respectively	[72]
American cranberry (<i>Vaccinium macrocarpon</i>)	Anthocyanin glycosides (cyanidin-3-galactoside, cyanidin-3-arabinoside, peonidin-3-galactoside, and peonidin-3-arabinoside)	Cell cycle arrest	DU145 human PCa cells.	6-h	In vitro (human PCa cells)	Viability decreased by 26%, 32% and 46% at 10, 25 and 50 mg/ml of WCE	[73]
Olive leaves	Oleuropein	Antiangiogenic	LNCaP & DU145 PCa cell lines & on BPH-1 non-malignant cells	72 h	In vivo and in vitro studies	100-500 μ M oleuropein causes significant reduction in cell viability (Particularly in LNCaP & DU145 cells)	[74]
Chinese medicinal herbs(<i>Salvia miltiorrhiza Bunge</i>)	Tanshinones	Inhibitory potency to the PCa cell lines.	PCa cells	24 h	In vitro, in vivo(mice)	For androgen-dependent LNCaP cells, Shows strong inhibitory potency having order of THIA>cryptotanshinone>tanshinone I	[75]
Tomato Powder and Soy Germ	Lycopene (tomatoes) & Parent Isoflavones ,isoflavone metabolites(soy germ)	Reduces prostate carcinogenesis	mouse prostate (TRAMP)model	14 week	In mice	Mice consuming TP (61%, $P < 0.001$), SG (66%, $P < 0.001$), and TPpSG (45%, $P < 0.001$) Having lower incidences of PCa.	[76]
Black pepper	Piperine	Reduces tumor growth, anti-migratory effects.	LNCaP, PC-3 and DU-145 PCa cells	24 h, 48h,& 72 h.	In vivo(in mice) and in vitro	LNCaP (AD), PC3, 22Rv1 & DU-145 (AI) cell lines shows reduction of proliferation with an IC ₅₀ value of 60 μ m, 75 μ m, 110 μ m and 160 μ m	[77]

						respectively.	
<i>O. gratissimum</i> leaf	Ethanollic extracts (anti-oxidants)	Anti-inflammatory and anti-angiogenesis properties	PC3•AR cells	24, 48, & 72 hours.	In-vitro	The three extracts P2,P3-2 and PS/PT1 in a dose dependent way(P2>P3-2>PS/PT1), inhibits proliferation of PC3•AR cells	[78]
Turmeric and Chinese goldthread	Curcumin and <i>ar</i> -turmerone, berberine and coptisine	Induce cell-cycle arrest, inhibition of cell invasion ,cellular apoptosis and metastasis	CWR22Rv1 and HEK293 cells	24h	In-vitro	IC ₅₀ value of bioactives (combined phytochemical), inhibited the cell proliferation in PCa cell lines that are studied.	[79]
Dried ginger (<i>Zingiber officinale</i> Roscoe)	6-Shogaol, 6-paradol (6-PAR) & 6-GIN.	Cause apoptosis	DU145, LNCaP, and PC3 (human) & mouse (HMVP2) PCa cell lines.	24h (human prostate cells) , 32 days (mice)	In vitro (human cultured cells), in vivo (in mouse)	6-SHO was the most chmopreventive than other two bioactives in inhibiting PCa cells (in vivo & in vitro) by apoptosis.	[80]
Cucumber	Cucurbitacin B	Inhibits cell growth, induces apoptosis.	LNCaP and PC-3	24h(in vitro), 30 days (in vivo)	In-vitro , in vivo(mouse)	IC ₅₀ of CuB results in inhibiting cell viability of prostate cncer cells; also (0.1 μ mol/day of CuB) inhibits the growth in athymic mice PC-3 xenografts.	[81]
<i>Alnus japonica</i> (bark)	Hirsutenone	Induce apoptosis	PC3 and LNCaP PCa cells	72h	in silico, in vitro (human PCa cells)	Hirsutenone induces apoptosis by targeting Akt1 and 2 in human PCa cells.	[82]
Cruciferous vegetables	Erucin (isothiocyanates)	induce a proliferation- arrest state	prostate adenocarcinoma cells (PC3)	24 h	In vitro	ER concentration up to 15 μ M caused a significant decrease in proliferation of PC3 cell at 25 μ M($P \leq 0.01$)	[83]
Arctium lappa (seed), green tea, Curcuma longa (root)	Arctigenin (Arctium lappa), epigallocatechin gallate(green tea), curcumin	Cell cycle arrest, apoptosis	LNCaP PCa	48 h	In vitro	IC ₅₀ values of EGCG, curcumin, arctigen induces antiproliferative effect in combination &individually induces apoptosis LNCaP cells.	[84]
<i>Salvia triloba</i> (Lamiaceae)	1,8- cineole, β –pinene, β -caryophyllene , camphor	Induced cytotoxicity, apoptosis, angiogenesis	PC-3, DU-145 & HUVEC cells	72 h	In vitro	IC ₅₀ values of extract was 287 \pm 8 & 456 \pm 15 μ g/ml in PC-3& DU-145 cells shows that it induces apoptosis to them and no cyto-toxic affect to normal cells.	[85]

Hedyotis diffusa (Leaves & root)	Diffusa cyclotide 1 to 3 (DC1-3)	Induces cytotoxicity, hepatoprotective, neuroprotective activities inhibited cell migration	PC3, LNCap and DU145(in vitro) Mouse xenograft model (in vivo)	72 h	In vitro and In vivo	IC ₅₀ value of bioactives is shown at the level below 10 μ M for three cancer cell lines. These bioactives shows anticancer affects in vivo and in vitro.	[86]
Milk thistle	Silibinin	Induces autophagy	PC-3 cells	48 h.	In vitro	Silibin induces autophagy (apoptosis) in PC-3 cells by the production of Reactive Oxygen Species.	[87]
Eurycoma longifolia	Quassinoids	Induced cytotoxicity, anti-tumorigenic activity, inhibition of LNCaP cells,	LNCaP cancer cells.	72 h(in vitro, in vitro (6 week)	In vitro(human) , In vivo (mice)	IC ₅₀ value of SQ40 at level of 5.97 μ g/mL inhibits growth of LNCaP while the injecton of 5 and 10 mg/kg of SQ40 inhibits LNCaP tumor growth in mice xenograft.	[88]
Carica Papaya	Crude flavnoid extract (CFE), ELE & MLE	Anti-cancer activity, Induces inhibition of cancer cell growth.	DU-145	48-72h	In vitro	Growth inhibition of DU-145 cancer cells induced at IC ₅₀ of CFE, ELE and MLE at the level of 2.2 μ g/ml, 2.4 μ g/ml & 2.6 μ g/ml respectively.	[89]
Pumpkin (seed)	Cucurbitin	Inhibiting cell growth	DU145 (androgen insensitive) & LNCaP (androgen sensitive)		In vitro	The considered curcurbitin is not the component that causes the Inhibition of cancerous cells. Although the seed extract are considered safe for the PCa.	[90]
Luobuma (leaves)	Sterols (Sitgmasterol, sitosterol) , Triterpenoid (Lupeol) , Flavonoids (Kaempferol, Isorhamnetin)	Inhibits cell proliferation, induce apoptosis, augment cell cytotoxicity	PC3 cells	24h	In vitro	Lupeol accounted for (w/w) 19.3% of F8 and inhibits proliferation of androgen-insensitive-prostate-cancer cells. Other bioactives also exerts anti-cancer effects by different mechanisms.	[91]
Ginger	6-shogaol, 10-shogaol 6-gingerol, & 10-gingerol,	Inhibit proliferation, induce apoptosis	PC3R, PC3 cells	24h	in vitro	6-shogaol, 10-shogaol 6-gingerol, & 10-gingerol at 100 μ M inhibits proliferation in PC3R, while same results also observe in PC3 by 6-gingerol, 6-shogaol and 10-shogaol.	[92]

<i>Salvia miltiorrhiza</i> Bunge (Danshen)	dihydroisotanshinone I (DT)	Increases survival rate of patients, inhibits cancer migration.	PC3, DU145, 22Rv1 cells	15year (in vivo), 24h (in vitro)	in vivo (human), In vitro,	Danshen induces in vivo protective effect on the patients that survival rate increases. While in-vitro DT inhibits the migration ability of PCa by different mechanisms.	[93]
Soybean (seed)	Bioactive peptides	Inhibits cancerous cells	PC-3 cells	48–60 h	In vitro	Different soybean lines shows different inhibitory percentage .S03-543CR soybean line shows highest (63%) inhibitory effect to PCa cells.	[94]
<i>Scutellaria altissima</i> L.	Scutellarin (flavon)	Induces G2/M arrest, apoptosis, inhibits proliferation	PC-3 cells	24h	In vitro	Scutellarin induces apoptosis, G2/M arrest, and inhibits the proliferation of PCa. Sensitized the PC-3 cells to chemotherapy.	[95]
<i>Solanum nigrum</i> L.	Solanine	Reduces tumor growth, induce apoptosis	DU145 cells(human ,in vitro), DU145 cell (mouse xenograft, in vivo)	30 days(In vivo), 24h (invitro)	In vivo, in vitro	Solanine in vivo and in vitro regulated the cell cycle proteins i.e. Cyclin E1, P21, Cyclin D1, CDK4, CDK2, CDK6. IC ₅₀ of solanine at level32.18 μ mol/L causes apoptosis. Decrease in tumor in mouse xenograft was observed.	[96, 97]
<i>Citrus aurantium</i> L. (stem bark)	acridone alkaloids (citrusinine-I, citracridone-I, 5-hydroxynoracronycin, natsucitrine-I, glycofolinine, citracridone-III)	Induces cyto-toxicity	PC3 cells	72 h	In vitro	IC ₅₀ of Citracridone-I shows more antiproliferative activity at the level of 12.5 – 14.8 μ M than the other alkaloids.	[98]
<i>Plagiochila disticha</i> (Plagiochilaceae)	plagiochiline A	Induces Cell cycle arrest &cancer cell death	DU145 cell	24 h	In vitro	1.75 μ g/mL of plagiochiline A causes cell cycle arrest and cell death in DU145 cell.	[99]
<i>Erythrina Excels</i> (stem bark)	Excelsanone	Induces cyto-toxicity , inhibits cell growth	PC3 & DU145 cell lines	24, 48 and 72 h	In vitro	IC ₅₀ of 1.31mg/ml of Excelsanone together with 6, 8-diprenylgenistein has moderate potential toward cyto-toxicity & also Inhibits cell growth in DU145 cell lines.	[100]
<i>Punica granatum</i> (juice and peel extract)	Ellagic acid and its derivatives, α & β -punicalagin(juice), punicalagin, ellagic acid and its derivatives (peel extract)	Inhibits migration, proliferation and colony formation	PC3 & DU145 cell lines	24 h or 48 h	In vitro	Pomegranate juice and peel extract both shows the antiproliferative effect for PCa cells. But peel extract show more robust result towards cancer than juice at similar concentration.	[101]

<i>Silybum marianum</i>	Silychristine, silibinin & Silymarin-enriched extract (SEE)	G2/M blockade, inhibits anti-proliferative effect	PC-3 cells	24 ,48 and 72h	In vitro	Silychristine, silibinin IC ₅₀ value of 3–120 µg/mL and SEE have IC ₅₀ of 44–52 µg/mL inhibits proliferation in dose dependent way. DXR-SEE co-treatment enhances the cell death than the SEE alone.	[102]
Rooibos (<i>Aspalathus linearis</i>)	Flavonoid (aspalathin)	G2/M cell cycle arrest, apoptosis	LNCaP 104-R1 cells xenografted in mice.	96h	In vivo (mouse xenograft)	GRT extract aspalathin majorly inhibits the proliferation and suppressed the CRPC cells. Causes apoptosis in LNCaP 104-R1 xenografts in mice.	[103]
<i>Paederia foetida</i> (leaf extract)	Lupeol, β-sitosterol and MEPL.	Induces cyto-toxicity,	PC-3 and DU-145, THP-1 cells	24h	In vitro	Lupeol, β-sitosterol and MEPL at their respective IC ₃₀ values exhibits cyto-toxicity, apoptosis & inhibits proliferation.	[104]
<i>Citrus sinensis</i> L. (peel extract)	Citric acid, narirutin & hesperidin	Suppresses DNA synthesis rate in PC cells, induce apoptosis, inhibits cell cycle re-entry	LNCaP, RWPE-1, GM3348 & PC-3	24h & 48h	In vitro	Narirutin & hesperidin was not the bioactives responsible for inhibiting cell cycle re-entry but it was the citric acid. So, citric acid along other bioactives can be act as chemopreventive.	[105]
Green tea	Epigallocatechin-3-gallate (EGCG)	Inhibits migration and invasiveness of cancer, upregulate TIMP-3 level, decreases class I EZH2 & HDACs.	LNCaP & DUPRO cells	6week (in vivo), 48h (in vitro)	In vivo (human), In vitro	EGCG/GTP inhibits migration & invasive capability of cancer cells. In addition, EGCG in patients increases TIMP-3 levels by balancing MMP: TIMP suppresses PCa.	[106]
<i>Glycyrrhiza glabra</i>	GGE (Glycyrrhiza Extract)	Inhibits proliferation, induce apoptosis	PC-3 cells, WI-38 cells	96h	In vitro	GGE treatment causes proliferation at IC ₅₀ value of PC-3 and WI-38 cells are at the level of 35.7 ± 2.0 lg/m and 96 ± 1.6 lg/ml. while ADR+GGE causes proliferation at IC ₅₀ 11.6 ± 0.6nM.	[107]
<i>Rosa canina</i>	Phenolics (ascorbic acid, p-coumaric acid, gallic acid, quercetin, 3, 4- dihydroxy benzoic acid, rutin hydrates and chlorogenic acid).	Induces cyto-toxicity, apoptosis, cell cycle arrest, increases caspase activity.	PC-3 cells	72h	In vitro	Significant increase in M phase cells at observed at IC ₉₀ of 257 and 378 mg/mL of <i>Rosa canina</i> extract. Apoptosis, cell cycle arrest and increase in caspase activity also observed that may be due to phelonic content of extract.	[108]

<i>Cymbopogon citrates</i> (lemon grass)	Citral	Induce apoptosis, inhibits colonogenic formation and proliferation of PCa cells.	PC3 and PC-3M cells	72h	In silico , in vitro	Citral significantly reduces the colonogenic potential, proliferation, cell viability, changes the morphology and inhibits the lipogenesis of cancerous cells.	[109]
<i>Rhizoma Curcuma</i>	Germacrone	Reduces the viability, induces apoptosis and autophagy.	PC-3 & 22RV1 human PCa cells	48h	In vitro	Germacrone in dose dependent manner with IC ₅₀ have the value for PC-3 were 259 μ M and for 22RV1 were 396.9 μ M induces apoptosis and inhibits cells proliferation.	[110]
<i>Orobancha crenata</i>	Orobancha crenata methalonic extract	Inhibits PCa cells,	PC-3 PCa cells	24h	In vitro	O. crenata extract exhibits the anticancer, cytotoxic and antiproliferative activity due to the bioactive methalonic components present in it.	[111]
<i>Moringa oleifera</i> (Leaves)	Methalonic extract	Induces G0/G1 cell cycle arrest, anti-cancer potential and ROS-mediated apoptosis.	PC-3 cells	24h	In vitro	Moringa oleifera methalonic leaves extract demonstrates ROS-mediated apoptosis and reduction in proliferation by suppressing deregulated Hedgehog signaling in PCa.	[112]
<i>Paris forrestii</i>	Total saponins (polyphillin D, paris saponin Tg).	Induces apoptosis,PCT3 treatment changes mRNA and lncRNA.	LNCAP, DU145, PC3, RWPE	24h	In vitro	PCT3 exhibits the anticancer activity on PCa and also reveals some crucial mRNAs and lncRNAs that take part in the anticancer activity of PCa.	[113]

5. Multi-targeted Chemo-prevention

Assembling evidences describes that a lot of phytochemicals are acting via multiple mechanisms involving modulating pathways of signal transduction, interconnections with receptors and the genes includes in the control of apoptosis, cell cycle, cell proliferation and regulating transcription by exerting their chemotherapeutic and antitumor effects. Some of the potential phytochemicals are described under that are proven to be having the chemo-preventive effects towards the PCa [15].

5.1 Tanshinones

Tanshinones are abietane diterpene compounds found in *Salvia miltiorrhiza*. They include tanshinone-I "T1" (Compound 1), tanshinone-IIA "T2A" (Compound 2), and cryptotanshinone "CT" (Compound 3). (a traditional Chinese medicine). These bioactive elements are used to cure disorders and display anti-cancerous action by anti-angiogenesis, anti-proliferation, pro-apoptosis, reducing adhesion, metastasis, invasion, and migration, and inducing differentiation, with no negative effects on normal cells. [114, 115].

Tanshinones showed the anti-cancerous results while doing invitro study in the dose dependent manner by inducing apoptosis and cell cycle arrest. Tanshinone-I exhibits the potential activity with IC_{50} value around 3–6 μ M. Aurora A kinase were identified as the probable target of these phytochemicals actions (tanshinones), as in the cell lines of PCa. Aurora "A" were over-expressed and hence decreases the PCa cell growth. Its expression was significantly downregulated by tanshinones. Tanshinones especially "T1" exhibits the anti-angiogenesis effects in-vivo and in-vitro suggesting that these are the safe anti-cancerous and therapeutic agents against PCa[72]. T1 also increases TRAIL mediated apoptosis through the miR135a-3p arbitrated DR5 up-regulation in the PCa cells as an effective TRAIL sensitizer [116]. In another study tanshinone IIA isolated from *Salviae Miltiorrhizae* (root extract) exhibits the antiproliferative

effects to PCa in a dose dependent way. Tan- IIA causes the cell death and cell cycle arrest in LNCaP cells at G0/G1 phase and correlating it with the enhanced CDK inhibitors levels. These tanshinones induces ER stress, induces the cell death with the blockage of the expression GADD153/CHOP via siRNA reduced tanshinone IIA, increases the expression of down-stream of different molecules and suppresses the tumor growth and reduces tumor volume to 86.4% in xenograft model within the 13 days of treatment. In PC-3, LNCaP cells the IC_{50} value for the bioactives Tanshinone IIA were 2.54 μ g/mL and 5.77 μ g/mL[117]. Tanshinone IIA also exhibits the inhibitory effects on the proliferation and growth of the LNCaP cells via BrdU incorporation assays and colony formation respectively and induces the cell cycle arrest at G1 phase by the activation of p53 signaling, also the down regulating Cyclin D1, CDK2 and CDK4 and inhibiting androgen receptor (AR) in LNCaP cells [118].

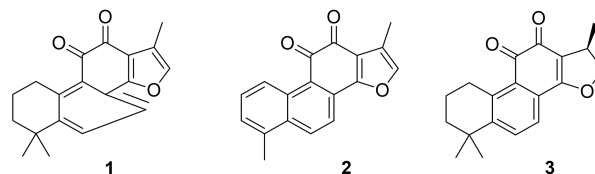


Figure 2: Molecular structures of tanshinone-I (1), tanshinone-IIA (2) and cryptotanshinone (3). Reproduced with permission: Copyright 2015, MDPI [119]

5.2 Biochanin-A

Iso-flavones are the most common plant-based bioactive chemicals. Biochanin-A (compound 4) in red clover and soy has chemo-preventive, anti-proliferative, and anti-cancerous activities. Biochanin-A significantly enhances the Trail mediated apoptosis and cytotoxicity in LNCaP and DU145 PCa cell lines. TRAIL is actually the innate potent anti-cancerous agent that inequitably induces the apoptosis in the malignant cells and cause no damage or toxicity to normal cells. In vitro study shows TRAIL cytotoxicity at 50-100ng/mL for 48h was 2.8% -1.4% to 6.2% -1.7% for DU145 and 8.3% -1.2% to 19.6%-1.1% for LNCap. Biochanin-A sensitized the LNCaP cells that are TRAIL-resistant by inhibiting the activity of transcription

factor NF- κ B (p65). This compound enhanced the expression of TRAIL-R2 (DR5) a death receptor and disrupted the potential of mitochondrial membrane. Apoptosis is enhanced by inducing the potential of sensitized TRAIL and TRAIL resistant PCa. This isoflavone regulated NF- κ B activity and also affected the intrinsic and extrinsic apoptotic pathways [120-122].

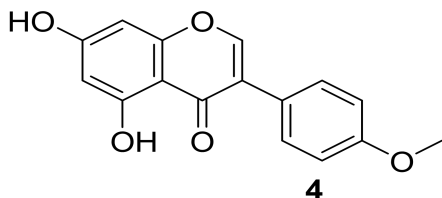


Figure 3: Molecular structure of Biochanin-A (4). Reproduced with permission: Copyright 2014, PLOS [123]

5.3 Oleuropein

Olive leaves, fruits, and oil contribute to the Mediterranean diet's health benefits. Oleuropein (Compound 5) is an anti-tumor polyphenol found in olive leaves. Olive leaves and oil contain polyphenols. Many of the invitro studies demonstrated the apoptotic and anti-proliferative effects in many of the cancer cell lines. In a study using MMT test to assess cell proliferation, 100-500M oleuropein treated over 72 hours on LNCaP, DU145, and non-malignant BPH-1 cells suppressed cell viability, especially in DU145 and LNCap cells. Hydrolysis of oleuropein produces the compounds such as hydroxytyrosol and eleonolic acid that are also the bioactive compounds. This polyphenol induces the decrease in cell viability and modification in the thiol group, ROS (reactive oxygen species), γ -glutamylcysteine synthetase, heme oxygenase-1 and pAkt. Oleuropein induces the antioxidant effect while exposing cell culture on the BPH-1 cells, a non-malignant cell line. Oleuropein proves to be an adjuvant agent while treating the prostatic, so as for preventing the modification of hypertrophic to malignant (cancerous) cell [74, 124-126].

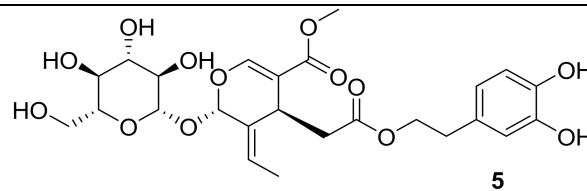


Figure 4: Molecular structure of Oleuropein (5). Reproduced with permission: Copyright 2015, Scientific Research Publishing, Inc. [127]

5.4 Anthocyanins and phenolic acid

Anthocyanins are phenolic pigments found in berries and grapes. Anthocyanins are also found in cereals, tubers, and other plants. These bioactive components have proven to be beneficial for health [128]. Sweet potato leaves contain anthocyanins and phenolic acid. Polyphenol rich sweet potato green extract (SPGE) stimulates anti-proliferative activity in prostate epithelial cells without injuring normal cells, modifies the cell cycle, lowers colonogenic survival, and induces apoptosis in human PCa "PC-3 cell line" in-vivo and in-vitro. Alterations in apoptosis regulatory constituents e.g. Bcl2 inactivation, BAX upregulation, release of cytochrome and the activation of the downstream apoptotic signaling were observed by the action of SPGE. SPGE also cause the degradation of DNA as obvious via TUNEL (terminal deoxynucleotidyl transferase-mediated dUTP-nick-end labeling) staining of enhanced 3'-DNA ends concentration. In-vivo 400 mg/kg SPGE oral administration show the reticent progression and growth approximately 69% in prostate tumor xenograft model of mice and exhibits that normal tissues are also not affected[129].

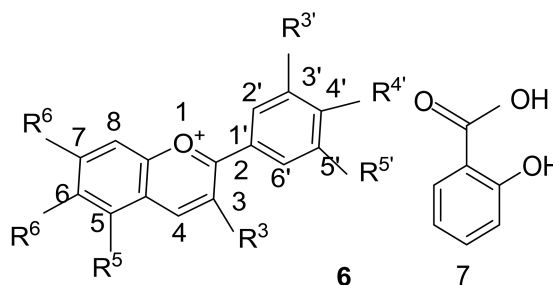


Figure 5: Molecular structure of Anthocyanins (6) and phenolic acid (7). Reproduced with permission: Copyright 2017, MDPI [130]

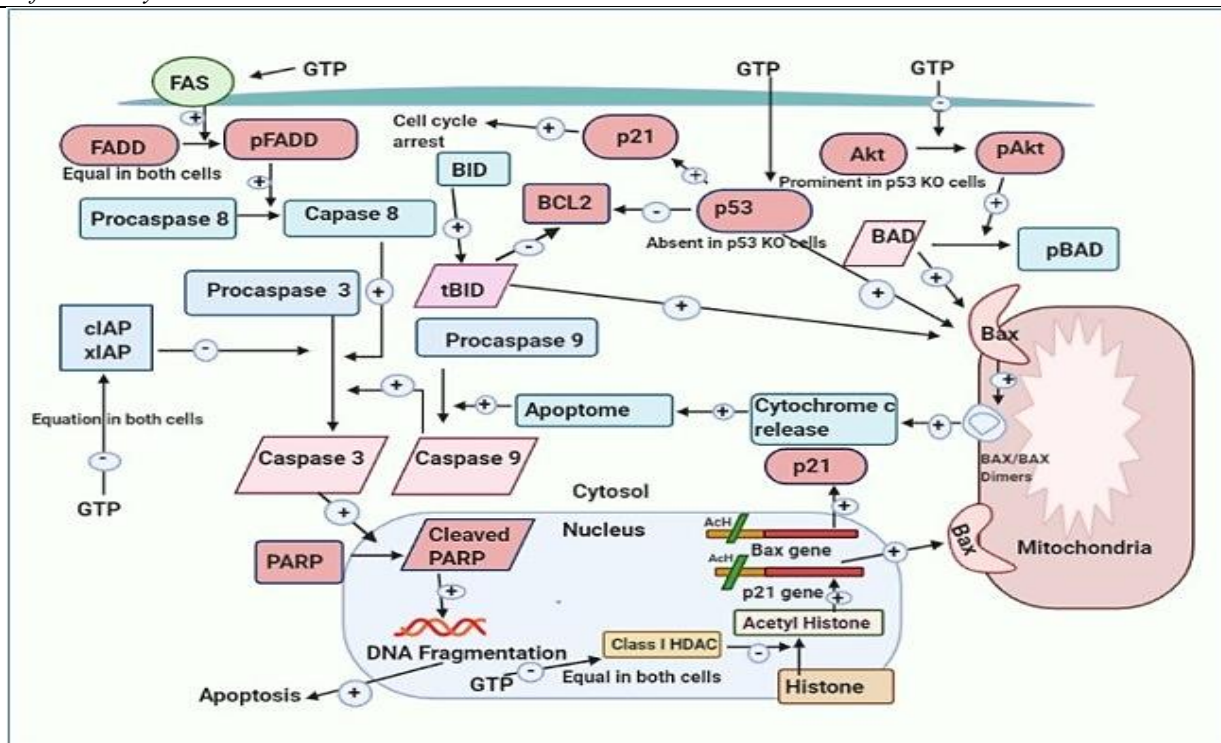


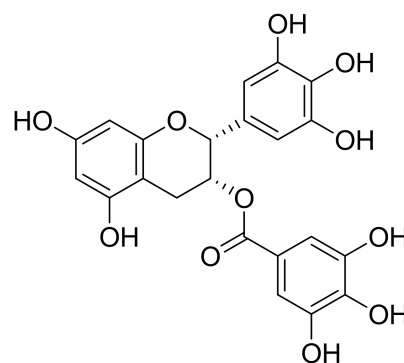
Figure 6: Schematic model illustration of the green tea polyphenol induced activation of intrinsic (death cascade of mitochondria) and extrinsic (death receptor pathways) molecular pathways in the presence and absence of p53. Reproduced with permission: Copyright 2012, PLOS [131].

5.5 Epigallocatechin-3-gallate (EGCG)

Epigallocatechin-3-gallate (EGCG) is the major green tea polyphenol. Green tea polyphenol induced P53 activation and stabilization of down-stream targets Bax and p21/waflare induced by the GTP treatment in a dose dependent manner especially in LNCaP cells. These polyphenols promotes the apoptosis in cancerous cells effectively both in absence and presence of p53 function via agitation in signaling pathways involving the extrinsic FAS-FADD death receptor and constancy pathways that intersects in the induction of apoptosis via mitochondrial death cascade (**Figure 6**) [132].

An analytical study reported that EGCG in combination with quercetin induces apoptosis, cell cycle arrest and inhibits the cell proliferation in PCa in vitro by enhancing the EGCG intracellular concentration and lessen the EGCG methylation. As compared to the sum rate of inhibition of EGCG and quercetin individually their combination with 10 μ M or 20 μ M respectively enhances the reduction in PC-3 cell proliferation at 24h and 48h by

15% and 20%, or 21% and 19%, respectively. The combined effect of these agents based on the certainty that quercetin decreases the quantity of catechol-*O*-methyl transferase (COMT) activity while EGCG inhibits activity of catechol-*O*-methyl transferase (COMT). EGCG and quercetin leads to the additive effects by executing the strong anti-proliferative effects in LNCaP cells. Combination of these two bioactive molecules proved to be much effective in order to induce chemotherapeutic and chemo-preventive effects towards PCa[133].



8

Figure 7: Molecular structure of Epigallocatechin-3-gallate

(8). Reproduced with permission: Copyright 2006, Elsevier [134]

5.6 Resveratrol

Resveratrol is a natural polyphenol found in peanuts, berries, and grapes. Many pre-clinical investigations suggest resveratrol is a promising natural bioactive anticancer drug [135]. These research showed that resveratrol (Compound-9) shields various biological systems, especially in cancer[136]. By altering androgen receptor signaling in PCa, resveratrol inhibits androgen-regulated gene expression and cell proliferation. Anti-androgenic resveratrol analogues were extracted from plants or semi-synthesized. LNCaP prostate cell lines were seeded in the luciferase assay along with MMTV-luc reporter plasmid for the measurement of androgen dependent (AR) activity. 4'-O-methylresveratrol (3, 5-dihydroxy-49-methoxystilbene) resveratrol analog were proved to be most potent abstractor of AR transcriptional activity as IC_{50} value for the resveratrol and its analogs were to be $5\mu M$ and $2\mu M$ respectively. The hydroxyl (OH) in the ring of resveratrol plays the major role in the anti-androgenic effects via modulation of androgen dependent (AR) activity [137]. Peanut stem extract (PSE) contains high content of resveratrol that augments its radio-sensitization affects in PCa which is likely to be mediated through the apoptotic pathway activation, DSB (DNA double-strand break) repair attenuation and the arrest of cell cycle in G2/M phase. Resveratrol and PSE inhibits proliferation in LAPCD-KD cells for 48h treatment with IC_{50} value 25 and $500\mu g/mL$, respectively. In addition, co-administration of PSE or resveratrol and radiation, induced the apoptosis in radio-resistant PCa cells. Radiation therapy were enhances effectively by exploration of PSE and resveratrol in the shDAB2IP PCa mouse xenograft model [138].

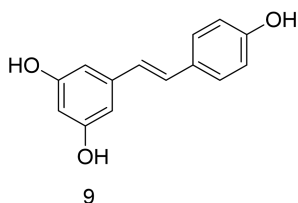


Figure 8: Molecular structure of resveratrol (9). Reproduced with permission: Copyright 2019, MDPI [139]

5.7 Piperine

Black pepper contains the medicinal alkaloid piperine (*Piper nigrum* Linn.). Pepper has wide-ranging pharmacological effects and is used to treat numerous diseases. Piperine is anti-asthmatic, immune-modulatory, anti-ulcer, anti-oxidant, anti-inflammatory, and anti-carcinogenic, according to human research [140-143]. A study provide evidence that piperine exerts the antitumor activities towards the PCa, in-vivo and in-vitro. Piperine was pre-treated with DU145 cells for 48h and then their viability was examined by the CCK-8 assay. It clearly caused apoptosis and inhibited cell migration and proliferation in DU145 prostate cell lines by downregulating MMP-9 and Akt/mTOR signaling, also Akt/mTOR signalling appears to be MMP-9 protein upstream regulator (**Figure 9**) [144].

Piperine in the dose dependent manner suppresses different metastatic behavior and proliferation of PCa by inducing the G⁰/G1 phase arrest. The bioactive component piperine shows the IC_{50} value for the PC-3, DU145 and androgen-dependent LNCap cells were $111\mu M$, $226.6\mu M$ and $74.4\mu M$ respectively¹⁰⁶. In another in-vivo and in-vitro studies the effectiveness of piperene were examined. It induces apoptosis and inhibits proliferation in both the androgen independent PC-3, 22RV1 and DU145 and the androgen dependent LNCap cells in vitro. PC-3, 22RV1 and DU145 PCa cell line while treating with piperine results in the lessened expression of nuclear factor-kB (NF-kB) and phosphorylated STAT-3 transcription factors. In-vivo study shows that xeno-transplanted model with PCa in mice results in the reduction of androgen dependent (AD) and androgen independent (AI) tumor growth. Significant reduction in viability and proliferation of PC-3 (AI) and LNCaP (AD) cells with piperine were exhibits while assessing as MMT assay with the IC_{50} values of $75\mu M$ and $60\mu M$ respectively in a dose dependent way [77].

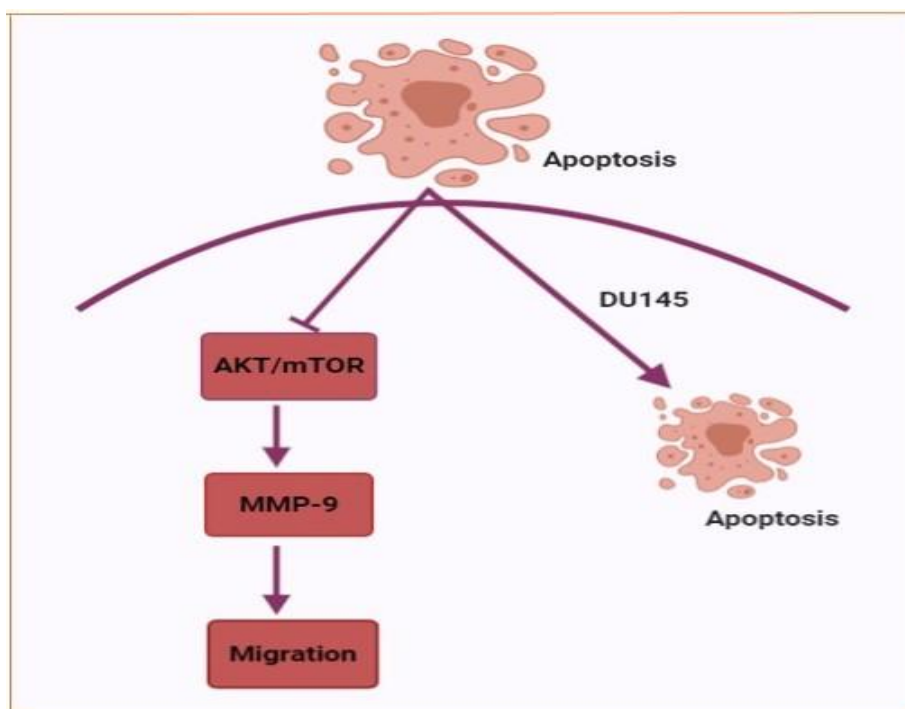


Figure 9: Piperine inhibits the continuation of migration via downregulating signaling pathway Akt/mTOR/MMP-9 in DU145 PCa cells. Reproduced with permission: Copyright 2018, Spandidos publications [145].

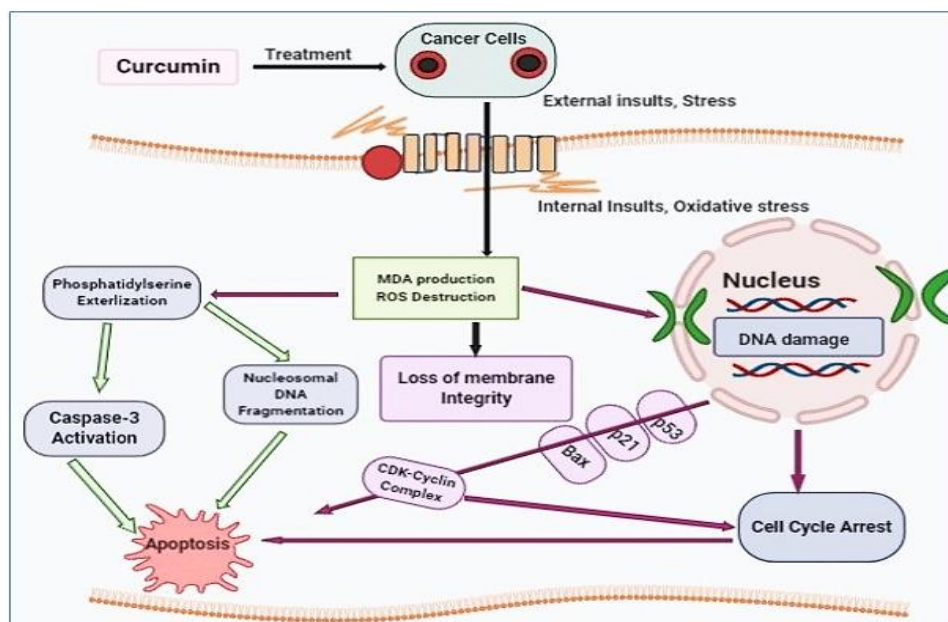
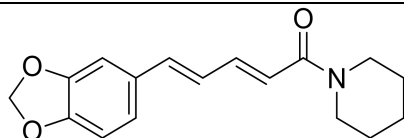


Figure 10: Schematic model representation of curcumin molecular mechanism, in malignancies management as a therapeutic agent. Reproduced with permission: Copyright 2019, MDPI [146].



10

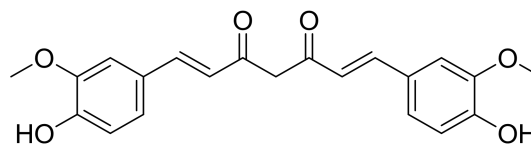
Figure 11: Molecular structure of piperine (9) Reproduced with permission: Copyright 2022, Springer [147].

5.8 Curcumin

Curcumin a pleiotropic curcuma longa constituent is a polyphenol with therapeutic properties. Curcumin has anti-arthritis, antioxidant, anticancer, and anti-inflammatory properties, according to in-vivo and in-vitro studies. Due to its regulation and efficacy towards multiple targets, as well as its tolerability, safety, and non-toxicity for human use, curcumin is a potential therapeutic agent for the treatment and/or prevention of chronic diseases [148-151]. Curcumin (*Curcuma longa*) is a potential chemo-preventive for early-stage PCa. It affects cell proliferation by reducing the expression of β -catenin-targeted genes, which links cell death with autophagy in androgen-dependent prostate cells. Curcumin cell viability were assessed by trypan-blue exclusion test that reveals that curcumin exhibits cytotoxic effect for the concentration $>75\mu\text{M}$, both in androgen dependent and independent PCa. Androgen dependent PCa cells were more sensitive for the natural compound curcumin (IC_{50} value were 44 and $48\mu\text{M}$ for the cells 22rv1 and LNCaP, respectively) than in androgen independent PCa cells (IC_{50} value were 115 and $170\mu\text{M}$ for PC-3 and DU145 cells respectively) [152]. Curcumin inhibited the cell growth and induces cell growth arrest via DNA damage, cell cycle arrest, stress genes (Bax, p21, p53 and CDK Cyclin complex) expression, and induces apoptosis through the phosphatidylserine externalization modulation, fragmentation of nucleosomal DNA and caspase-3 activation (**Figure 10**) [146].

In PCa metastasis liable phenotype can be induced as a result of chronic inflammation via sustaining pro-

metastatic and a positive pro-inflammatory feedback loop between CXCL1/-2 and NF κ B. This feedback loop is disrupted from curcumin by suppression of NF κ B signaling that leads to the lessened in-vivo metastasis formation [153]. Curcumin's anticancer effects were studied in nude mice. PC-3 cells were subcutaneously injected to the nude mice for establishing the tumor model. Nude mice were divided into different groups, group B (6% polyethylene glycol and 6% anhydrous ethanol, group C (normal saline), and group H, M, L (100 mg/kg, 50 mg/kg, and 25 mg/kg curcumin). Tumor growth was measured every 6th day and after 30 days they were killed to weigh the tumor. Cell apoptosis was determined by TUNEL assay. In group H, M, L the volume and weight of tumor was lower remarkably than that of the control groups (C, B) ($P<0.05$), and as the dose for curcumin increases the inhibitor rate also increases. While comparing with that of the control group, in H, M, L group Bcl-2 gradually decreased and Bax protein expression was enhanced ($p<0.05$). So, this study leads to the result that curcumin has the ability to inhibit PC-3 cells growth, reduces the weight and volume of tumor and also induces apoptosis under the nude mice skin by up regulating Bax and down regulating Bcl-2 [154]. Curcumin repudiates cancer associated fibroblasts (CAF) induced capture/invasion and epithelial to mesenchymal-transition and suppresses CXCR4, IL-6 receptor expression and Reactive oxygen species (ROS) in the PCa cells via suppressing HIF 1 α /mTOR/MAOA signaling so that exhibiting the potential therapeutic effects of curcumin in PCa [155].



11

Figure 12: Molecular structure of Curcumin (9) Reproduced with permission: Copyright 2018, Frontiers [156].

6. Future Prospective

Health claims are highly concerns with the nutrition

regulation in order to protect and inform the public about the fallacious health declarations. Although it's challenging but human intrusion studies are important in supporting the plant derived bio-actives, for the validated scientific findings [157-159]. However, with the advancement in cancer studies, characterization of neoplastic transformations due to the aberration in several signaling pathways arise the need for the identification of chemo-preventives that must be target specific towards the carcinogenesis. Hence, unraveling the bio-actives synergistic interactions and their potential impact on humans would considerably help in attaining success in the chemo-prevention via the plant bio-actives [15]. Pure plant derive bioactive compounds individually are needed for determining their potential chemo-preventive effects from the dietary supplements. However, isolation of the pure bioactive compound is sometime become difficult and challenging because of the stability issue, and missing their potential or in some of the cases unknown constituents may also demonstrate bioactivity either synergistically or additively from the same plant of interest[160].

Nutraceuticals and dietary supplements exert chemo-preventive effects that vary within the populations and also largely rely on microbiota gastro-intestinal composition, which in turn affect the level of anticancer compounds and bio-available nutrients. So, studies that exhibit the distinction in microbiome betwixt high and low risk populations, or in-between patients and healthy person with metastatic or dormant and androgen insensitive disease may lead to the valuable insight into the microbiome role in the progression and development of PCa. Human microbiome modulation may exert beneficial effects in chemoprevention of PCa [161]. Even though unique chemotherapeutic constituents would be more and more efficacious against the cancerous cells, their drug resistance as well as toxicity to normal tissues remain the extensive obstacle for its clinical use. Using various plant derived bio-actives for the personalized approach provides with the new dimensions for the

standard cancerous growth therapy for the betterment of its outcome in complementary and complex way [47].

Despite, a lot of the data involvement for the carcinogenic studies and its treatment, only arbitrary controlled trial is able to assess adequate evidences for creating the universal guidelines. Additionally, only a few of the plant derive bio-actives have been taken for the reasonable clinical trials to evaluate their potential anti-PCa activity [162]. Many more efforts are needed in clinical, epidemiological research, as well as in Phyto-biology that must be addressed, before the potential health effect of these phytochemicals on human[163].

7. Conclusion

Finally, many cancer treatment strategies are still in clinical trials, and many are on the way to improvement despite the enormous amount of work that has already gone into them. Because of their proven effectiveness against a wide range of acute diseases, low cost, and widespread availability, the scientific community is also making headway in treating malignant PCa with natural plant sources. Several useful plants, shrubs, and herbs have been shown to have chemo-preventive effects against PCa malignancies due to the presence of novel bioactive components. Being the active constituent bio-actives of the plants act as an agent that distressing the signaling of the prostate cells in several of the pathways, causes blockage of cell cycle at various phases, induces alternations and killing of the PCa cells with the less chances of drug resistance. Numerous in-vivo and in-vitro clinical studies have been conducted to better understand the precise protocol pathway of these bioactives in their interaction with and effect on PCa cells. However, much more of the research and clinical trials are needed for the detection of chemo-preventive effects of different plants bio-actives, while watching towards the future prospective.

Conflict of interest

The authors declare no conflicts of interest.

Authors Contribution

Hira Zulfiqar convinced the main idea and wrote the

manuscript. Hunain Zulfikar, M. Furqan Farooq, Iqbal Ahmed, Iqra Rani revised the manuscript and prepared figures and references. Farman Ullah helps in scientific writing of the paper.

Data Availability Statement

The data presented in this study are available on request from the corresponding author.

REFERENCES

- Pandey, M.K., et al., Regulation of cell signaling pathways by dietary agents for cancer prevention and treatment. *Semin Cancer Biol*, 2017. 46: p. 158-181.
- Szliszka, E., et al., Enhanced TRAIL-mediated apoptosis in prostate cancer cells by the bioactive compounds neobavaisoflavone and psoralidin isolated from *Psoralea corylifolia*. *Pharmacol Rep*, 2011. 63(1): p. 139-48.
- Rawla, P., Epidemiology of Prostate Cancer. *World J Oncol*, 2019. 10(2): p. 63-89.
- Nguyen-Nielsen, M. and M. Borre, Diagnostic and Therapeutic Strategies for Prostate Cancer. *Semin Nucl Med*, 2016. 46(6): p. 484-490.
- Chen, R., et al., Prostate cancer in Asia: A collaborative report. *Asian Journal of Urology*, 2014. 1(1): p. 15-29.
- Yedjou, C.G., et al., Prostate Cancer Disparity, Chemoprevention, and Treatment by Specific Medicinal Plants. *Nutrients*, 2019. 11(2).
- Holm, H.V., et al., Modern treatment of metastatic prostate cancer. *Tidsskr Nor Lægeforen*, 2017. 137(11): p. 803-805.
- Atun, R., et al., Expanding global access to radiotherapy. *The Lancet Oncology*, 2015. 16(10): p. 1153-1186.
- Emmett, L., et al., Lutetium (177) PSMA radionuclide therapy for men with prostate cancer: a review of the current literature and discussion of practical aspects of therapy. *J Med Radiat Sci*, 2017. 64(1): p. 52-60.
- Aghdam, R.A., et al., Efficacy and safety of (177)Lutetium-prostate-specific membrane antigen therapy in metastatic castration-resistant prostate cancer patients: First experience in West Asia - A prospective study. *World J Nucl Med*, 2019. 18(3): p. 258-265.
- Iravani, A., et al., Lutetium-177 prostate-specific membrane antigen (PSMA) theranostics: practical nuances and intricacies. *Prostate Cancer Prostatic Dis*, 2020. 23(1): p. 38-52.
- Brahmbhatt, M., et al., Ginger phytochemicals exhibit synergy to inhibit prostate cancer cell proliferation. *Nutr Cancer*, 2013. 65(2): p. 263-72.
- Singh, A.K., et al., Emerging importance of dietary phytochemicals in fight against cancer: Role in targeting cancer stem cells. *Crit Rev Food Sci Nutr*, 2017. 57(16): p. 3449-3463.
- Komakech, R., et al., A Review of the Potential of Phytochemicals from *Prunus africana* (Hook f.) Kalkman Stem Bark for Chemoprevention and Chemotherapy of Prostate Cancer. *Evidence-Based Complementary and Alternative Medicine*, 2017. 2017: p. 3014019.
- Priyadarsini, R.V. and S. Nagini, Cancer chemoprevention by dietary phytochemicals: promises and pitfalls. *Curr Pharm Biotechnol*, 2012. 13(1): p. 125-36.
- Bishayee, A. and G. Sethi, Bioactive natural products in cancer prevention and therapy: Progress and promise. *Semin Cancer Biol*, 2016. 40-41: p. 1-3.
- Salehi, B., et al., Phytochemicals in Prostate Cancer: From Bioactive Molecules to Upcoming Therapeutic Agents. *Nutrients*, 2019. 11(7): p. 1483.
- Prostate cancer. *Nurs Stand*, 2016. 30(40): p. 17.
- Mokbel, K., U. Wazir, and K. Mokbel, Chemoprevention of Prostate Cancer by Natural Agents: Evidence from Molecular and Epidemiological Studies. *Anticancer Res*, 2019. 39(10): p. 5231-5259.
- Prostate cancer. *Nurs Stand*, 2014. 28(26): p. 18.
- Wang, G., et al., Genetics and biology of prostate cancer. *Genes Dev*, 2018. 32(17-18): p. 1105-1140.
- Schatten, H., Brief Overview of Prostate Cancer Statistics, Grading, Diagnosis and Treatment Strategies. *Adv Exp Med Biol*, 2018. 1095: p. 1-14.
- Ritch, C. and M. Cookson, Recent trends in the management of advanced prostate cancer. *F1000Res*, 2018. 7.
- Kgatlhe, M.M., et al., Prostate Cancer: Epigenetic Alterations, Risk Factors, and Therapy. *Prostate Cancer*, 2016. 2016: p. 5653862.
- Cuzick, J., et al., Prevention and early detection of prostate cancer. *Lancet Oncol*, 2014. 15(11): p. e484-92.

26. Salehi, B., et al., Phytochemicals in Prostate Cancer: From Bioactive Molecules to Upcoming Therapeutic Agents. *Nutrients*, 2019. 11: p. 1483;.
27. Brookman-May, S.D., et al., Latest Evidence on the Impact of Smoking, Sports, and Sexual Activity as Modifiable Lifestyle Risk Factors for Prostate Cancer Incidence, Recurrence, and Progression: A Systematic Review of the Literature by the European Association of Urology Section of Oncological Urology (ESOU). *European Urology Focus*, 2019. 5(5): p. 756-787.
28. Leitzmann, M. and S. Rohrmann, Risk factors for the onset of prostatic cancer: Age, location, and behavioral correlates. *Clinical epidemiology*, 2012. 4: p. 1-11.
29. Rebbeck, T.R., Prostate Cancer Genetics: Variation by Race, Ethnicity, and Geography. *Semin Radiat Oncol*, 2017. 27(1): p. 3-10.
30. Biró, K. and L. Géczi, [The role of exercise in prostate cancer prevention and treatment]. *Magy Onkol*, 2019. 63(1): p. 60-64.
31. Bernard, B., et al., Impact of age at diagnosis of de novo metastatic prostate cancer on survival. *Cancer*, 2020. 126(5): p. 986-993.
32. Siegel, R.L., K.D. Miller, and A. Jemal, Cancer statistics, 2019. *CA Cancer J Clin*, 2019. 69(1): p. 7-34.
33. Perdana, N.R., et al., The Risk Factors of Prostate Cancer and Its Prevention: A Literature Review. *Acta Med Indones*, 2016. 48(3): p. 228-238.
34. Mazzone, E., et al., The effect of race on survival after local therapy in metastatic prostate cancer patients. *Can Urol Assoc J*, 2019. 13(6): p. 175-181.
35. Abdel-Rahman, O., Prostate Cancer Incidence and Mortality in Relationship to Family History of Prostate Cancer; Findings From The PLCO Trial. *Clin Genitourin Cancer*, 2019. 17(4): p. e837-e844.
36. Kimura, T. and S. Egawa, Epidemiology of prostate cancer in Asian countries. *Int J Urol*, 2018. 25(6): p. 524-531.
37. Giri, V.N. and J.L. Beebe-Dimmer, Familial prostate cancer. *Semin Oncol*, 2016. 43(5): p. 560-565.
38. Dickerman, B.A., et al., Weight change, obesity and risk of prostate cancer progression among men with clinically localized prostate cancer. *Int J Cancer*, 2017. 141(5): p. 933-944.
39. Bandini, M., G. Gandaglia, and A. Briganti, Obesity and prostate cancer. *Current Opinion in Urology*, 2017. 27(5): p. 415-421.
40. Zhang, X., et al., Impact of obesity upon prostate cancer-associated mortality: A meta-analysis of 17 cohort studies. *Oncol Lett*, 2015. 9(3): p. 1307-1312.
41. Golabek, T., et al., Obesity and prostate cancer incidence and mortality: a systematic review of prospective cohort studies. *Urol Int*, 2014. 92(1): p. 7-14.
42. Barsouk, A., et al., Epidemiology, Staging and Management of Prostate Cancer. *Med Sci (Basel)*, 2020. 8(3).
43. Peisch, S.F., et al., Prostate cancer progression and mortality: a review of diet and lifestyle factors. *World Journal of Urology*, 2017. 35(6): p. 867-874.
44. Riviere, P., et al., Tobacco smoking and death from prostate cancer in US veterans. *Prostate Cancer and Prostatic Diseases*, 2020. 23(2): p. 252-259.
45. Murta-Nascimento, C., et al., The effect of smoking on prostate cancer survival: a cohort analysis in Barcelona. *European journal of cancer prevention : the official journal of the European Cancer Prevention Organisation (ECP)*, 2015. 24(4): p. 335-339.
46. Nussbaumer, S., et al., Analysis of anticancer drugs: a review. *Talanta*, 2011. 85(5): p. 2265-89.
47. Sak, K., Chemotherapy and dietary phytochemical agents. *Chemother Res Pract*, 2012. 2012: p. 282570.
48. Huang, B., et al., PSMA-Targeted Stably Linked "Dendrimer-Glutamate Urea-Methotrexate" as a Prostate Cancer Therapeutic. *Biomacromolecules*, 2014. 15(3): p. 915-923.
49. Baskar, R., et al., Cancer and radiation therapy: current advances and future directions. *Int J Med Sci*, 2012. 9(3): p. 193-9.
50. Lumen, N., et al., Developments in external beam radiotherapy for prostate cancer. *Urology*, 2013. 82(1): p. 5-10.
51. Chaiswing, L., et al., Profiles of Radioresistance Mechanisms in Prostate Cancer. *Crit Rev Oncog*, 2018. 23(1-2): p. 39-67.
52. Moschini, M., et al., External Beam Radiotherapy Increases the Risk of Bladder Cancer When Compared with Radical Prostatectomy in Patients Affected by

- Prostate Cancer: A Population-based Analysis. *Eur Urol*, 2019. 75(2): p. 319-328.
53. Lin, Y., Internal radiation therapy: a neglected aspect of nuclear medicine in the molecular era. *J Biomed Res*, 2015. 29(5): p. 345-55.
54. Chagari, C., et al., Brachytherapy: An overview for clinicians. *CA Cancer J Clin*, 2019. 69(5): p. 386-401.
55. Czerwińska, M., et al., Targeted Radionuclide Therapy of Prostate Cancer-From Basic Research to Clinical Perspectives. *Molecules*, 2020. 25(7).
56. Zaorsky, N.G., et al., The evolution of brachytherapy for prostate cancer. *Nat Rev Urol*, 2017. 14(7): p. 415-439.
57. Ferdinandus, J., et al., Prostate-specific membrane antigen theranostics: therapy with lutetium-177. *Current Opinion in Urology*, 2018. 28(2): p. 197-204.
58. Kuo, H.T., et al., Enhancing Treatment Efficacy of (177)Lu-PSMA-617 with the Conjugation of an Albumin-Binding Motif: Preclinical Dosimetry and Endoradiotherapy Studies. *Mol Pharm*, 2018. 15(11): p. 5183-5191.
59. Assadi, M., et al., Potential application of lutetium-177-labeled prostate-specific membrane antigen-617 radioligand therapy for metastatic castration-resistant prostate cancer in a limited resource environment: Initial clinical experience after 2 years. *World J Nucl Med*, 2020. 19(1): p. 15-20.
60. Silvestri, I., et al., A Perspective of Immunotherapy for Prostate Cancer. *Cancers (Basel)*, 2016. 8(7).
61. Rekoske, B.T. and D.G. McNeel, Immunotherapy for prostate cancer: False promises or true hope? *Cancer*, 2016. 122(23): p. 3598-3607.
62. Comiskey, M.C., M.C. Dallos, and C.G. Drake, Immunotherapy in Prostate Cancer: Teaching an Old Dog New Tricks. *Curr Oncol Rep*, 2018. 20(9): p. 75.
63. Venturini, N.J. and C.G. Drake, Immunotherapy for Prostate Cancer. *Cold Spring Harb Perspect Med*, 2019. 9(5).
64. Schepisi, G., et al., Immunotherapy for Prostate Cancer: Where We Are Headed. *Int J Mol Sci*, 2017. 18(12).
65. Fujita, K. and N. Nonomura, Role of Androgen Receptor in Prostate Cancer: A Review. *World J Mens Health*, 2019. 37(3): p. 288-295.
66. Crawford, E.D., et al., Androgen-targeted therapy in men with prostate cancer: evolving practice and future considerations. *Prostate Cancer Prostatic Dis*, 2019. 22(1): p. 24-38.
67. Liu, J.M., et al., Androgen deprivation therapy for prostate cancer and the risk of autoimmune diseases. *Prostate Cancer Prostatic Dis*, 2019. 22(3): p. 475-482.
68. Nead, K.T., et al., Androgen Deprivation Therapy and Future Alzheimer's Disease Risk. *J Clin Oncol*, 2016. 34(6): p. 566-71.
69. Chen, F.Z. and X.K. Zhao, Prostate cancer: current treatment and prevention strategies. *Iran Red Crescent Med J*, 2013. 15(4): p. 279-84.
70. Wang, Z., et al., The efficacy and safety of radical prostatectomy and radiotherapy in high-risk prostate cancer: a systematic review and meta-analysis. *World Journal of Surgical Oncology*, 2020. 18(1): p. 42.
71. Kim, E.H. and A.D. Bullock, Surgical Management for Prostate Cancer. *Mo Med*, 2018. 115(2): p. 142-145.
72. Gong, Y., et al., Bioactive tanshinones in *Salvia miltiorrhiza* inhibit the growth of prostate cancer cells in vitro and in mice. *Int J Cancer*, 2011. 129(5): p. 1042-52.
73. Déziel, B., et al., American cranberry (*Vaccinium macrocarpon*) extract affects human prostate cancer cell growth via cell cycle arrest by modulating expression of cell cycle regulators. *Food & Function*, 2012. 3(5): p. 556-564.
74. Acquaviva, R., et al., Antiproliferative effect of oleuropein in prostate cell lines. *Int J Oncol*, 2012. 41(1): p. 31-8.
75. Zhang, Y., et al., Tanshinones from Chinese Medicinal Herb Danshen (*Salvia miltiorrhiza* Bunge) Suppress Prostate Cancer Growth and Androgen Receptor Signaling. *Pharmaceutical Research*, 2012. 29(6): p. 1595-1608.
76. Zuniga, K.E., S.K. Clinton, and J.W. Erdman, The Interactions of Dietary Tomato Powder and Soy Germ on Prostate Carcinogenesis in the TRAMP Model. 2013. 6(6): p. 548-557.
77. Samykutty, A., et al., Piperine, a Bioactive Component of Pepper Spice Exerts Therapeutic Effects on Androgen Dependent and Androgen Independent Prostate Cancer Cells. *PLoS One*, 2013. 8(6): p. e65889.

78. Ekunwe, S.I., et al., Fractionated *Ocimum gratissimum* leaf extract inhibit prostate cancer (PC3-AR) cells growth by reducing androgen receptor and survivin levels. *J Health Care Poor Underserved*, 2013. 24(4 Suppl): p. 61-9.
79. Zhao, Y., et al., Turmeric and Chinese goldthread synergistically inhibit prostate cancer cell proliferation and NF- κ B signaling. *Funct Foods Health Dis*, 2014. 4: p. 312-339.
80. Saha, A., et al., 6-Shogaol from Dried Ginger Inhibits Growth of Prostate Cancer Cells Both *In Vitro* and *In Vivo* through Inhibition of STAT3 and NF- κ B Signaling. 2014. 7(6): p. 627-638.
81. Gao, Y., et al., Inactivation of ATP citrate lyase by Cucurbitacin B: A bioactive compound from cucumber, inhibits prostate cancer growth. *Cancer Letters*, 2014. 349(1): p. 15-25.
82. Kang, S., et al., Hirsutenone in *Alnus* extract inhibits akt activity and suppresses prostate cancer cell proliferation. *Mol Carcinog*, 2015. 54(11): p. 1354-62.
83. Melchini, A., et al., Antiproliferative activity of the dietary isothiocyanate erucin, a bioactive compound from cruciferous vegetables, on human prostate cancer cells. *Nutr Cancer*, 2013. 65(1): p. 132-8.
84. Wang, P., et al., Increased chemopreventive effect by combining arctigenin, green tea polyphenol and curcumin in prostate and breast cancer cells. *RSC Advances*, 2014. 4(66): p. 35242-35250.
85. Atmaca, H. and E. Bozkurt, Apoptotic and anti-angiogenic effects of *Salvia triloba* extract in prostate cancer cell lines. *Tumour Biol*, 2016. 37(3): p. 3639-46.
86. Hu, E., et al., Novel cyclotides from *Hedyotis diffusa* induce apoptosis and inhibit proliferation and migration of prostate cancer cells. *Int J Clin Exp Med*, 2015. 8(3): p. 4059-65.
87. Kim, S.H., et al., Autophagy inhibition enhances silibinin-induced apoptosis by regulating reactive oxygen species production in human prostate cancer PC-3 cells. *Biochem Biophys Res Commun*, 2015. 468(1-2): p. 151-6.
88. Tong, K.L., et al., The in vitro and in vivo anti-cancer activities of a standardized quassinoids composition from *Eurycoma longifolia* on LNCaP human prostate cancer cells. *PLoS One*, 2015. 10(3): p. e0121752.
89. Bhaumik, A., et al. THE BIOACTIVE COMPOUNDS OBTAINED FROM THE PAPAYA (*CARICA PAPAYA*) ACT AS POTENTIAL ANTICANCER AGENTS AGAINST THE HUMAN PROSTATE CANCER CELL LINE DU-145. 2015.
90. Medjakovic, S., et al., Pumpkin seed extract: Cell growth inhibition of hyperplastic and cancer cells, independent of steroid hormone receptors. *Fitoterapia*, 2016. 110: p. 150-6.
91. Huang, S.P., et al., Chemopreventive Potential of Ethanolic Extracts of *Luobuma* Leaves (*Apocynum venetum* L.) in Androgen Insensitive Prostate Cancer. *Nutrients*, 2017. 9(9).
92. Liu, C.M., et al., Ginger Phytochemicals Inhibit Cell Growth and Modulate Drug Resistance Factors in Docetaxel Resistant Prostate Cancer Cell. *Molecules*, 2017. 22(9).
93. Wu, C.Y., et al., Anti-cancer effect of danshen and dihydroisotanshinone I on prostate cancer: targeting the crosstalk between macrophages and cancer cells via inhibition of the STAT3/CCL2 signaling pathway. *Oncotarget*, 2017. 8(25): p. 40246-40263.
94. Rayaprolu, S.J., et al., Soybean peptide fractions inhibit human blood, breast and prostate cancer cell proliferation. *J Food Sci Technol*, 2017. 54(1): p. 38-44.
95. Gao, C., et al., Cytotoxic and chemosensitization effects of Scutellarin from traditional Chinese herb *Scutellaria altissima* L. in human prostate cancer cells. *Oncol Rep*, 2017. 38(3): p. 1491-1499.
96. Butt, G., et al., Emerging themes of regulation of oncogenic proteins by *Solanum nigrum* and its bioactive molecules in different cancers. *J Cell Biochem*, 2018. 119(12): p. 9640-9644.
97. Pan, B., et al., Inhibition of prostate cancer growth by solanine requires the suppression of cell cycle proteins and the activation of ROS/P38 signaling pathway. *Cancer Med*, 2016. 5(11): p. 3214-3222.
98. Segun, P.A., et al., Acridone alkaloids from the stem bark of *Citrus aurantium* display selective cytotoxicity against breast, liver, lung and prostate human carcinoma cells. *J Ethnopharmacol*, 2018. 227: p. 131-138.
99. Stivers, N.S., et al., Plagiocichiline A Inhibits Cytokinetic Abscission and Induces Cell Death. *Molecules*, 2018. 23(6).

100. Gbaweng, A.J.Y., et al., Excelsanone, a new isoflavonoid from *Erythrina excelsa* (Fabaceae), with in vitro antioxidant and in vitro cytotoxic effects on prostate cancer cells lines. *Nat Prod Res*, 2020. 34(5): p. 659-667.
101. Chaves, F.M., et al., Pomegranate Juice and Peel Extracts are Able to Inhibit Proliferation, Migration and Colony Formation of Prostate Cancer Cell Lines and Modulate the Akt/mTOR/S6K Signaling Pathway. *Plant Foods Hum Nutr*, 2020. 75(1): p. 54-62.
102. Gioti, K., et al., Silymarin Enriched Extract (*Silybum marianum*) Additive Effect on Doxorubicin-Mediated Cytotoxicity in PC-3 Prostate Cancer Cells. *Planta Med*, 2019. 85(11-12): p. 997-1007.
103. Huang, S.H., et al., Rooibos suppresses proliferation of castration-resistant prostate cancer cells via inhibition of Akt signaling. *Phytomedicine*, 2019. 64: p. 153068.
104. Pradhan, N., et al., *Paederia foetida* induces anticancer activity by modulating chromatin modification enzymes and altering pro-inflammatory cytokine gene expression in human prostate cancer cells. *Food Chem Toxicol*, 2019. 130: p. 161-173.
105. Shammugasamy, B., et al., Effect of citrus peel extracts on the cellular quiescence of prostate cancer cells. *Food Funct*, 2019. 10(6): p. 3727-3737.
106. Deb, G., et al., Green tea-induced epigenetic reactivation of tissue inhibitor of matrix metalloproteinase-3 suppresses prostate cancer progression through histone-modifying enzymes. *Mol Carcinog*, 2019. 58(7): p. 1194-1207.
107. Gioti, K., et al., *Glycyrrhiza glabra*-Enhanced Extract and Adriamycin Antiproliferative Effect on PC-3 Prostate Cancer Cells. *Nutrition and Cancer*, 2020. 72(2): p. 320-332.
108. Kilinc, K., et al., *Rosa canina* Extract has Antiproliferative and Proapoptotic Effects on Human Lung and Prostate Cancer Cells. *Nutr Cancer*, 2020. 72(2): p. 273-282.
109. Balusamy, S.R., et al., Citral Induced Apoptosis through Modulation of Key Genes Involved in Fatty Acid Biosynthesis in Human Prostate Cancer Cells: In Silico and In Vitro Study. *BioMed Research International*, 2020. 2020: p. 6040727.
110. Yu, Z., et al., Germacrone Induces Apoptosis as Well as Protective Autophagy in Human Prostate Cancer Cells. *Cancer Manag Res*, 2020. 12: p. 4009-4016.
111. Hegazy, M.G., A.M. Imam, and B.E. Abdelghany, Evaluation of cytotoxic and anticancer effect of *Orobancha crenata* methanolic extract on cancer cell lines. *Tumor Biology*, 2020. 42(5): p. 1010428320918685.
112. Pandey, P., et al., *Moringa oleifera* methanolic leaves extract induces apoptosis and G0/G1 cell cycle arrest via downregulation of Hedgehog Signaling Pathway in human prostate PC-3 cancer cells. *Journal of Food Biochemistry*, 2020. 44.
113. Xia, C., et al., Total saponins from *Paris forrestii* (Takht) H. Li. show the anticancer and RNA expression regulating effects on prostate cancer cells. *Biomedicine & Pharmacotherapy*, 2020. 121: p. 109674.
114. Zhang, Y., et al., Tanshinones: sources, pharmacokinetics and anti-cancer activities. *Int J Mol Sci*, 2012. 13(10): p. 13621-66.
115. Dong, Y., S.L. Morris-Natschke, and K.H. Lee, Biosynthesis, total syntheses, and antitumor activity of tanshinones and their analogs as potential therapeutic agents. *Nat Prod Rep*, 2011. 28(3): p. 529-42.
116. Shin, E.A., et al., Upregulation of microRNA135a-3p and death receptor 5 plays a critical role in Tanshinone I sensitized prostate cancer cells to TRAIL induced apoptosis. *Oncotarget*, 2014. 5(14): p. 5624-36.
117. Chiu, S.C., et al., Tanshinone IIA inhibits human prostate cancer cells growth by induction of endoplasmic reticulum stress in vitro and in vivo. *Prostate Cancer Prostatic Dis*, 2013. 16(4): p. 315-22.
118. Won, S.H., et al., Activation of p53 signaling and inhibition of androgen receptor mediate tanshinone IIA induced G1 arrest in LNCaP prostate cancer cells. *Phytother Res*, 2012. 26(5): p. 669-74.
119. Wang, D., et al., Unveiling the Mode of Action of Two Antibacterial Tanshinone Derivatives. *International journal of molecular sciences*, 2015. 16: p. 17668-81.
120. Szliszka, E., et al., The dietary isoflavone biochanin-A sensitizes prostate cancer cells to TRAIL-induced apoptosis. *Urologic Oncology: Seminars and Original Investigations*, 2013. 31(3): p. 331-342.
121. Szliszka, E. and W. Krol, The role of dietary polyphenols in tumor necrosis factor-related apoptosis inducing ligand

- (TRAIL)-induced apoptosis for cancer chemoprevention. Eur J Cancer Prev, 2011. 20(1): p. 63-9.
122. Yu, C., et al., Perspectives Regarding the Role of Biochanin A in Humans. Front Pharmacol, 2019. 10: p. 793.
123. Hanski, L., et al., Inhibitory activity of the isoflavone biochanin A on intracellular bacteria of genus Chlamydia and initial development of a buccal formulation. 2014. 9(12): p. e115115.
124. Niedzwiecki, A., et al., Anticancer Efficacy of Polyphenols and Their Combinations. Nutrients, 2016. 8(9).
125. Barbaro, B., et al., Effects of the olive-derived polyphenol oleuropein on human health. Int J Mol Sci, 2014. 15(10): p. 18508-24.
126. Omar, S.H., Oleuropein in olive and its pharmacological effects. Sci Pharm, 2010. 78(2): p. 133-54.
127. Al-Rimawi, F., I. Afaneh, and H. Jaraiseh, Effect of Olive Leaves Drying on the Content of Oleuropein. American Journal of Analytical Chemistry, 2015. 6: p. 246-252.
128. Khoo, H.E., et al., Anthocyanidins and anthocyanins: colored pigments as food, pharmaceutical ingredients, and the potential health benefits. Food Nutr Res, 2017. 61(1): p. 1361779.
129. Karna, P., et al., Polyphenol-rich sweet potato greens extract inhibits proliferation and induces apoptosis in prostate cancer cells in vitro and in vivo. Carcinogenesis, 2011. 32(12): p. 1872-80.
130. Altemimi, A., et al., Phytochemicals: Extraction, Isolation, and Identification of Bioactive Compounds from Plant Extracts. Plants, 2017. 6: p. 42.
131. Gupta, K., et al., Green tea polyphenols induce p53-dependent and p53-independent apoptosis in prostate cancer cells through two distinct mechanisms. 2012. 7(12): p. e52572.
132. Gupta, K., et al., Green tea polyphenols induce p53-dependent and p53-independent apoptosis in prostate cancer cells through two distinct mechanisms. PLoS One, 2012. 7(12): p. e52572.
133. Wang, P., D. Heber, and S.M. Henning, Quercetin increased the antiproliferative activity of green tea polyphenol (-)-epigallocatechin gallate in prostate cancer cells. Nutr Cancer, 2012. 64(4): p. 580-7.
134. Nagle, D.G., D. Ferreira, and Y.-D. Zhou, Epigallocatechin-3-gallate (EGCG): Chemical and biomedical perspectives. Phytochemistry, 2006. 67(17): p. 1849-1855.
135. Shukla, Y. and R. Singh, Resveratrol and cellular mechanisms of cancer prevention. Ann N Y Acad Sci, 2011. 1215: p. 1-8.
136. Walle, T., Bioavailability of resveratrol. Ann N Y Acad Sci, 2011. 1215: p. 9-15.
137. Iguchi, K., et al., Anti-Androgenic Activity of Resveratrol Analogs in Prostate Cancer LNCaP Cells. Journal of andrology, 2012. 33.
138. Chen, Y.A., et al., Sensitization of Radioresistant Prostate Cancer Cells by Resveratrol Isolated from Arachis hypogaea Stems. PLoS One, 2017. 12(1): p. e0169204.
139. Springer, M. and S.J.N. Moco, Resveratrol and its human metabolites—Effects on metabolic health and obesity. 2019. 11(1): p. 143.
140. Umadevi, P., K. Deepti, and D.V.R. Venugopal, Synthesis, anticancer and antibacterial activities of piperine analogs. Medicinal Chemistry Research, 2013. 22(11): p. 5466-5471.
141. Ba, Y. and A. Malhotra, Potential of piperine in modulation of voltage-gated K⁺ current and its influences on cell cycle arrest and apoptosis in human prostate cancer cells. Eur Rev Med Pharmacol Sci, 2018. 22(24): p. 8999-9011.
142. Meghwal, M. and T.K. Goswami, Piper nigrum and piperine: an update. Phytother Res, 2013. 27(8): p. 1121-30.
143. Gorgani, L., et al., Piperine-The Bioactive Compound of Black Pepper: From Isolation to Medicinal Formulations: Piperine isolation from pepper.... Comprehensive Reviews in Food Science and Food Safety, 2016. 16.
144. Zeng, Y. and Y. Yang, Piperine depresses the migration progression via downregulating the Akt/mTOR/MMP-9 signaling pathway in DU145 cells. Mol Med Rep, 2018. 17(5): p. 6363-6370.
145. Zeng, Y. and Y.J.M.m.r. Yang, Piperine depresses the migration progression via downregulating the Akt/mTOR/MMP-9 signaling pathway in DU145 cells. 2018. 17(5): p. 6363-6370.

146. Yedjou, C.G., et al., Prostate cancer disparity, chemoprevention, and treatment by specific medicinal plants. 2019. 11(2): p. 336.
147. Tripathi, A.K., A.K. Ray, and S.K. Mishra, Molecular and pharmacological aspects of piperine as a potential molecule for disease prevention and management: evidence from clinical trials. Beni-Suef University Journal of Basic and Applied Sciences, 2022. 11(1): p. 16.
148. Zhou, H., C.S. Beevers, and S. Huang, The targets of curcumin. *Curr Drug Targets*, 2011. 12(3): p. 332-47.
149. Gupta, S.C., S. Patchva, and B.B. Aggarwal, Therapeutic roles of curcumin: lessons learned from clinical trials. *Aaps j*, 2013. 15(1): p. 195-218.
150. Esatbeyoglu, T., et al., Curcumin--from molecule to biological function. *Angew Chem Int Ed Engl*, 2012. 51(22): p. 5308-32.
151. Wei, X., et al., Effects of cyclohexanone analogues of curcumin on growth, apoptosis and NF- κ B activity in PC-3 human prostate cancer cells. *Oncol Lett*, 2012. 4(2): p. 279-284.
152. Teiten, M.H., et al., Anti-proliferative potential of curcumin in androgen-dependent prostate cancer cells occurs through modulation of the Wntless signaling pathway. *Int J Oncol*, 2011. 38(3): p. 603-11.
153. Killian, P.H., et al., Curcumin inhibits prostate cancer metastasis in vivo by targeting the inflammatory cytokines CXCL1 and -2. *Carcinogenesis*, 2012. 33(12): p. 2507-2519.
154. Yang, J., et al., Effect of curcumin on Bcl-2 and Bax expression in nude mice prostate cancer. *Int J Clin Exp Pathol*, 2015. 8(8): p. 9272-8.
155. Du, Y., et al., Curcumin inhibits cancer-associated fibroblast-driven prostate cancer invasion through MAOA/mTOR/HIF-1 α signaling. *Int J Oncol*, 2015. 47(6): p. 2064-72.
156. Zheng, J., et al., Curcumin, a polyphenolic curcuminoid with its protective effects and molecular mechanisms in diabetes and diabetic cardiomyopathy. 2018. 9: p. 472.
157. Pressman, P., R.A. Clemens, and A.W. Hayes, Bioavailability of micronutrients obtained from supplements and food: A survey and case study of the polyphenols. *Toxicology Research and Application*, 2017. 1: p. 2397847317696366.
158. Lucey, A., C. Heneghan, and M.E. Kiely, Guidance for the design and implementation of human dietary intervention studies for health claim submissions. *Nutrition Bulletin*, 2016. 41(4): p. 378-394.
159. Livingstone, T.L., et al., Plant Bioactives and the Prevention of Prostate Cancer: Evidence from Human Studies. *Nutrients*, 2019. 11(9).
160. Weaver, C.M. and J.W. Miller, Challenges in conducting clinical nutrition research. *Nutr Rev*, 2017. 75(7): p. 491-499.
161. Kallifatidis, G., J.J. Hoy, and B.L. Lokeshwar, Bioactive natural products for chemoprevention and treatment of castration-resistant prostate cancer. *Semin Cancer Biol*, 2016. 40-41: p. 160-169.
162. Salehi, B., et al., Phytochemicals in Prostate Cancer: From Bioactive Molecules to Upcoming Therapeutic Agents. *Nutrients*, 2019. 11(7).
163. Chirumbolo, S., Plant phytochemicals as new potential drugs for immune disorders and cancer therapy: really a promising path? *J Sci Food Agric*, 2012. 92(8): p. 1573-7.

How to cite this article:

Zulfiqar H, Zulfiqar H, Farooq F, Ahmed I, Rani I, Ullah F. (2022). Advancement and Future Perspectives of Prostate Cancer Treatment by Using Plant Bio-actives: A Review. 1(1).p.80-106